A Study on Dynamic Behavior for Buried Pipe Rehabilitation

Izumi, Akira

(Degree)
博士（農学）

(Date of Degree)
2016-03-25

(Date of Publication)
2017-03-01

(Resource Type)
doctoral thesis

(Report Number)
甲第6652号

(URL)
https://hdl.handle.net/20.500.14094/D1006652

Doctoral Dissertation

A Study on Dynamic Behavior for Buried Pipe Rehabilitation

埋設更生管の動的挙動に関する研究

January 2016

Graduate School of Agricultural Science,
Kobe University

Akira IZUMI

The research reported in this thesis was carried out at the Laboratory of Geotechnical and Environmental Engineering for Agricultural Land, Graduate School of Agricultural Science, Kobe University, Japan.

Acknowledgements

I would like to express my sincere gratitude to Dr. Toshinori Kawabata, Professor of Graduate School of Agricultural Science, Kobe University for his encouragement and advice. He encouraged me to come back to the college as a doctoral student when I had been working at Incorporated Administrative Agency Japan Water Agency. Thanks to him, I gained a chance to research again.

I am indebted to Dr. Tsutomu Tanaka, Professor and Dr. Kazuya Inoue, Associate Professor of Graduate School of Agricultural Science, Kobe University for constructive suggestions in reviewing this thesis. In my research debrief, they gave me many advices.

I would like to acknowledge to Dr. Yutaka Sawada, Assistant Professor of Graduate School of Agricultural Science, Kobe University. I completed this thesis by his advice. I was strongly inspired by his insight and enthusiasm for research.

I wish to grateful to Dr. Takashi Kimata, Lecturer and Dr. Yosuke Kudo, Assistant Professor of Graduate School of Life and Environmental Sciences, Osaka Prefecture University. They gave me valuable advices in the joint seminar of Osaka Prefecture University and Kobe University.

I wish to express my appreciation to Dr. Yoshiyuki Mohri, Professor of College of Agriculture, Ibaraki University for his excellent cooperation during shaking table tests in National Agriculture and Food Research Organization. Further acknowledgement is also due to Mr. Mitsuru Ariyoshi for his kind cooperation.

I would like to thank Dr. Joji Hinobayashi, Dainippon Plastics Co., Ltd. for

providing polyethylene pipes and allowing me to conduct two point loading tests in Ako factory. He encouraged me and taught me the knowledge about polyethylene pipes.

My thanks extend to Dr. Kazunori Uchida, Professor and many other faculty members of Graduate School of Agricultural Science, Kobe University. They warmly accepted me who came back to the college after three and half year's absence.

I wish to extend my thanks to Dr. Akira Murakami, Professor and Dr. Kazunori Fujisawa, Associate Professor of Graduate School of Agricultural, Kyoto University. They taught me the fundamentals of continuum mechanics, how to write papers.

I am very grateful to Mr. Taiki Miki. He helped me to laboratory experiments and DEM analyses every day. This thesis would not have been completed without his support. I expect his success in Tokyo.

Thanks are due to Dr. Daisuke Shoda, Mr. Yuta Nadamoto, Mr. Takafumi Hanazawa and Ms. Chifumi Shigemura who belonged to the same laboratory. We have conducted laboratory experiments together and discussed about test results.

My sincere appreciation will go to Dr. Mariko Suzuki, Assistant Professor of Department of Civil Engineering, National Institute of Technology, Kagawa College, for her warm encouragement. She organized laboratory members and provided me suitable environment to research. I wish also acknowledge Mr. Yoshinori Itani, Mr. Takumi Ibata and Mr. Kohei Ono; they are doctoral course students and supported me a lot.

I am really thankful for Mr. Kazuki Murai, Mr. Sho Takahara, Mr. Seita Kobayashi, Ms. Yui Yokota, Mr. Naoki Takegawa, Mr. Kenji Terada, Mr. Zenko Ueda and Mr. Rintaro Shigemoto in the same laboratory. In particular, acknowledgements are due to Mr. Ono and Mr. Takahara for their kind cooperation in shaking table tests.

Finally, I am deeply grateful for my wife, my parents and her parents. I owe what I am now to them. They have forgave my selfishness that I wanted to research again and supported in my life.

Contents

List of Tables

List of Figures

Notations

C_h	:	Decreasing coefficient
C_i	:	Damping constant
D_{50}	:	Mean particle size
D_c	:	Center diameter of pipe (mm)
D_i	:	Damping constant
D_{out}	:	Outer diameter of pipe (N/mm)
Dr	:	Relative density (%)
D'	:	Diameter of flexible pipe
E_{50}	:	Deformation modulus (MN/m^2)
E_p	:	Elastic modulus of pipe (N/mm^2)
$E_{p'}$	:	Elastic modulus of pipe per unit depth ($N/mm^2/mm$)
F_i	:	Resultant force acted on element (N)
F_n	:	Normal force at each contact (N·m)
I	:	Moment of inertia of area (mm^4/mm)
I_i	:	Inertia moment of element (m^4/m)
K_n	:	Normal spring coefficient
K_s	:	Tangential spring coefficient
M_i	:	Resultant moment acted on element
M_r	:	Rolling friction (N·m)
P	:	Linear load (N/mm)
R	:	Radius of element (m)

R_{ij}	:	Center distance between two elements, i and j (m)
S	:	Vertical deflection (mm)
a	:	Length of long axis of ellipse
b	:	Length of short axis of ellipse
d_c	:	Center diameter of model pipe (mm)
d_n	:	Normal damping force (N)
d_s	:	Tangential damping force (N)
e_n	:	Normal elastic force (N)
e_s	:	Tangential elastic force (N)
f_c	:	Compressive strength (N/mm^2)
f_n	:	Normal compressive force (N)
f_s	:	Tangential compressive force (N)
i	:	Number of strain gauge
l	:	Distance between two elements of outer circumferential of polygonal element (mm)
m_i	:	Element mass (g)
p	:	Asymptotic value
q_n	:	Maximum deviator stress (kN/m^2)
r_i	:	Radius of an element (m)
t	:	Time
t_m	:	Normal distance between inner and outer circumferential of polygonal element (mm)
t_p	:	Thickness of pipe (mm)
u	:	Displacement vector of element (m)
ϕ	:	Angle of internal friction (deg.)
α	:	Change rate
α_{ij}	:	Angle making straight line connecting center of element i with a center of element j and x axial (deg.)
ε_b	:	Bending strain (μ)
ε_{in}	:	Inner circumferential strain on pipe (μ)
ε_{out}	:	Outer circumferential strain on pipe (μ)

ε_r	:	Axial strain (μ)
ε_{50}	:	Axial strain to half maximum deviator stress (μ)
σ_L	:	Vertical load (kN/m^2)
σ_m	:	Absolute maximum axial stress (m)
σ_r	:	Axial stress (MN/m^2)
σ_{rn}	:	Axial stress at measurement point n (MN/m^2)
Δ	:	Oblique deflection
Δu_i	:	x direction displacement increment of element *i* (m)
Δu_n	:	Normal relative displacement between two elements (m)
Δu_s	:	Tangential relative displacement between two elements (m)
Δv_i	:	y direction displacement increment of element *i* (m)
Δ'	:	Half oblique deflection
$\Delta\varphi_i$	:	Rotation increment of element *i* (m)
α'	:	Shear angle (deg.)
γ	:	Shear strain (%)
δ	:	45-225 deg. deflection of pipe
η_n	:	Normal damping coefficient
η_s	:	Tangential damping coefficient
θ_r	:	Rolling friction angel (deg.)
μ	:	Frictional coefficient
ρ_{dmax}	:	Maximum dry density (g/cm^3)
ρ_{dmin}	:	Minimum dry density (g/cm^3)
ρ_s	:	Density of soil particles (g/cm^3)
φ	:	Rotational displacement of element (m)

CHAPTER 1

Chapter 1

Introduction

1.1 Background

An irrigation canal plays an important role to apply irrigation water from a source to fields. In Japan, agricultural water requirements demand is 54.4 billion m^3 in 2010 (MLITT, 2013). The water requirements is approximately twice as much as municipal water. The main irrigation canal networks extend over a length of 49,000 km (MAFF, 2012). After World War 2, the networks were developed in order to increase yields of foods associated with an expansion of an urban area and economic development.

In recent years, the aging irrigation canal increases as shown in **Figure 1.1** and requires a repair work. A standard economic life of irrigation facilities is 40 years and the aging irrigation canals have a risk for a leakage and a decrease of a capacity of flow. In addition, since the aging irrigation canals do not have a resistance of major earthquake such as Nankai Trough earthquake which will happen in the near future, the aging irrigation canals have a risk for a serious damage.

As a repair work for an aging pipeline, Pipe rehabilitation has been used. In this method, the inner pipe (rehabilitated pipe) is inserted into the outer aging pipe as shown in **Figure 1.2**. This method was recognized to use firstly in 1971 (Anzaki, 2013) and

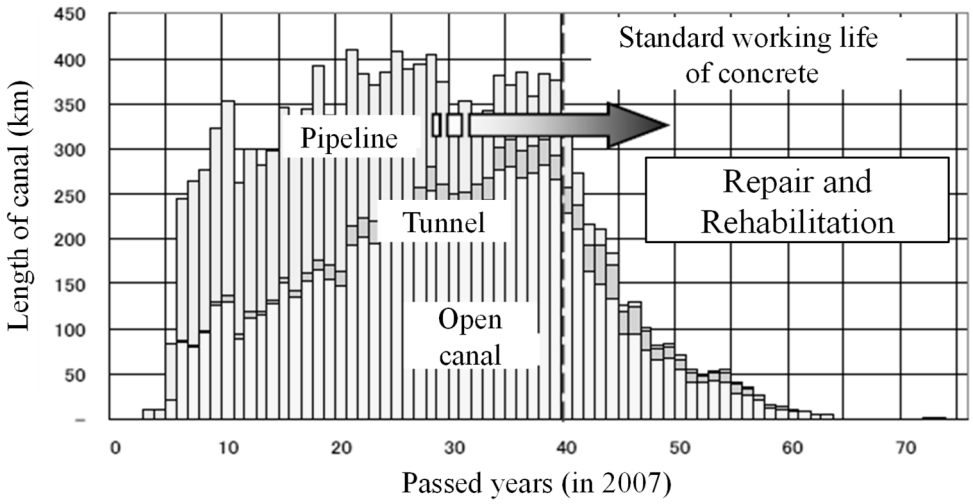

Figure 1.1 Service period of irrigation canal (M.A.F.F., 2010)

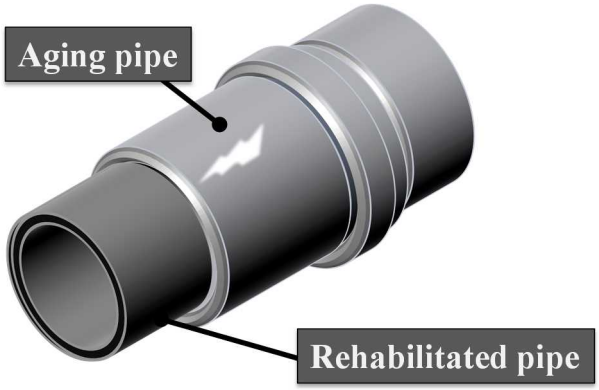

Figure 1.2 Pipe rehabilitation

developed at a sewerage filed. This method has four merit (J.P.R.Q.A.A., 2007a). Firstly, the strength, capacity of flow, water-tightness, anticorrosion property and rub resistance on the aging pipeline can be greatly improved. Secondly, the influence of the construction by this method on fields, residents and traffic conditions can be lower since a large excavation does not need. Thirdly, the less construction cost is anticipated for the same reason as the second. Finally, an amount of industrial waste can be reduced since the aging pipeline was remained to be buried. The method is categorized in terms of the

Table 1.1 Categorization of Pipe rehabilitation (J.P.R.Q.A.A., 2007b).

Structure	Function	Method	Name(construction method)
Non-integrated	Only inner pipe resist the force (single layer) / Outer and Inner pipes share the force (double layer)	Cured-in-place	ICP BREATHE SD LINER IN SITU FORM ALL LINER GROW HORSE LINING IN PIPE
		Close-Fit	EX OMEGA LINER FFT-S ALL LINER PALTEM HL-E PALTEM SZ SEAMLESS SYSTEM
Integrated	Integrated pipe resist the force	Spirally-wound	SPR DANBY PALTEM FLOORING

structure and production as shown in **Table 1.1**.

In the design standard (MAFF, 2009) for pipeline in Japan, the design of the pipe rehabilitation is not described. In the design standard of this method for the sewerage filed (JSWA, 2001), a stiffness of an aging outer pipe is negligible. Thus, it is assumed that all earth pressure acts on the inner pipe. In the design standard for the irrigation pipeline, a pipeline is designed with consideration of the stiffness around the pipeline on the basis of Marston-Spangler theory (Spangler, 1941 and Marston, 1930). It is needed to clear an influence of an aging outer on an inner pipe in order to apply the pipe rehabilitation to the design standard for irrigation pipeline.

1.2 Literature Review

Almost researches related to rehabilitated pipeline have been made for sewage pipeline. As an initial study, Falter (1996) suggested the need of new method and solution for the design of rehabilitated sewage pipeline from the analysis. In addition,

22 series of centrifuge test were performed using different pipe stiffness, burying way and ground condition in order to evaluate the behavior of buried flexible pipe. Takahashi et al. (2002) conducted the full-scale loading test, centrifuge test and FEM analyses in order to evaluate the deformation behavior of the rehabilitated pipe under different damage level of the outer pipe and it was found that the outer aging pipe reinforced the ground and bending strain of inner rehabilitated pipe decreased by about 60% relative to that of single buried pipe. Nakano et al. (2002) developed the separate non-linear analysis method to design the reinforced the aging sewerage pipe. In addition, Nakano et al. (2003) conducted the destructive test and FEM analysis for RC box culvert. As the results, it was found that the load bearing capacity of the rehabilitated RC box culvert depended on the damage level of the outer pope. Gumbel et al. (2003) and Spasojevic et al. (2007) conducted centrifuge tests using PVC as inner rehabilitated pipe and duralumin as outer aging pipe in order to evaluate the influence of the damage of outer pipe on the behavior of inner pipe. The results indicated that bending strain of inner pipe increased as the damage of outer pipe developed. Inoue et al. (2005) discussed about the buckling behavior and design of sewer pipes cured with plastic inner liners. The effect of the aging outer pipe on the buckling of inner pipes was estimated through the buckling theory. As the results, the critical buckling occurs when the external hydraulic pressure acts on the inner pipe. In addition, both standards of ASTM and JSWA were compared, indicating that JSWA was more reasonable than ASTM for the design of two layer pipe. Yoshimura et al. (2006) conducted two-edge loading test and FEM analyses for sewer concrete pipes which rehabilitated by cured-in-place pipes (CIPP). It was suggested that the effect of outer pipe of CIPP on the deformation response of the rehabilitated pipe was slight from the test and analyses results. In addition, from the result for the full scale test that simulated vehicle loading and adjacent excavation, Inoue et al. (2006) indicated that the rehabilitated pipes by CIPP were fully safe. In the test, the outer pipe had an inner diameter of 300 mm and four crossed cracks. Tohda, et al. (2006) conducted fourteen dynamic centrifuge model tests to investigate the response and safety of sewer concrete pipes rehabilitated by CIPP under strong seismic loading. The outer pipe and the inner pipe were hypothesized as

the integrated structure and two model pipes with different flexibilities which was simulated damaged levels of the outer pipes were used. From the test results, safety of a rehabilitated pipe under strong seismic loading was confirmed. Law et al. (2007) discussed about the influence of slip between the outer pipe and the inner pipe in detail by FEM analyses. Miyashita and Kuwano (2008) and Ko and Kuwano (2010) conducted cyclic loading test to evaluate the relationship between the effects of backfill material density and damage level on the double layer pipe. As the test results, it was revealed that the inner pipe was retained in loose sand by the restraint effect from the outer pipe when the deterioration level was low.

In recent years, studies on pipe rehabilitation for irrigation field has been conducted. Sawada et al. (2014) conducted the model experiments under different damage levels of the aging pipe and loading positions. Experimental results indicated that the strain concentration occurred at the top and the bottom of the rehabilitated pipe due to the point contact of the edge of the aging pipe. In addition, Ono et al. (2015) conducted the centrifuge model tests under various conditions including the damage levels of the outer pipe, the positions of surcharge load, the ring stiffness of the inner pipe, and the density of the backfill material. The test results show that the strain concentration of the inner pipe was reduced by 20% as the ring bending stiffness of the inner pipe increased, and that the strain concentration appears for loose and dense ground.

Although the following studies on the dynamic behavior of the buried pipe such as the floatation, deformation and lateral displacement were conducted by the shaking table tests and the analyses and so on, studies in order to verify the dynamic behavior of the rehabilitated pipe was almost not conducted. Nasu (1972) conducted dynamite tests, plank hammering tests, gas gun tests to verify dynamic behavior of the buried pipeline. As the test results indicated that the period spectrum of the pipeline was corresponding to that of the ground, and the axial strain was larger than the bending strain. Ohara and Yamamoto (1976) conducted shaking table tests for the buried pipe in order to measure the shaking earth pressure. From the tests results, it was cleared that a damage of the pipe due to the seismic force was small when the pipe was buried nearly on the base

rock and backfill material was sufficiently compacted. Oishi and Sekiguchi (1984) observed the strain and the acceleration of the buried pipe in order to investigate the dynamic behavior of buried pipelines. On the base of the observed earthquake, the spectra analysis and phase velocity analysis were conducted to make clear the relationship between the strain and the ground motion. They proposed the method of the seismic response analysis of the buried pipeline. Mohri et al. (1998) conducted the large scale shaking tests for the shallowly buried pipe to investigate the amount floatation of the pipe during earth quake. The test results show that the velocity and the amount of floating of the buried pipe depended on the degree of liquefaction, the shaking time and the vertical shaking. They proposed the effectiveness of three types of the floatation restraint. In addition, the pipe for the protection method with geogrid and gravel as backfill material did not float even the cover depth of approximately zero (Mohri et al. 2000). Yuasa et al. (2000) conducted the shaking table tests for buried pipes in liquefaction and finite element analysis as the purpose of the clarification of the floatation mechanism of the buried pipe. As the results, it was revealed that the floatation was influenced by the difference in external pressure acted on the pipe and that the floatation could be reproduced by the analysis. Sato et al. (2003) predicted the amount of the floatation of the buried pipe by FEM (FLIP). The floatation behavior of the buried pipe was partially simulated. Kawabata et al. (2005) conducted DEM analyses in order to clarify the uplift mechanism of the buried pipe to cyclic simple shear in dry sand. As the analyses results, the buried pipe uplifted due to the reaction force from the lower ground as the lateral displacement of the pipe increased. Kawabata et al. (2011) conducted the shaking table test in order to verify the dynamic behavior for the bend of pressure pipeline with a concrete block and the thrust restraint using geogrids (Kawabata et al., 2006, Kawabata et al., 2009, Sawada et al., 2010). As the results, the horizontal displacement of the bend with the concrete block was extremely larger than that with the thrust restrain using geogrid.

In addition, since a damage of joint of pipes and a settlement of pipes may be caused by earthquake, their dynamic behavior was investigated. Kitaura et al. (1982) proposed a model test using a sinking-soil-box and measured stress acting on pipes and

deformation of joints of pipes when ground sank. Colton et al. (1982) conducted the dynamic test for full-scale buried pipelines to measure the soil-pipe axial interaction. As the test results, when the displacement of the pipe was less than 0.01in., the pipe did not slip relative to the sand. At displacement greater than about 0.01 in., the irreversibility was observed in the sand deformation. In addition, the relationship between the force and the displacement of the pipe was highly nonlinear. Miyajima (1983) conducted shaking table test for a model pipe fixed at one end in liquefied ground to verify a destruction of pipes due to floating of its. Hachiya et al. (2005) proposed a rational design method for buried pipelines subjected to differential ground settlement on the basis of a data set from 3D centrifuge model tests. From test results of shaking table test, Fujita et al. (2007) evaluated an allowable range of joint for expansion and bending on pipeline that formed with flexible joints and Tanaka et al. (2005) cleared that the use of ball type flexible joint has reduced significantly the vertical thrust on the joint that usually observed during the ground settlement after the liquefaction. Da et al. (2008) were conducted two pairs of centrifuge tests designed to investigate the differences in behavior of buried high-density polyethylene pipelines subjected to normal and strike -strip faulting. Alireza et al. (2014) monitoring the performance of pipe rehabilitation using acoustic emission technique, subjected to static and dynamic loading. Particularly, two damage mechanisms are investigated-delamination between outer pipe and inner pipe, and incipient failure of the inner pipe.

In Discrete Element Method (DEM) (Cundall and Strack, 1979), a micro mechanical quantity which do not measure in laboratory tests can be evaluated. In recent years, DEM is widely used in order to verify a theory and to support a date obtained from the tests in geotechnical engineering field. Meguro and Hakuno (1988) developed Modified Distinct Element Method and conducted the fracture analyses of the concrete structure. This method was introduced into the non-linear spring to mortar. The numerical results obtained in this method agreed well with the results of laboratory tests. Sakaguchi et al. (1993) introduced the rolling friction into DEM analyses. The rolling friction was formulated by the term of resisting moment and could be expressed as a shear strength which had an actual soil material. Matsuoka and Yamamoto (1994)

compared the result for direct shear box tests and biaxial compression tests on granular assemblies of aluminum rods to the result for DEM by which their tests was simulated in order to investigate the quantitative applicability of DEM to stress-strain behavior of granular material. They concluded that DEM could be a useful tool to elucidate the microscopic mechanism of the behavior of granular materials. Nakase et al. (2002) proposed that any structures are modeled using a polygonal element which consisted of a circle element and an edge element. Suehiro et al. (2003) conducted the shaking table test to clarify the mechanism of floatation behavior of underground structure using the polygonal element by DEM. Kawabata et al. (2003) evaluated the characteristic behavior of shallowly buried pipeline under wheel load using DEM analyses. The model pipe was expressed as 20 beam elements, all elements was coupled by contacting element and elastic spring at each element. As the analyses results, it was found that the load of the traveling force distributed in the flexible pipe in the whole and surrounding ground, and the stress concentration to the top of the pipe was remarkable for the rigid pipe. Murakami et al. (2004) incorporated a numerical model where both the adhesive force and the lubricative effect due to liquid bridges in order to capture the mechanism of soil compaction from micro-mechanical viewpoint. They carried out numerical simulation of soil compaction test by the proposed model and the results were found to be in good agreement with the compaction curve obtained through usual experiments. Mori and Ogawa (2007) conducted the liquefaction analysis for the river dike by DEM and compared the analysis result to the damage of the river dike due to the 1995 Hyogoken-Numbu earth quake. It was found that the settlement of the river dike obtained from the analysis result could reproduce the actual settlement. Fukumoto et al. (2011) proposed a simple model for DEM with fewer parameters. The interparticle contact bond model and the rolling friction model were introduced into the conventional contact model.

1.3 Aim of This Study

As described above, studies on the dynamic behavior of the rehabilitated pipe are much less studies relative to the static behavior although many researchers have evaluated the influence of the aging outer pipe on the static behavior of the inner pipe by the model test, the centrifuge test and the analyses such as FEM.

It was not cleared that the influence of the aging outer pipe with cracks on the dynamic behavior of the inner pipe although Tohda et al. (2006) conducted fourteen dynamic centrifuge model tests assuming the outer pipe and the inner pipe as the integrated structure and concluded that the safety of a rehabilitated pipe under strong seismic loading was confirmed. In addition, the pipe rehabilitation has added two issues to be resolved. One is a reduction of cross-sectional area of water flow due to construction or insert of inner pipes into outer pipes. Another is the dynamic behavior of joints of outer pipes. The mail purposes in this study are shown as followings.

- To verify an influence of a pipe thickness on a static and dynamic behavior of a pipe
- To verify an influence of a shear deformation of a backfill material on a rehabilitated pipe
- Formularization of a deflection of a rehabilitated pipe to shear deformation of a backfill material
- To verify an influence of a joint of an outer pipe on an inner pipe during earthquake

1.4 Overview of This Thesis

The thesis is organized into seven chapters. Chapter 1 provides a brief introduction, literature reviews with respect to Marston-Spangler theory and pipe rehabilitation, and the aim of this thesis.

In chapter 2 the model tests for several flexible pipes, which each pipe has a

different thickness and equivalent bending ring stiffness were conducted in a steel pit to discuss the influence of the thickness of pipe and ground stiffness behavior of pipes. In chapter 3, shaking table tests using these pipes were conducted in order to verify the influence of the thickness of pipe, a condition of test pit and bedding material on the dynamic behavior of pipes due to a shear deformation of a backfill material. In chapter 4, in order to verify the influence of a damage of the outer pipe on the dynamic behavior of the inner pipe, cyclic shear test using a lamina box was a conducted under a different damage of outer pipes and a different density of backfill material. In chapter 5, two dimensional discrete element method (DEM) analyses were conducted in order to verify the deformation mechanism of the inner pipe with and without the outer pipe during earthquake and formulate the oblique deflection of the inner pipe to shear strain of the backfill material. In chapter 6, shaking table tests were conducted to verify the dynamic behavior of the axial direction of the inner pipe used for the method. Finally, Chapter 7 describes the conclusions and perspectives of the present study.

References

Alireza, F., Ehsan D., Zilan, Z., Salvatore S., Amjad A. and Andre, F. (2014): Post-earthquake Evaluation of Pipelines Rehabilitated with Cured in Place Lining Technology Using Acousitic Emission, *Construction and Building Materials*, Vol.54, pp.326-338.

American Society for Testing Materials (2004): Annual Book of ASTM Standards, Vol.08.04, pp.1078-1084.

Anzaki, T. (2013) : Pipe rehabilitation method “Insituform method “, *Agricultural and Rural Development Information Center*, No.111, 32-37.

Colton, J.D., Cang, P.H.P. and Lindberg, H.E. (1982): Measurement of Dynamic Soil-pipe Axial Interaction for Full-scale Buried Pipeline, *Soil Dynamics and Earthquake Engineering*, Vol. 1, pp.183-188.

Cundall, P.A. and Strack, O.D.L. (1979): A Discrete Numerical Model for Granular

Assemblies, *Géotechnique*, 29, No.1. pp. 47-65.

Da Ha, Tarek H. Abdoun, Michael J. O'Rourke, Michael D. Symans, Thomas D. O'Rourke, Michael C. Palmer and Harry E. Stewart (2008): Buried High-density Polyethylene Pipelines Subjected to Normal and Strike-slip Faulting- A Centrifuge Investigation, *Canadian Geotechnical Journal*, Vol. 45, pp.1733-1742.

Falter, B. (1996): Structural analysis of sewer linings, *Trenchless Technol*, Vol.11, No.2, pp.27-41.

Fujita, N., Mohri, Y. and Suzuki, H. (2007): Performance of Flexible Joints Formed Underground Pipeline for Seismic Motion, *Trans. of JSIDRE*, No. 249, pp.63-73 (in Japanese with English Summary).

Fukumoto, Y., Sakaguchi, H. and Murakami, A. (2011): Failure Criteria for Geomaterials in Simple Discrete Element Modeling, *Trans. of JSIDRE*, A2, Vol. 67, pp.105-112 (in Japanese with English Summary).

Gumbel, J., Spasojevic, A., Robert, J.M. (2003): Centrifuge Modeling of Soil Load Transfer to Flexible Sewer Liners, New Pipeline Technologies, Security, and Safety, pp.352-362.

Hachiya, M., Tohda, J., Tokumasu, K., Takatsuka, Y. and Sano Y. (2005): A New Design Method for Buried Pipelines Subjected to Differential Ground Settlement, Journal of JSCE, JSCE, No. 799, pp.109-122 (in Japanese with English Summary).

Inoue, Y., Tohda, J., Yoshimura, H., Shirai, H., Ohsugi, A. (2005): Buckling behavior and design of sewer pipes cured with plastic inner liners, 50th Geotechnical Symposium, pp.271-278.

Inoue, Y., Yoshimura, H., Tohda, J. and Ohsugi, A. (2006): Response of Sewer Concrete Pipes Rehabilitated by CIPP through Full-Scale Model Tests, International Conference on Physical Modeling in Geotechnics, pp.735-740.

Japan Pipe Rehabilitation Quality Assurance Association (2007a): Classification of rehabilitation method, Design-approach introduction of pipe rehabilitation, No.1, pp. 22-25 (in Japanese).

Japan Pipe Rehabilitation Quality Assurance Association (2007b): ABCs of pipe rehabilitation method, Design-approach introduction of pipe rehabilitation, No.1,

pp. 32-34 (in Japanese).

Japan Sewage Works Association (2001): Guideline of Rehabilitated Pipe (Proposed), pp.11-40 (in Japanese).

Japan Sewage Works Association (2004): Fiberglass Reinforced Plastic Mortar Pipes for Sewerage (JSWAS K-16) (in Japanese).

Kawabata, T., Sawada, Y. and Mohri, Y. (2009): Large Scale Experiments on Lightweight Thrust Restraint for Buried Bend under Internal Pressure, Trans. JSIDRE, No.262, pp.111-117 (in Japanese with English Summary).

Kawabata, T., Sawada, Y. Mohri, Y. and Ling, H.I. (2011): Dynamic Behavior of Buried Bend with Trust Restraint in Liquefying Ground, Journal of JSCE, C, No.63, pp.399-406 (in Japanese with English Summary).

Kawabata, T., Sawada, Y. Mohri, Y. and Uchida, K. (2006): Verification of Effectiveness for Lightweight Thrust Restraint Method of Buried Bend and Mechanism of Lateral Resistance by Model Tests, Trans. JSIDRE, No.244, pp.179-185 (in Japanese with English Summary).

Kawabata, T., Uchida, K., Ariyoshi, M., Nakase, H., Mohri, Y. and Ling, H.I. (2003): D.E.M. Analysis on Behavior of Shallow Buried Pipe Subject to Traffic Loads, Proc. of the Int. Conf. of pipeline 2003, pp.1218-1227.

Kawabata,T., Ooishi, J., Nakase, H., Mohri, Y. and Uchida K. (2005): Mechanism of Uplifting for Buried Pipe Subjected to Cyclic Simple Shear, Trans. JSIDRE, No.239, pp.59-66 (in Japanese with English Summary).

Kitara, M. and Miyajima, M. (1983): Dynamic Behavior of a Model Pipe Fixed at One End during Liquefaction, Journal of JSCE, No. 336, pp.31-38 (in Japanese).

Ko, D.H. and Kuwano, R. (2010) : Model tests of buried double-layer pipe and design of flexible liner, Institute of Industrial Science, the University of Tokyo, Vol.62, No.4, 77-81.

Kobayashi, M., Ando, H. and Oguchi, N. (1998): Effects of Velocity and Cyclic Displacement of Subsoil on Its Axial Restraint Force Acting on Polyethylene Coated Steel Pipes during Earthquakes, Journal of JSCE, JSCE, No. 591, pp.299-312 (in Japanese with English Summary).

Law, T.C.M. and Moore, I.D. (2007): Numerical modeling of tight fitting flexible liner in damaged sewer under earth loads, Tunneling and Underground Space Technology 22, 655-665.

Marston, A. (1930) : The theory of external loads on closed conduits in the light of the latest experiments, Bulletin 96, Iowa Engineering Experiment Station.

Matsuoka H. and Yamamoto, S. (1994): A Microscopic study on Shear Mechanism of Granular Materials by DEM, Journal of JSCE, No.487, pp.167-175 (in Japanese with English Summary).

Meguro, K. and Hakuno, M. (1988) :Fracture Analysed of Concrete Structure by Granular Assembly Simulation, Buu. Earthq. Res. Inst. Univ. Tokyo, Vol.63, pp. 409-468 (in Japanese with English Summary).

Ministry of Agriculture, Forestry and Fisheries of Japan (2009) : Design standard for pipeline (in Japanese).

Ministry of Agriculture, Forestry and Fisheries of Japan (2010) (Reference in 2015.11.29): For the development of “Guidance of function conservation of irrigation and drainage facilities for open canal” ver. 2010 (in Japanese), available from http://www.maff.go.jp/j/council/seisaku/nousin/bukai/h22_1/pdf/data3-2.pdf

Ministry of Agriculture, Forestry and Fisheries of Japan (2012) (Reference in 2015.11.29): Maintenance conditions of agricultural production base ver. 2013, (in Japanese) available from http://www.maff.go.jp/j/council/seisaku/nousin/bukai/h24_4/pdf/ref-data4.pdf

Ministry of Land, Infrastructure, Transport, Tourism (2013) (Reference in 2015.11.29): Water Resources in JAPAN Ver. 2013 (in Japanese), available from http://www.mlit.go.jp/mizukokudo/mizsei/mizukokudo_mizsei_fr2_000004.html

Miyashita, T. and Kuwano, R. (2008) : Effects of backfill density and degree of deterioration on the deformation characteristics of double layer pipe under cyclic loading,Institute of Industrial Science, the University of Tokyo, Vol.60, No.3, 221-224 (in Japanese with English Summary).

Mohri, Y., Kawabata, T. and Fujita, N. (2000): Verification of Shallow Cover for Buried Pipeline Reinforced with Geogrids, Trans. JSIDRE, No.208, pp.127-135 (in

Japanese with English Summary).

Mohri, Y., Kawabata, T. and Ling, H.I. (1998): Experiments on Shallowly Buried Pipeline using Shaking Table, The 10th Earthquake Engineering Symposium Proc., pp.1913-1916 (in Japanese with English Summary).

Mori, H., and Ogawa, Y. (2007): Liquefaction Analysis of River Dike by Distinct Element Method, Trans. JSIDRE, No.249, pp. 9-16 (in Japanese with English Summary).

Murakami, T., Sakaguchi, H. and Murakami, A. (2004): Applicability of DEM Simulation for Soil Compaction, Trans. JSIDRE, No.229, pp.79-84 (in Japanese with English Summary).

Nakano, M., Si, J., Kawase, T. and Deguchi, T. (2002); Introduce of Separate Non-linear Analysis Method and Development of Design System in Reinforcement Design for Aging Sewerage Pipe, Proc. of the Japan Concrete Institute,Vol.24, pp.1561-1566 (in Japanese with English Summary).

Nakano, M., Si, J., Natsui, K. and Deguchi, T. (2003); Load Bearing Capacity Assessment on Rehabilitation of Aging Sewerage Pipe, Proc. of the Japan Concrete Institute, Vol.25, pp.1861-1866 (in Japanese).

Nakase, H., Miyata, M., Nagao, T., Honda, A., Kyouno, T., Yasuda, K. and Sugano, T. (2002) : Application of DEM to Deformation Analysis for Caisson Type Breakwater, Journal of Applied Mechanics, vol.5, pp. 461-472 (in Japanese).

Nasu, N. (1972): Shaking Test for Buried Pipe, Soil and Foundation, No. 167, pp.21-30 (in Japanese).

Ohara S. and Yamamoto, T. (1976) : On the Seismic Earth Pressure Acts on the Buried Pipe, Memoirs of the Faculty of Engineering, Yamaguchi University, Vol.27, pp.45-50 (in Japanese).

Oishi, H. and Sekiguchi, K. (1984): Consideration on Strain-Occurance Mechanism of Underground Pipelines during Earthquake, Journal of JSCE, No.350, pp. 227-267 (in Japanese with English Summary).

Ono, K., Sonoda, Y., Sawada, Y., Ling, H.I. and Kawabata, T. (2015): Centrifuge Modeling for Mechanical Behavior of Liners in Damaged Host Pipes, Transp.

Infrastruct. Geotech., 2, 139-154.

Sakaguchi H., Ozaki, E. and Igarashi, T. (1993) : Plugging of flow of granular materials during the discharge from a silo, Int. Journal of Modern Physics B, Vol. B7, pp. 1949-1963.

Sato, S., Ichii, K., Nishiyama, S., Ooshima, T., Inoue, Y., Sato, S., Ikeda, T., Araki, S., Hyoudo, T., Umeki, T. and Imai, S. (2003): Accuracy of up lift evaluation for buried pipe in liquefied ground by a FEM, The 48th Geotechnical Society symposium, pp.225-232 (in Japanese with English Summary).

Sawada, Y., Kawabata, T. and Mohri, Y. (2010): Design for Lightweight Thrust Restraint of Pipe Bend, Trans. JSIDRE, No.265, pp.33-40 (in Japanese with English Summary).

Sawada, Y., Sonoda, Y., Ono, K., Inoue, K., Mohri, Y., Ariyoshi, M. and Kawabata, T. (2014) : Influences of damage levels of outer aging pipes on mechanical behavior of rehabilitated pipes, Transactions of JSIDRE, No.291, 25-31 (in Japanese with English Summary).

Spangler, M.G. (1941) : The structural design of flexible pipe culverts, Bulletin 153, Iowa Engineering Experiment Station.

Spasojevic, A., Robert, J.M., Gumbel, J. (2007): Centrifuge modeling of the effects of soil loading on flexible sewer liners, Geotechnique 57, No.4, pp.331-341.

Suehiro, T., Nakase, H., Mohri, U., and Yasuda, S. (2003): Shaking Table Test to Underground Structures and Simulation Study on Mechanism of Uplifting Using Distinct Element Method, Journal of JSCE, Earthquake Engineering, No.27,0323, pp.1-8 (in Japanese with English Summary).

Takada, S. and Yamabe, Y. (1982): An Experiment on A Seismic Behavior of Buried Pipelines Subjected to Large Ground Deformations Using The Sinking-Soil-Box, Journal of JSCE, JSCE, No. 323, pp.55-65 (in Japanese).

Takahashi, Y., Li, L., Deguchi, T., Yamada, K. (2002): A study on the bedding effects of the deteriorated existing pipe on the flexible rehabilitated pipe and its mechanism, Journal of Japan Sewage Works Association Research journal, No471, pp.103-113 (in Japanese with English Summary).

Tanaka, Y., Arimura, T. and Jibu M. (2005): Behavior of Buried Pipe with Flexible Joint in Liquefied Ground, Report of Research Center for Urban Safety and Security, Research Center for Urban Safety and Security Kobe University, No. 8, pp.63-71 (in Japanese with English Summary).

Tohda, J., Nakamura, Y., Inoue, Y., Yoshimura, H., Ko, H.Y. and Ohsugi, A. (2006): Dynamic Response of Sewer Concrete Pipes Rehabilitated by CIPP through Centrifuge Model Tests, International Conference on Physical Modeling in Geotechnics, pp.759-764.

Yoshimura, H., Tohda, J., Inoue, Y. and Ohsugi, A. (2006): Response of Sewer Concrete Pipes Rehabilitated by CIPP through Two-Edge Loading Tests, International Conference on Physical Modeling in Geotechnics, pp.1587-1592.

Yuasa, A., Kawakami. T. and Yaoita, A. (2000): Fundamental Study on Floatation of Underground Structure during Earthquake, Trans. JSIDRE, No.208, pp.91-97 (in Japanese with English Summary).

CHAPTER 2

The contents of this chapter are based on:

Kawbata, T., Nadamoto, Y., Izumi, A., Shimamoto, C., Shoda, D., Inoue, K., Mohri, Y., Ariyoshi, M., Hinobayashi, J., Tokiyoshi, M.. and Uchida K.: Effect of pipe thickness on the behavior of flexible pipes with equivalent bending ring stiffness, *Proceedings of 19th Int. Offshore and Polar Engineering Conf.,* ISOPE, pp.404-408 (2009)

Izumi, A., Sawada, Y. and Hinobayashi, J., Mohri, Y., Ariyoshi, M. and Kawabata, T.: Characteristic Mechanical Behavior for Flexible Pipes Having Different Thickness and Equivalent Bending Ring Stiffness, *Trans. JSIDRE,* JSIDRE, No. 292, pp.231-239 (2015) (in Japanese with English Summary)

Chapter 2

Mechanical Behavior for Flexible Pipe Having Different Thickness and Equivalent Bending Ring Stiffness

2.1 Introduction

The pipe rehabilitation has a demerit that a cross sectional area of water flow of an inner pipe is smaller than that of an existing outer pipe due to construction or insert of inner pipes into outer pipes although this method has a great merit that is trenchless repair work. To control the reduction rate at the cross sectional area of water flow, thinning of pipe thickness is desirable.

Design standard (MAFF, 2009) for pipeline in Japan is based on Marston-Spangler theory (Marston, 1930 and Spangler, 1941). Structural calculation of flexible pipeline is based on bending ring stiffness $E_p I/D_c^3$, where E_p is the elastic modulus, I is the moment of inertia of area ($I = t_p^3 / 12$, t_p is the thickness of a pipe), D_c is the center diameter of a pipe. Bending ring stiffness is defined from the following formula that indicates relationships vertical deflection of flexible pipe and linear load.

$$P = \frac{E_p I S}{0.149\left(D_c / 2\right)^3} \tag{2.1}$$

where P is the linear load, S is the vertical deflection. Depending on the formula, behavior of buried flexible pipes having different thickness and equivalent bending ring stiffness

are identical in theory. However, it is reported that a pipeline which met the design standard buckled (Tomita et al., 1999). Kawabata et al. (2008) conducted field buried test for a pipeline having a diameter of 3,000 mm and a thickness of 26~28 mm. As the results, it was revealed that the behavior of the buried pipe was different from the behavior on the basis of Marston-Spangler theory. Tohda and Yoshimura (1999) also indicated that earth pressure on buried pipes and deflection of buried pipes and verified the relationships vertical deflection ratio of flexible pipe and maximum of bending moment from the result of FEM analyses.

In this chapter, the model tests for several flexible pipes, which have a different thickness and equivalent bending ring stiffness, were conducted in a steel pit to discuss the influence of the thickness of pipe and ground stiffness behavior of pipes.

2.2 Outline of Shaking Table Test

2.2.1 Test Equipment

The test pit was made of steel and has a length of 1830 mm, a width of 1000 mm and a depth of 1230 mm as shown in **Figure 2.1**. Both side walls of the test pit had a hole with a diameter 300 mm from the bottom of the test pit of 600 mm in height to install measurement instruments. Two vinyl sheets which were applied silicon oil between two sheets were set inside.

2.2.2 Model Pipe

A steel pipe, a polyvinyl chloride pipe (abbr. as PVC) pipe, a high density polyethylene (abbr. as HDPE) pipe, a thin steel pipe and a low density polyethylene (abbr. as LDPE) were used. The steel pipe, the PVC pipe and the HDPE pipe had an equivalent bending ring stiffness. The thin steel pipe and the LDPE pipe had an equivalent bending stiffness. The bending ring stiffness of those three pipes was one-tenth of that of these two pipes. **Table 2.1** shows properties of pipes. Tests using the steel pipe, the PVC pipe and the HDPE pipe grouped under Case-A. Tests using the shin steel pipe and the LDPE

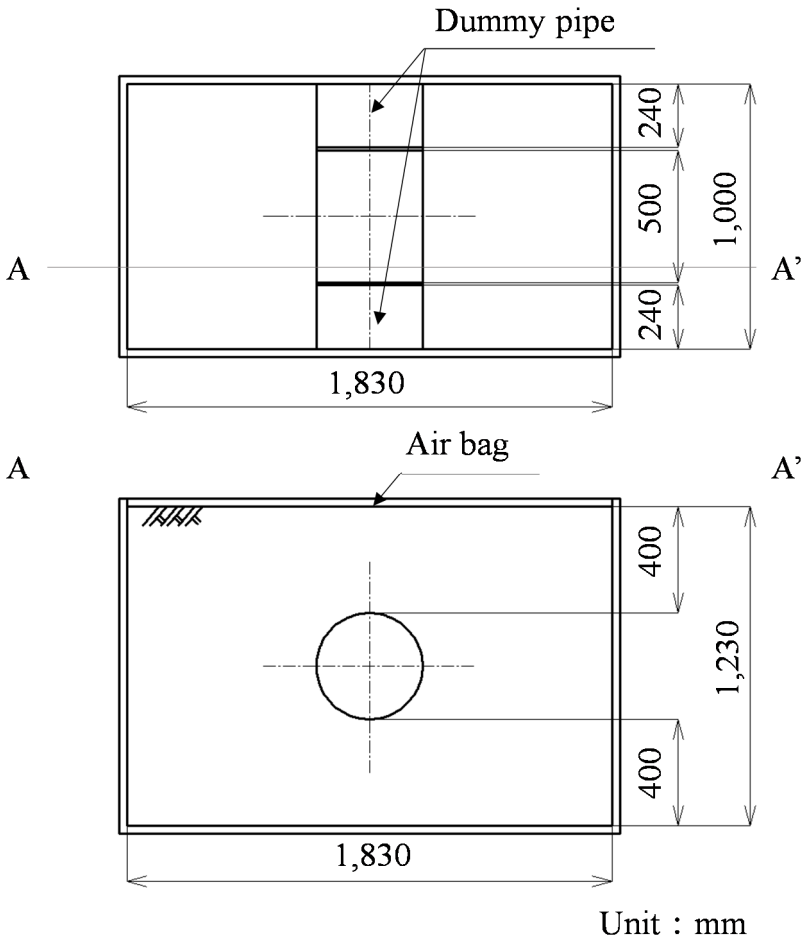

Figure 2.1 Schematic layouts of experiment

Table 2.1 Properties of pipes

Type of pipe	Thickness t_p (mm)	Center diameter D_c (mm)	Elastic modulus E_p (N/mm^2)	Ring Bending stiffness E_pI/D_c^3 (kN/m^2)
Steel	2.49	402.00	223,067	4.4
PVC	9.12	406.69	3,470	3.3
HDPE	14.26	422.79	1,223	3.9
Thin steel pipe	1.12	400.38	211,151	0.4
LDPE	11.68	408.63	275	0.5

pipe grouped under Case-B.

2.2.3 Model Ground

Silica sand was used as a soil material for the model ground. **Table 2.2** shows the

properties of silica sand. **Figure 2.2** shows a grain size accumulation curve for silica sand. The pit was backfilled with silica sand in two different relative densities of 95 % (dense ground) or 25 % (loose ground) from the bottom of the pipe to the ground surface. A bedding of 400 mm height was dense ground. In addition, as shown in **Figure 2.3**, concrete blocks were set in the area of from the bottom of the pipe to a height of half the pipe diameter. **Table 2.3** shows the mix design of concrete. Unconfined compression strength of 28 days curing the concrete was 17.97 N/mm^2.

Table 2.2 Properties of silica sand

Density of soil particles	ρ_s	2.59 g/cm^3
Minimum dry density	ρ_{dmin}	1.236 g/cm^3
Maximum dry density	ρ_{dmax}	1.566 g/cm^3
Mean particle size	D_{50}	0.19
Angle of internal friction	ϕ	39.76 deg.

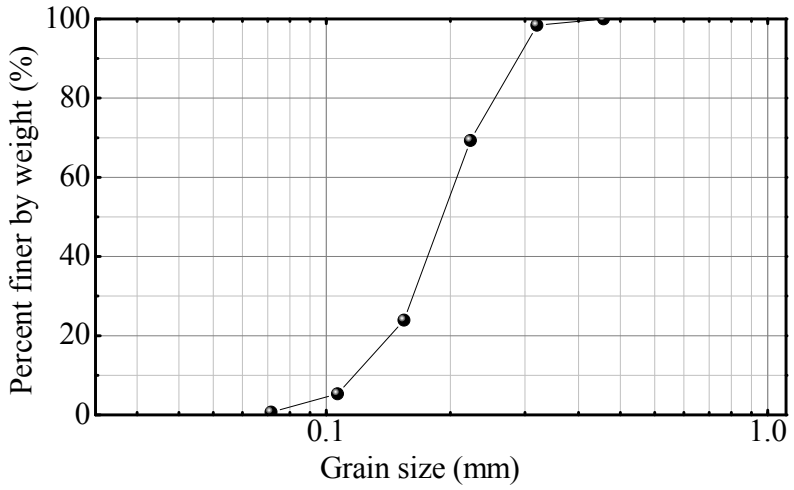

Figure 2.2 Grain size accumulation curve for silica sand

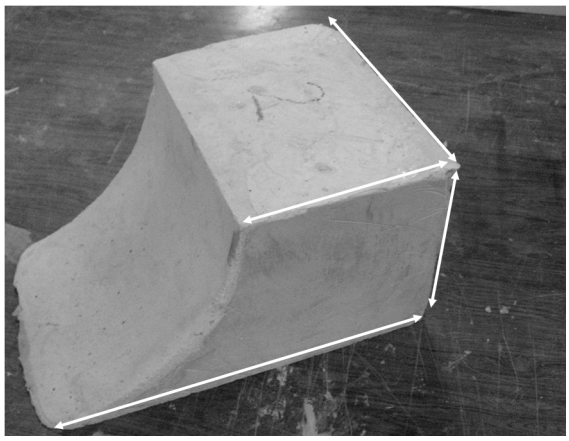

Figure 2.3 Concrete block

Table 2.3 Mix design of concrete

High early strength	20 kg
Gravel	4.4 kg
water	3.5 l

2.2.4 Procedure of Model Test and Test Condition

After backfilling, vertical pressure on the surface of the ground is given with an air bag up to 120 kPa in increments of 10 kPa. The model pipe and dummy pipes were buried under an overburden depth of 400 mm. Dummy pipes were set at both end of model pipes. Vertical pressure of 120 kPa corresponded about an overburden depth of 11m. **Table 2.4** shows test conditions.

2.2.5 Measurements

Strain of pipes, horizontal and vertical deflections of pipes and vertical pressure were measured. In steel pipe, PVC pipe and HDPE pipe, 120 strain gauges were attached circumferentially to the inner and outer surfaces of each pipe at intervals of 6 degrees. In thin steel pipe and LDPE pipe, 240 strain gauges were attached circumferentially to the inner and outer surfaces of each pipe at intervals of 3 degrees. Horizontal and Vertical deflections of pipes was measured by rotating a displacement transducer as shown in **Figure 2.4**. Vertical loading pressure by the air bag was measured by a pressure transducer.

Table 2.4 Test condition

	Type of pipe	Backfill material condition
Case-A-ST-D	steel	dense ground
Case-A-ST-L	steel	loose ground
Case-A-PE-D	PVC	dense ground
Case-A-PE-L	PVC	loose ground
Case-A-PVC-D	HDPE	dense ground
Case-A-PVC-L	HDPE	loose ground
Case-B-ST-D	thin steel	dense ground
Case-B-ST-L	thin steel	loose ground
Case-B-ST-C	thin steel	loose ground and concrete block
Case-B-PE-D	LDPE	dense ground
Case-B-PE-L	LDPE	loose ground
Case-B-PE-C	LDPE	loose ground and concrete block

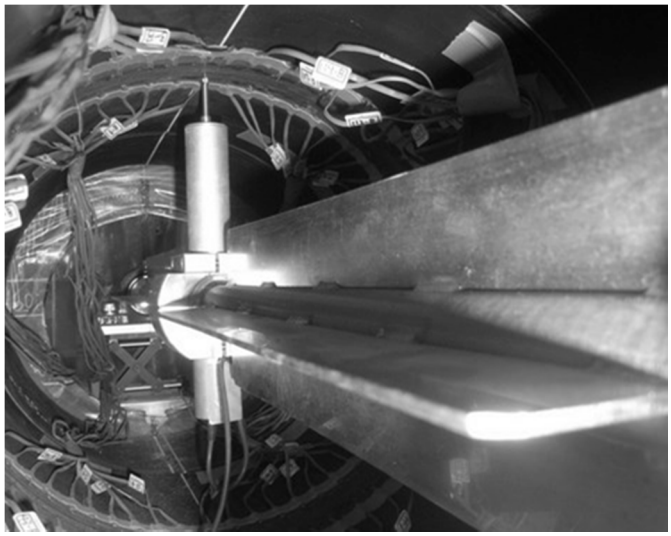

Figure 2.4 Displacement transducer

2.3 Relationships between Test Process and Deflection

In design standard (MAFF, 2009) for a pipeline in Japan, a securement of an area water cross of a pipeline and of a water tightness of joints of a pipeline were judged by a ratio of a deflection of a pipe. The ratio of deflection is calculated by dividing a deflection of a pipe into a center diameter of a pipe.

Figure 2.5(a) also shows relationships between the test process and ratio of

horizontal and vertical deflections of model pipes in Case-A. **Figure 2.5(b)** shows these relationships in Case-B. **Table 2.5** shows horizontal and vertical ratios of the deflection of pipes at the load of 120 kPa. When a pipe was deformed rectangularly, a change of a distance between a top of a pipe and a bottom of a pipe is a negative vertical deflection and a change of a distance between of sides of a pipe is a positive horizontal deflection of a pipe.

An influence of thickness of a pipe on horizontal and vertical deflection of a flexible pipe having an equivalent bending ring stiffness was small inspire of a density of a backfill material and .of a value of a bending ring stiffness. From **Figure 2.5(a)**, it was found that each pipe in Case-A was deformed longitudinally when the backfill material was filled from the bottom of the pipe to the top of the pipe in the case of dense ground. This result was similar to the result for the field test for a buried flexible pipe having a diameter of 1,500 mm in which Kawabata et al. (1993) conducted. The results were caused by a lateral pressure acting at the side of the pipe due to a compaction of the backfill material. According to an increment of vertical pressure due to the increment of the depth from the top of the pipe to the ground surface and vertical load by the air bag, the vertical deflection of each pipe was small. The ratio of the horizontal and the vertical defection of pipes were -0.3~0.0 % and 0.1~0.2 % respectively at vertical load of 120 kPa as shown in **Table 2.5**. The results indicated the longitudinal deformation of the pipe remained when the backfill material was density.

On the other hand, the ratio of the horizontal and vertical deflection of pipes in Case-A were approximately zero in the case of loose ground because of no compaction when pipes were buried from the bottom of pipes to the top of pipes as shown in **Figure 2.5(a)**.

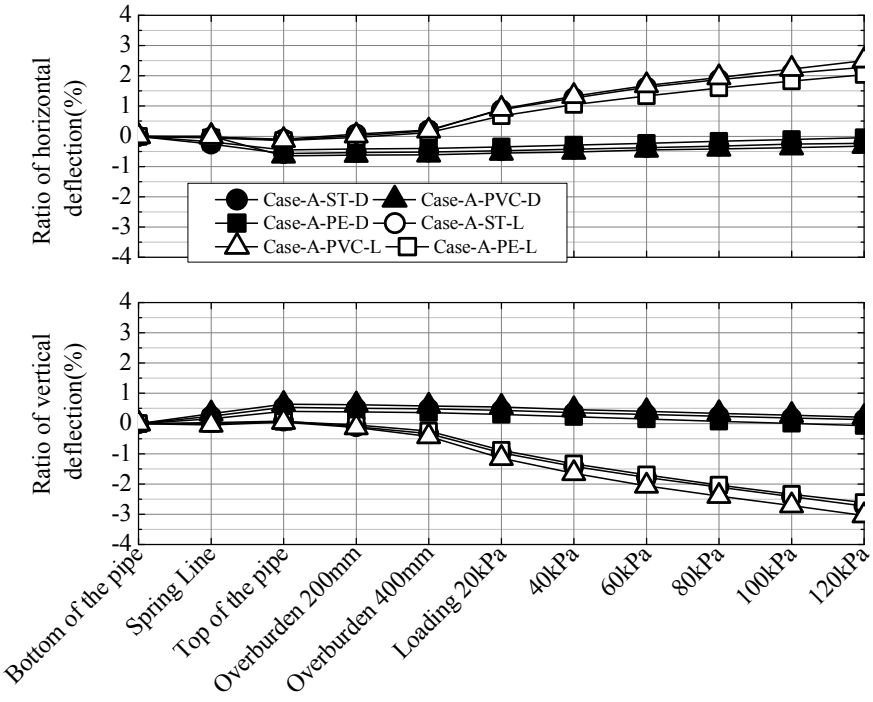

(a) Case-A

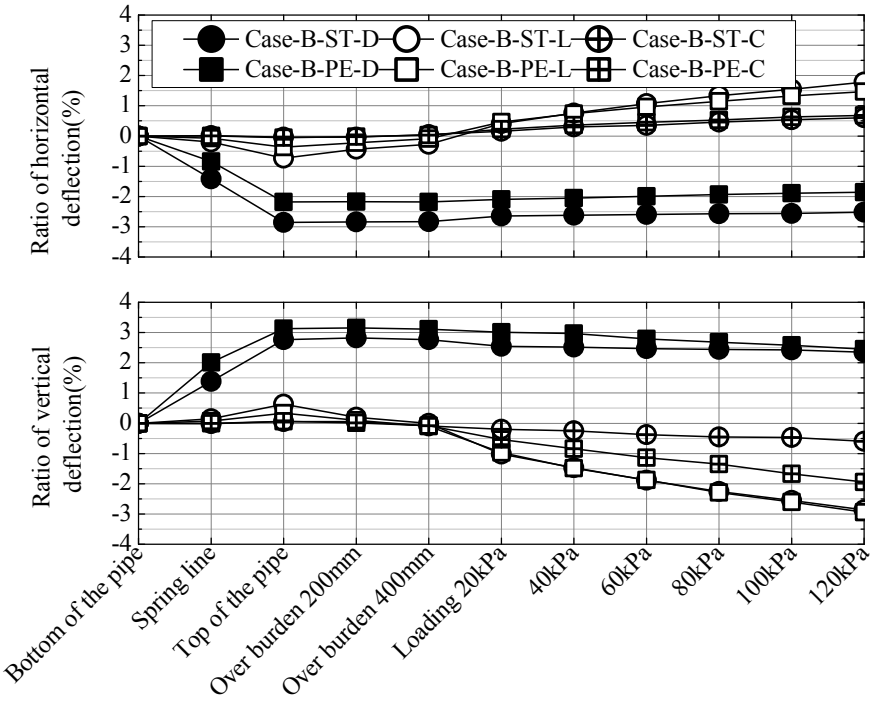

(b) Case-B

Figure 2.5 Relationships between test process and ratio of horizontal and vertical deflection of pipe

Table 2.5 Ratios of horizontal and vertical deflection at load of 120 kPa

	Case-A-ST-D	Case-A-PVC-D	Case-A-PE-D
Ratio of horizontal deflection	-0.2 %	-0.3 %	0.0 %
Ratio of vertical deflection	0.1 %	0.2 %	0.1 %
	Case-A-ST-L	Case-A-PVC-L	Case-A-PE-L
Ratio of horizontal deflection	2.3 %	2.5 %	2.0 %
Ratio of vertical deflection	-2.7 %	3.0 %	-2.6 %
	Case-B-ST-D	Case-B-PE-D	Case-B-ST-L
Ratio of horizontal deflection	-2.5 %	-1.9 %	1.8 %
Ratio of vertical deflection	2.4 %	2.5 %	-2.9 %
	Case-B-PE-L	Case-B-ST-C	Case-C-PE-C
Ratio of horizontal deflection	1.5 %	0.6 %	0.7 %
Ratio of vertical deflection	-2.9 %	-0.6 %	-1.9 %

The ratio of the horizontal deflection of pipes increased and the ratio of the vertical deflection decreased from the backfilling of the top of pipes at the load of 120 kPa. The ratio of the horizontal and the vertical defection of pipes were 2.0~2.5 % and -3.0~ -2.6 % respectively at the vertical load of 120 kPa as shown in **Table 2.5**. The result was caused by low confining pressure of loose ground in comparison with it of dense ground.

As shown in **Figure 2.5(b)**, for dense and loose ground, the tendency of the horizontal and vertical deflection to the process of backfilling and vertical load by the air bag in Case-B were similar to that in Case-A. Compared to the ratio of the horizontal and vertical deflection of the pipe in Case-A, that in Case-B was large as shown in **Table 2.5** since the bending ring stiffness of pipes in Case-B were one- tenth of that in Case-A.

When the concrete block was set from the bottom of the pipe to the spring line, the deformation of the pipe was restricted. Ratios of horizontal and vertical deflection of the pipe in Case-B-ST-C and Case-B-PE-C were approximately zero in the process of the filling as shown in **Figure 2.5(b)**. Absolutes of the ratio of the horizontal and vertical deflection of the pipe in Case-B-ST-C and Case-B-PE-C became smaller in comparison with those of in Case-B-ST-L and Case-B-PE-L. At the load of 120 kPa, the ratios of the vertical deflection of the pipe in Case-B-ST-C and Case-B-PE-C were -0.6 and -1.9 % respectively. This difference was caused by the shape of concrete block. The concrete formwork was made using the thin steel pipe. The concrete block was not fitted completely to the LDPE pipe since outer diameter of the LDPE pipe was larger than that of the thin steel pipe.

2.4 Influence of Pipe Thickness on Bending Strain

The distribution of the bending strain in each case shows **Figure 2.6** and **Figure 2.7** respectively. The bending strain is calculated by the following equation.

$$\varepsilon_b = \frac{\varepsilon_{out} - \varepsilon_{in}}{2} \tag{2.2}$$

where ε_b is the bending strain, ε_{out} is the outer circumferential strain on a pipe and ε_{in} is the inner circumferential strain on a pipe. A tensile outer circumferential strain is positive. For the setting of the concrete block, strain gauges were not attached from the bottom of the pipe to the spring line. In Case-A, the scales of the PVC and HDPE pipe are calibrated on the basis of thickness of the steel pipe, since the bending strain is proportional to a thickness of a pipe. In Case-B, the scale of the LDPE pipe was calibrated on the basis of thickness of the thin steel pipe.

The shape of the distribution of the bending strain in steel pipe in Case-A was similar to other pipes in spite of the density of the backfill material. For the dense ground, the tensile strain increased at the bottom and top of each pipe and the compressive strain increased at the side of each pipe due to compaction of the backfill material when the backfill material was filled from the bottom of the pipe to the top of the pipe in the case of dense ground as shown in **Figure 2.6(a)**, **(c)** and **(e)**. It was found that each pipe in Case-A was deformed longitudinally as well as the result of the deflection of each pipe. The stress concentration occurred at the bottom and top of each pipe since the bending strain on the bottom and top of each pipe decreased at the load of 120 kPa. As shown in **Figure 2.6(b)**, **(d)** and **(f)**, the strain of each pipes was not generated at the process of the filling for the loose ground. This was corresponding to the result as shown in **Figure 2.4**. At the load of 120 kPa, the compressive strain on the bottom and top of each pipes increased and the tensile strain on 30 and 150 degrees of each pipes increased due to the vertical load. As shown in **Figure 2.7(a)**, **(b)**, **(c)** and **(d)**, the similar shape of the distribution of the bending strain in each pipe in Case-B was found for the dense and loose ground as well as the shape in Case-A.

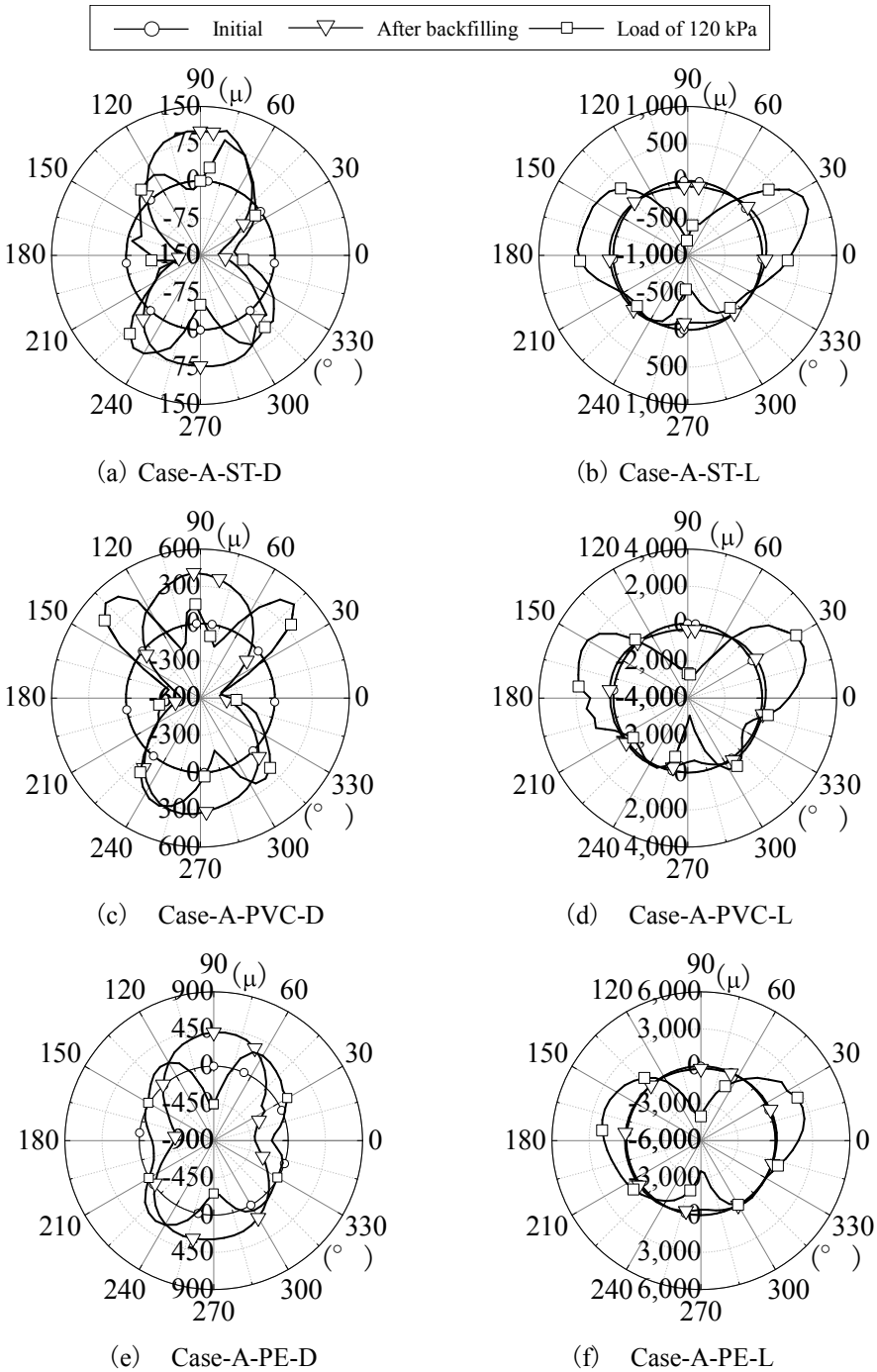

Figure 2.6 Bending strain distributions in Case-A

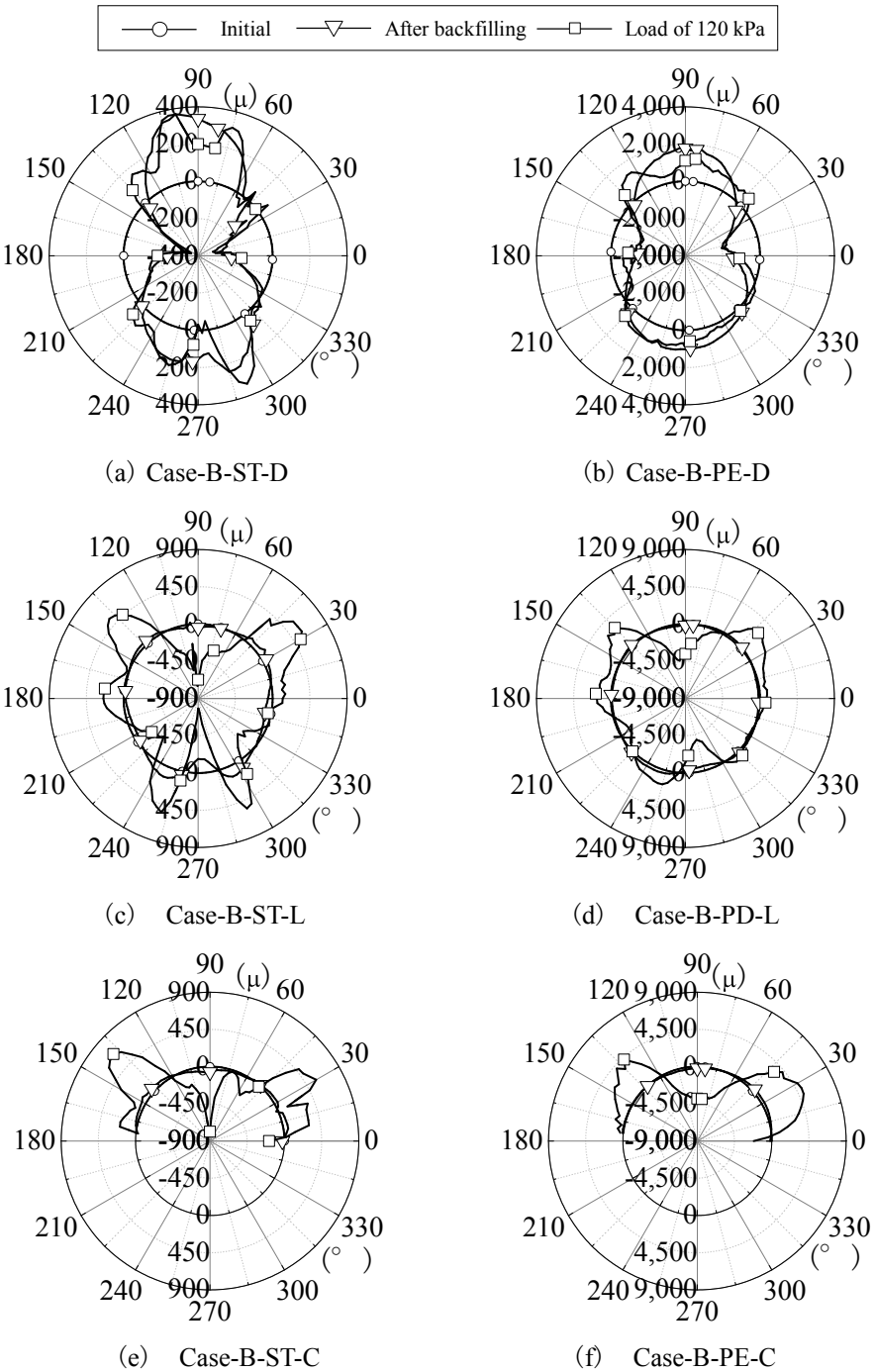

Figure 2.7 Bending strain distributions in Case-B

It was found that the boundary between the concrete block and the backfill material was influenced of the deformation of buried flexible pipes as shown in **Figure 2.7(c)**, **(d)**, **(e)** and **(f)**. The distribution of the bending strain from the spring line of the pipe to top of the pipe for the loose ground with using concrete block was similar to that for the loose ground only. However, it was assumed that the compressive strain was generated at the boundary between the loose ground and the concrete block for the load of 120 kPa.

2.5 Influence of Pipe Thickness on Axial Stress

The axial stress distribution in Case A and Case B shows **Figure 2.8** and **Figure 2.9**, respectively. The axial stress is calculated by the following equation.

$$\sigma_r = \varepsilon_r \times E_p \tag{2.3}$$

$$\varepsilon_r = \frac{\varepsilon_{out} + \varepsilon_{in}}{2} \tag{2.4}$$

where σ_r is the axial stress (MN/m^2), ε_r is the axial strain. A tensile stress is positive.

The compressive stress depended on the thickness as shown in **Figure 2.8**. The axial stress of pipes to the process of the backfilling for dense ground was not generated as shown in **Figure 2.8(a)**, **(c)** and **(e)** although the deflection and the bending strain of pipes to the process increased due to the ground compaction. The compressive stress was generated at the vertical load of 120 kPa and the maximum compressive stress in Case-A-ST-D, Case-A-PVE-D and CASE-A-PE-D was 5.3, 1.4 and 0.39 MN/m^2 respectively. For loose ground, the maximum compressive stress in Case-A-ST-L, Case-A-PVC-L and Case-A-PE-L was 8.2, 2.5 and 0.95 MN/m^2, respectively as shown in **Figure 2.8(b)**, **(d)** and **(f)**. In comparison with the axial stress distribution of the steel pipe for dense ground, that of the thin steel pipe for loose ground was non-uniform. The result indicated that a stress concentration on the pipe occurred since the difference between the ring bending stiffness and the ground stiffness for loose ground was larger than that for dense ground.

For Case-B that the ring bending stiffness was one tenth of that in Case-A, the compressive stress depended on the thickness as shown in **Figure 2.9** as well as the result

in Case-A. The axial stress of the thin steel pipe and LDPE pipe was not generated the process of the backfilling for dense and loose ground. The absolute maximum stress in Case-B-ST-D and Case-B-ST-L was 23.0 and 51.3 MN/m^2 respectively. The axial stress distribution of the thin steel pipe at the load of 120 kPa in spite of the density of the ground was more non-uniform than that of the HDPE pipe. In addition, the axial strain in Case-B-ST-C also distributed non-uniformly from the spring line to the pipe top when the concrete block was set as the base material.

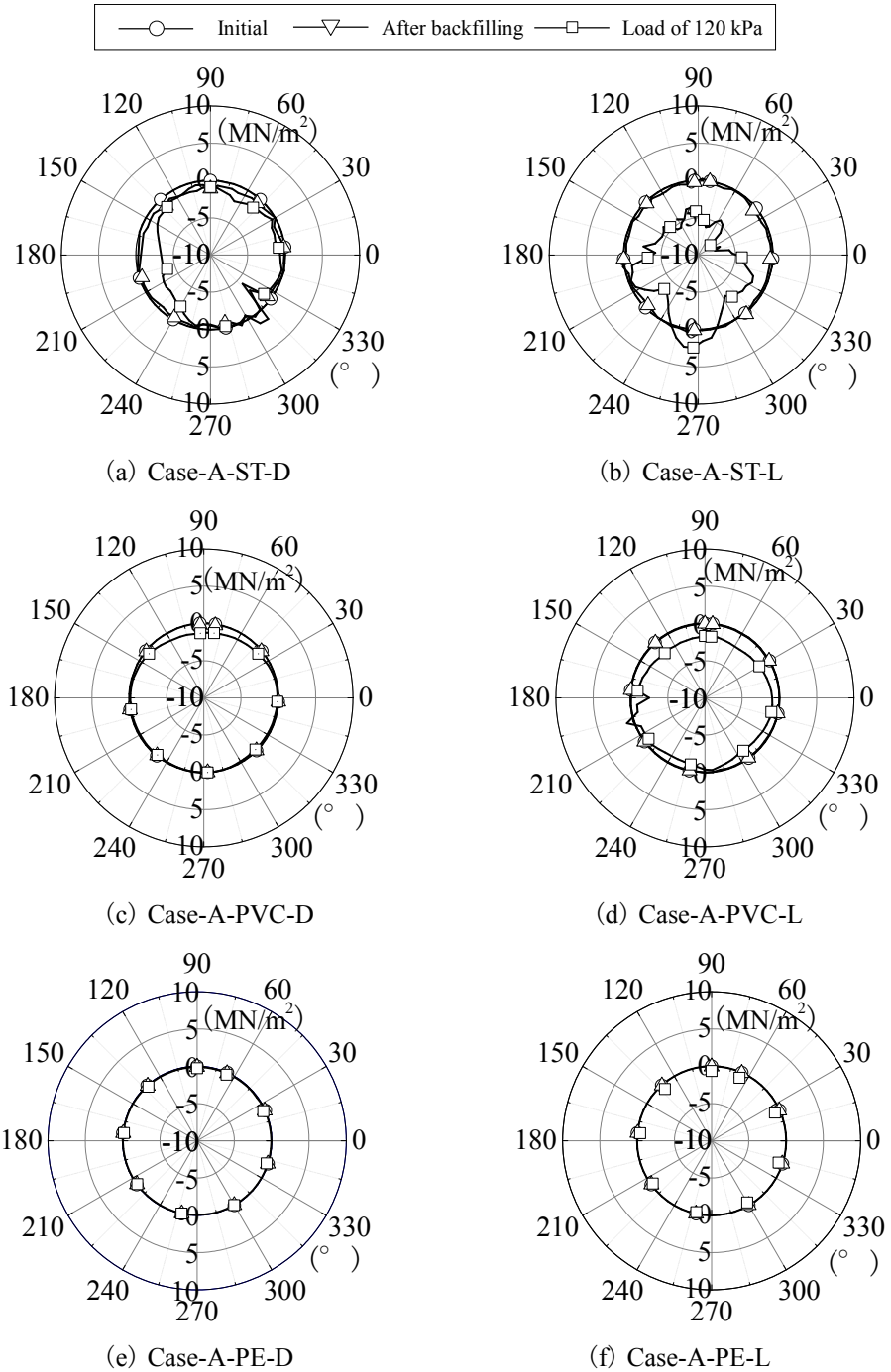

(a) Case-A-ST-D (b) Case-A-ST-L

(c) Case-A-PVC-D (d) Case-A-PVC-L

(e) Case-A-PE-D (f) Case-A-PE-L

Figure 2.8 Axial stress distributions in Case-A

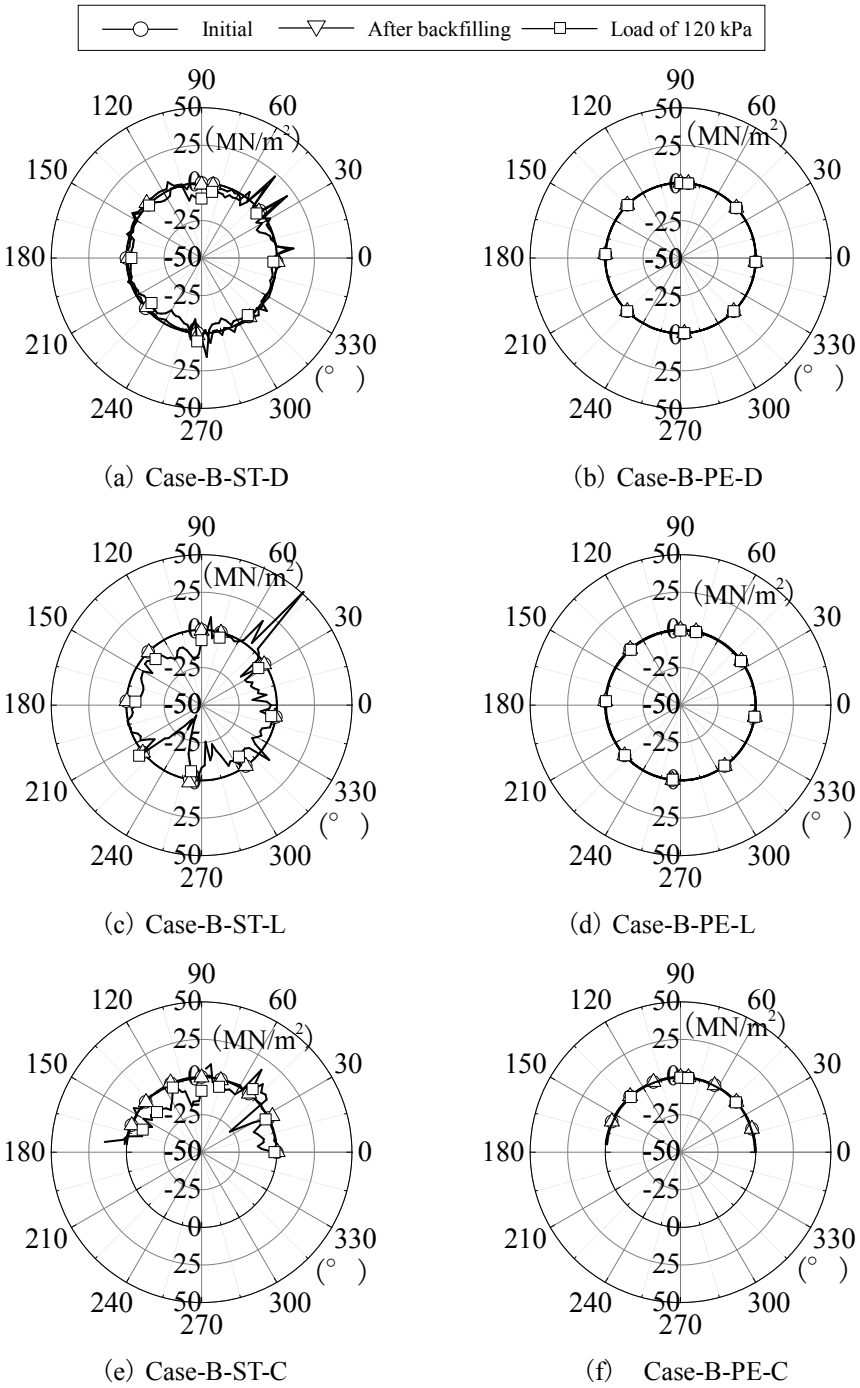

(a) Case-B-ST-D (b) Case-B-PE-D

(c) Case-B-ST-L (d) Case-B-PE-L

(e) Case-B-ST-C (f) Case-B-PE-C

Figure 2.9 Axial stress distributions in Case-B

In order to verify the influence of the thickness of pipes in Case-B for loose ground on the absolute maximum stress, **Figure 2.10** shows the relationships between $\sigma_L D_{out} L$ (σ_L : the vertical load (kN/m^2), D_{out} : the outer diameter of a pipe (m) and L : the length of a pipe (m)) and $\sigma_m tL$ (σ_m : the absolute maximum axial stress (kN/m^2). A broken line indicates linear approximation line of relationships. The absolute maximum axial stress increased according to the increment of the loading pressure. In design standard (MAFF, 2009) for pipeline in Japan, an allowable stress of type of a pipes is determined by dividing a tensile strength by a safety factor. The allowable stress of a steel pipe, STW290 is 123 N/mm^2 and that of PE pipe is 6.2 N/mm^2. The value of $\sigma_m tL$ converted from these allowable stress shows a solid line in **Figure 2.10**. It was found that the thin steel pipe reached the allowable stress earlier than the LDPE pipe since the slope of approximation line of the thin steel pipe was 7.9 times to that of the LDPE pipe. The result indicated that the relationship between the axial stress and the vertical pressure depended on the thickness of the pipe.

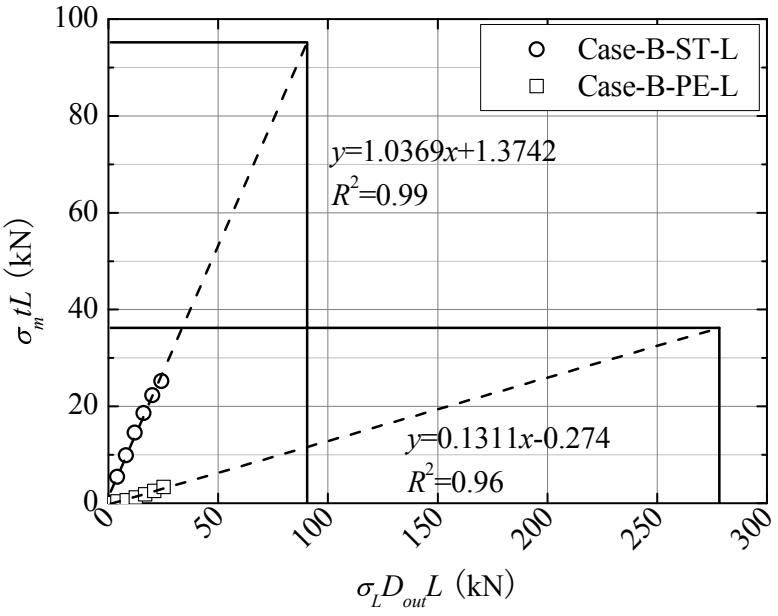

Figure 2.10 Relationships between $\sigma_L D_{out} L$ and $\sigma_m tL$ in Case-B

The non-uniformity of the axial stress distribution in Case-B was evaluated with a change rate of axial stress to the distance between a strain gauge and an adjacent strain gauge. The change rate, α is defined as the following equation.

$$\alpha = \frac{\sigma_{rn+1} - \sigma_{rn}}{\pi D_{out} / i} \tag{2.5}$$

where σ_{rn+1} is the axial stress at a measurement point n+1, σ_{rn} is the axial stress at a measurement point n and *i* is 120 (a number of strain gauge which was attached to the outer surface of pipes. **Figure 2.11** shows relationships between each measurement point and α at the load of 120 kPa. A spring line of pipes is zero degrees and a top of pipes is 90 degrees. α in Case-B-ST-D was large at 45 and 270 degrees and the absolute maximum change rate was 2,358. α in Case-B-ST-L varied widely and the absolute maximum α was 4,623. Since the deflection rate of the pipe in the loose ground was larger than that in the dense as shown in **Figure 2.5(b)**, the change rate depended on the deflection of the pipe. The change rate in Case-B-PE-D was extremely small. The absolute maximum α in Case-B-PE-D and Case-B-PE-L were 7.4 and 68, respectively. These results indicated that the dispersion of the axial stress was large according to the density of the backfill material.

The part of the sudden change of α was corresponding to a result of a previous study and a report of an accident during earthquake. α was suddenly changed at the inclined direction as shown in **Figure 2.11**. Tanaka and Mohri (1985) and Tanaka et al (2000) indicated that the fracture region at 45 degrees from the top of the pipe was generated from the result of the vertical loading test for the buried flexible pipe and that a shear strain of an underground dominated at 45 degrees from the top when an arched underground structure was buckled. Yoshida (1999) reported that cracks was generated at 45 degrees from the top of the shield tunnel during the Great Hanshin-Awaji Earthquake.

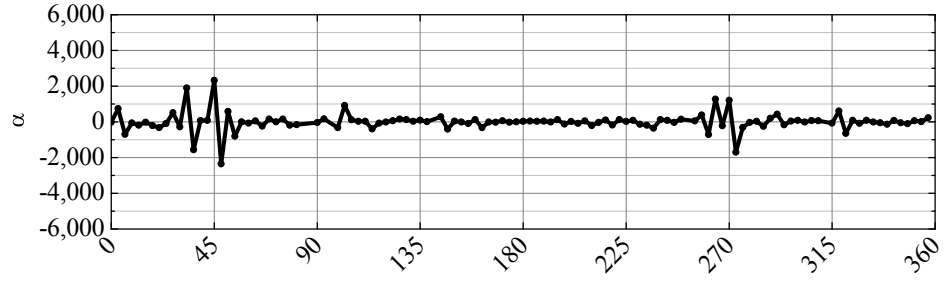

(a) Case-B-ST-D

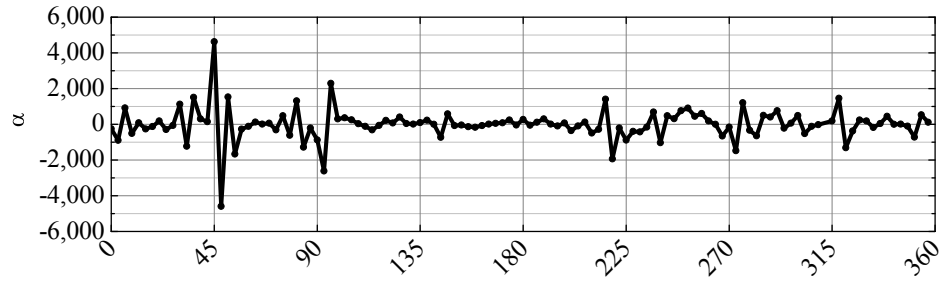

(b) Case-B-ST-L

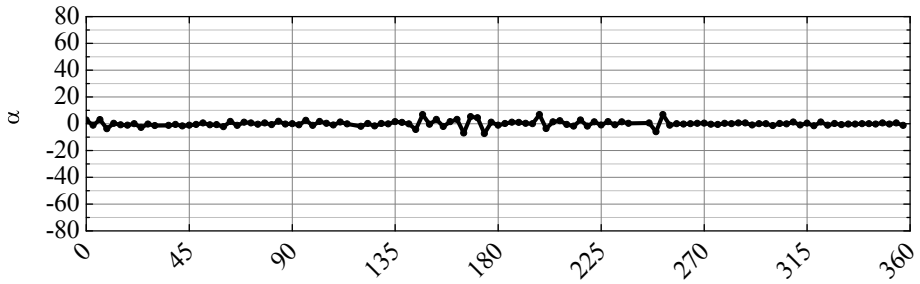

(c) Case-B-PE-D

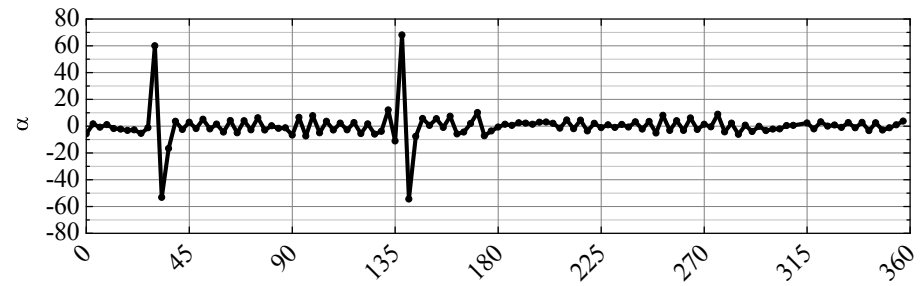

(d) Case-B-PE-L

Figure 2.11 Relationships between each measurement point and α at the load of 120 kPa.

2.6 Conclusions

In this chapter, the model tests for several flexible pipes, which have different thicknesses and equivalent bending ring stiffness were conducted in a steel pit to discuss the influence of the thickness of pipe and ground stiffness behavior of pipes. From the result of the model test, the following conclusions were obtained.

1. For flexible pipes having different thickness and equivalent bending ring stiffness, the influence of the thickness of the pipe on the deflection and the bending strain distribution of the pipe was extremely small.
2. For the dense ground, flexible pipes were deformed longitudinally due to the compaction of the ground. The compressive strain of the side of the pipe increased at the process of backfilling. The compressive strain of the bottom and top of the pipe increased due to the vertical pressure.
3. For the loose ground, the pipe was not deformed at the process of the backfilling. The deformation of the pipe depended on the increment of the vertical pressure.
4. The boundary between the concrete block and the backfill material was influenced of the deformation of buried flexible pipes.
5. The axial stress of the pipe which was generated due to the vertical pressure increased according to the decrease of the pipe thickness.
6. The more non-uniformity the axial stress distribution of the pipe was and the larger the axial stress was, the smaller the thickness of the pipe. In addition, the thin steel pipe reached the allowable stress earlier than the LDPE.
7. The non-uniformity of the axial stress distribution was evaluated with the change rate of axial stress to the distance between a strain gauge and an adjacent strain gauge.

References

Kawabata, T., Mohri, Y. and Kondo T. (1993): Behavior of Buried Large Thin Wall

Flexible Pipe – Field Test and Numerical Analysis Considered with Stage of construction of Buried Flexible Pipe -, *Trans. of JSIDRE*, No.167, pp.19-27 (in Japanese with English Summary).

Kawabata, T., Mohri, Y., Oda, T., Shoda, D., Ariyoshi, M. and Nakashima, H. (2008) : Field Measurement and Numerical Analysis for Buried Large Diameter Steel Pipes, *Proc. of the Int. Conf. of pipeline 2008*, Planning, Design and Construction, A1, pp.1-10.

Marston, A. (1930): The theory of external loads on closed conduits in the light of the latest experiments, Bulletin 96, IOWA Engineering Experiment Station, pp.1-37.

Ministry of Agriculture, Forestry and Fisheries of Japan (2009): Design standard for pipeline, pp.264-307 (in Japanese).

Spangler, M.G. (1941): The structural design of flexible pipe culverts, Bulletin 153, IOWA Engineering Experiment Station, pp.1-85.

Tanaka, T. and Mohri, Y. (1985): Movements of Buried Flexible Pipe – Non-linear Elasto-plastic Analyses and Experiments, Considering the Built-up Steps, *Trans. of JSIDRE*, No.118, pp.9-16 (in Japanese).

Tanaka, T., Nakamura, Y. and Kikuchi, M. (2000): Ground Collapse with Buckling of Arch Type Underground Structures, *Trans. of JSIDRE*, No.206, pp.29-37(in Japanese with English Summary).

Tohda, J. and Yoshimura, H. (2000): Proposal of a Rational Design Method for Buried Flexible Pipes, *Journal of JSCE*, No.617, pp.49-63 (in Japanese with English Summary).

Tomita, K., Ota H. and Nakano J. (1999): Accidents happened in such a way, Nikkei Construction, Nikkei BP, Inc. No.245, pp.50-53(in Japanese).

The Japanese Society of Irrigation, Drainage and Rural Engineering (2000): (in Japanese)

Yoshida, N. (1999): Underground and buried structures, Earthquake Geotechnical Engineering, BALKEMA, 987-992.

CHAPTER 3

The contents of this chapter are based on:

Izumi, A., Hinobayashi, J. Mohri Y., Ariyoshi, M. and Kawabata, T. : Characteristic Dynamic Behavior for Flexible Pipes Having Different Thickness and Equivalent Bending Ring Stiffness, Trans. of *JSIDRE*, JSIDRE (submitted)

Chapter 3

Dynamic Behavior for Flexible Pipe Having Different Thickness and Equivalent Bending Ring Stiffness

3.1 Introduction

In chapter 2, model test was conducted to verify the characteristic mechanical behavior for flexible pipes having different thickness and equivalent bending ring stiffness. From the test results, it is found that the influence of the thickness of the pipe upon the deflection and the distribution of bending strain was extremely small and the larger axial stress acts on the pipe with the thinner wall, and that the change of axial stress in infinitesimal section of pipe was larger with the thinner wall. In this chapter, shaking table tests using these pipes were conducted in order to verify the influence of the thickness of pipe, a condition of test pit and bedding material on the dynamic behavior of pipes due to a shear deformation of a backfill material.

3.2 Outline of Shaking Table Test

3.2.1 Test Equipment

The shaking table used for the test had plane dimensions of 6 m × 4 m, with the maximum loading capacity of 50 tf. Its excitation system was an electro-hydraulic servo. A rigid box (1,680 mm length, 400 mm width, and 825 mm height) and a laminar box (1,990 mm length, 1,500 mm width, and 970 mm height) were used as a test pit as shown in **Figure 3.1**. These test pits were installed on the shaking table. The laminar box consisted of fifteen flames having 55 mm height. A ground deformation is restricted due to the side wall of the rigid box. On the other hand, propagation of S-waves that horizontally vibrate a ground surface in the field is simulated by using the laminar box. Kokusho and Iwatate (1979) evaluated the nonlinear dynamic response of soft ground from a shaking table test results using a laminar box. Tanaka et al. (2005) evaluated the axial behavior of a buried pipe having a ball type flexible joint during earthquake. In this study, the condition that pipelines were buried on open channels (Harada, 1998), was simulated using the rigid box and the condition that flexible pipes were buried in the field was simulated using the laminar box.

3.2.2 Model Ground

In the test using the rigid box, Toyoura-sand was used as a soil material for the model ground. The density of soil particle of Toyoura-sand was 2.68 g/cm^3. In the test using the laminar box silica sand was used. The density of soil particle of silica-sand was 2.65 g/cm^3. **Figure 3.2** shows grain size accumulation curves for Toyoura-sand and silica sand. In both cases, relative density of backfill material was 40 %. In addition, as shown in **Figure 3.3**, concrete blocks were set in the area of from the bottom of the pipe to a height of half the pipe diameter. The concrete block consisted of high early portland cement, coarse aggregate and fine aggregate. The weight ratio of these was 1:2:3. Water cement ratio was 40 %. Unconfined compression strength of 3 days curing the concrete was 17.19 N/mm^2.

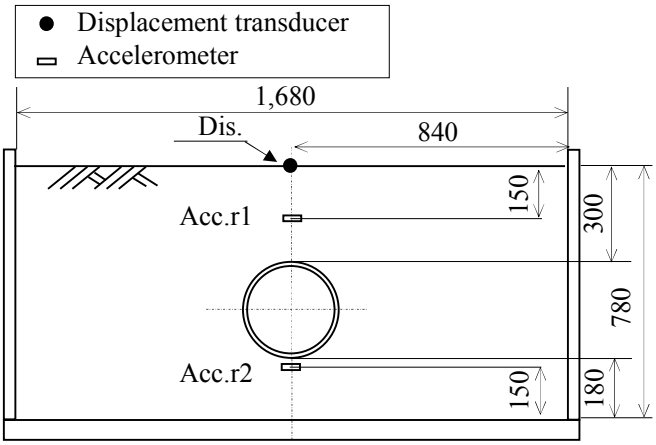

(a) Rigid box

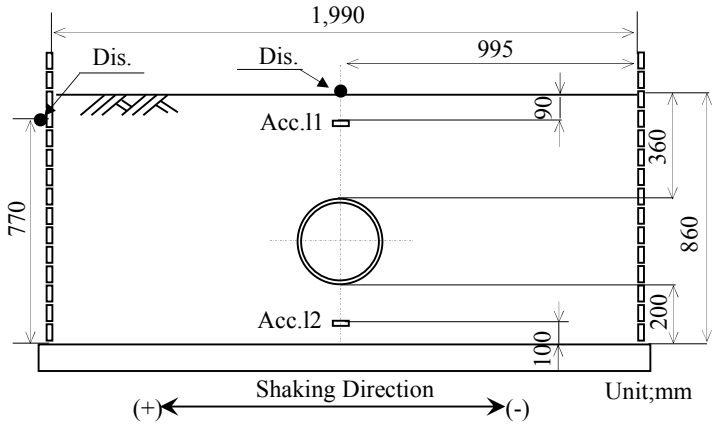

(b) Laminar box

Figure 3.1 Schematic layouts of experiment

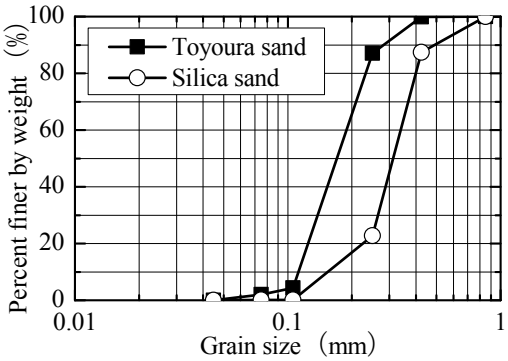

Figure 3.2 Grain size accumulation curves for Toyoura sand and silica sand

3.2.3 Model Pipe

A steel pipe, a PVC pipe, HDPE pipe were used as model pipes. The steel pipe, the PVC pipe and the HDPE pipe had an equivalent bending ring stiffness. **Table 3.1** shows properties of pipes. An inertia force acting on model pipes depends on the weight of pipes. Four vinyl hoses included lead shots were attached at the inner circumferential of The PVC pipe and the HDPE pipe to equalize a weight of the steel pipe.

Figure 3.3 Schematic diagram of concrete block

Table 3.1 Properties of pipes

Type of pipe	Thickness t_p (mm)	Center diameter D_c (mm)	Elastic modulus E_p (N/mm^2)	Ring Bending stiffness E_pI/D_c^3 (kN/m^2)
Steel	1.92	301.9	164,399	3.6
PVC	7.23	309.2	3,155	3.3
HDPE	11.52	311.8	1,390	3.9

3.2.4 Procedure of Test and Test Condition

Horizontal shakings were applied after backfilling as shown in **Figure 3.1**. In the test using the rigid box, an input acceleration generated a sinusoidal wave at a frequency of 2 Hz with the maximum acceleration of 6 m/s^2 as shown in **Figure 3.4(a)**. In the test using the laminar box, the input acceleration generated a sinusoidal wave at frequency of 2 Hz with the maximum acceleration of 4 m/s^2 as shown in **Figure 3.4(b)**. **Table 3.2** shows test conditions.

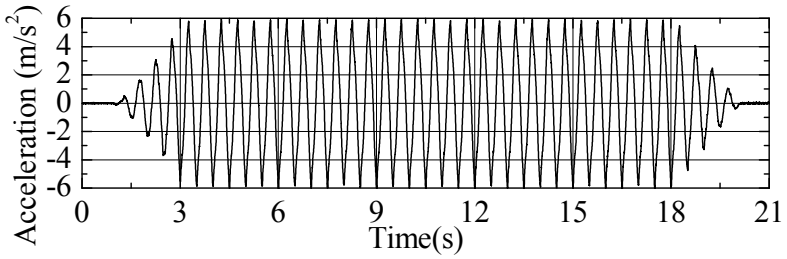

(a) Rigid box

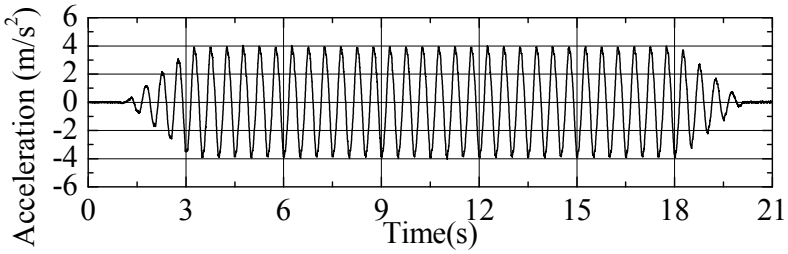

(b) Laminar box

Figure 3.4 Acceleration response of shaking table

Table 3.2 Test conditions

	Type of pipe	Test pit	Maximum acceleration	foundation
Case 1	Steel	Rigid Box	6 m/s^2	—
Case 2	PVC			
Case 3	HDPE			
Case 4	Steel	Laminar Box	4 m/s^2	—
Case 5	PVC			
Case 6	HDPE			
Case 7	Steel	Laminar box	4 m/s^2	Concrete
Case 8	PVC			
Case 9	HDPE			

3.2.5 Measurements

Strain and deflection of pipes, ground acceleration, ground settlement, horizontal displacement of the laminar box and acceleration of the shaking table were measured as shown in **Figure 3.1**. 32 strain gauges were attached circumferentially to the inner surfaces at intervals of 11.25 degrees. The deflection of pipes were measured using phosphor bronze that strain gauges were attached in both side. As a top of pipe was

defined as zero degrees, 0-180 (vertical), 45-225, 90-270 (horizontal) and 135-315 degrees were set inside pipe. The shear strain of the laminar box was calculated by dividing the height of the measurement position into the horizontal displacement of the laminar box.

3.3 Influence of Boundary Condition on Deflection

Figure 3.5 shows the time history of deflection of the pipe in Case 1 and Case 4. The ratio of deflection is calculated by dividing a deflection of a pipe into a center diameter of a pipe. The compression deflection of the pipe in each direction is negative. In both case, the amplitude of the deflection of the pipe in each direction increased from 3 seconds when the acceleration of the shaking table was reached at the peak. The

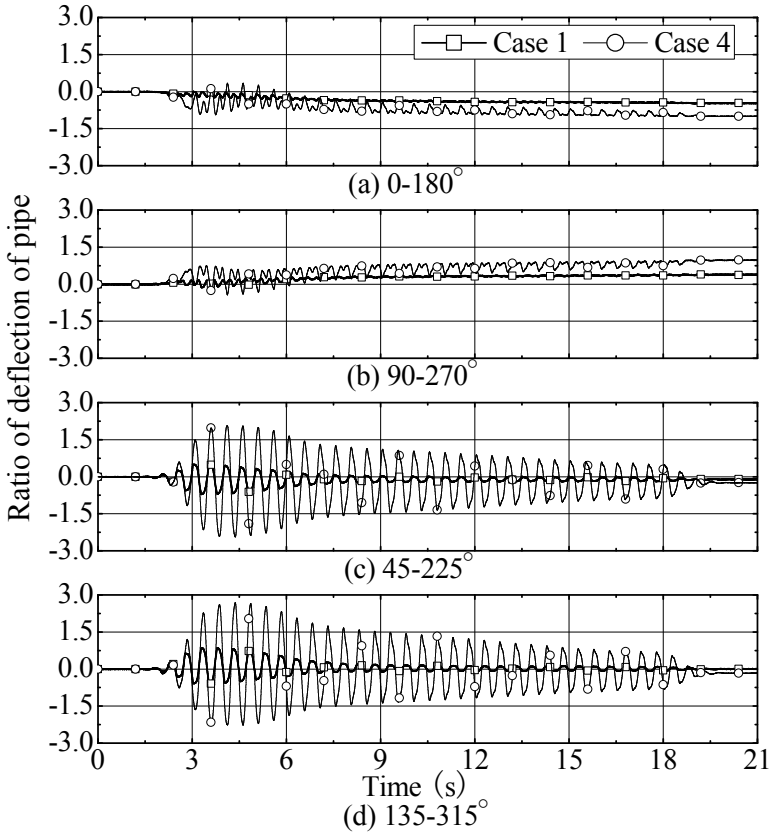

Figure 3.5 Time history of deflection ratio of pipe

amplitude oblique deflection of the pipe was larger than the amplitude vertical and horizontal deflection of the pipe in each case. As the result, it was confirmed that a buried flexible pipe was deformed obliquely during earthquake although a buried flexible pipe was deformed rectangularly by a vertical earth pressure of a backfill material and a wheel load in general.

Table 3.3 shows the absolute maximum deflection ratio of the pipe in Case 1 and Case 4. The vertical and horizontal deflection ratio of the pipe in Case 4 were more than double for that in Case 1. The oblique deflection ratio of the pipe in Case 4 was more than tripled for that in Case 1. The deflection of the pipe in Case 4 was larger than that in Case 1 although the maximum acceleration of the shaking table in Case 1 was half again that in Case 4. It was indicated that the side wall of the rigid box controlled the ground deformation.

The pipe was deformed obliquely by the difference between the displacement of the ground over and under the buried pipe. The amplitude of the deflection ratio in 45-225 and 135-315 degrees decreased after that reached at the peak as shown in **Figure 3.5**. **Figure 3.6** shows the acceleration response of the ground over and under the pipe from 3.0 to 4.5 seconds and from 15.5 to 17.0 seconds. The phase difference between the ground over and under the pipe for the laminar box was larger than that for the rigid box. On the other hand, the phase difference did not occur from 15.5 to 17.0 seconds in both cases.

For the loose ground, the acceleration response of the ground over the pipe corresponding to that under the pipe since the propagation velocity of the shear wave increased by the cyclic shaking. **Figure 3.7** shows the time history of the settlement of the ground in Case 1 and Case 4. The settlement of the ground increased from 3seconds due to the cyclic shaking. The density of the ground increase by the settlement. The results indicated that the negative dilatancy occurred by the cyclic shear deformation in the

Table 3.3 Absolute maximum of deflection ratio

	0-180 deg.	90-270 deg.	45-225 deg.	135-315 deg.
Case 1	0.49%	0.40%	0.71%	0.86%
Case 4	1.01%	0.99%	2.44%	2.69%

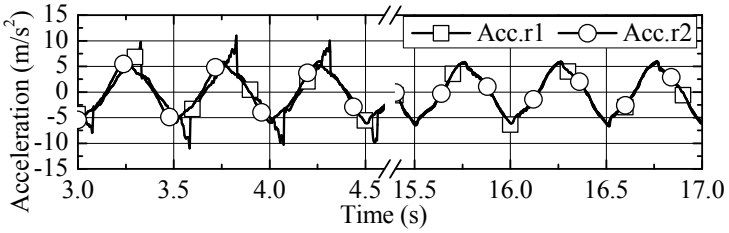

(a) Rigid Box

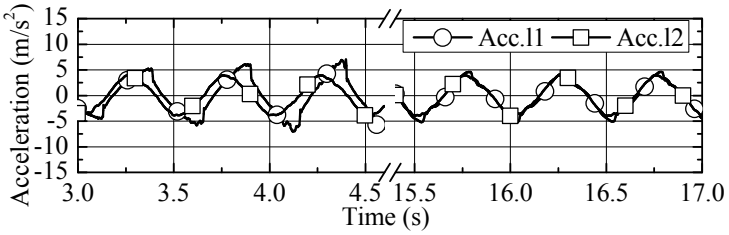

(b) Laminar box

Figure 3.6 Acceleration response of ground

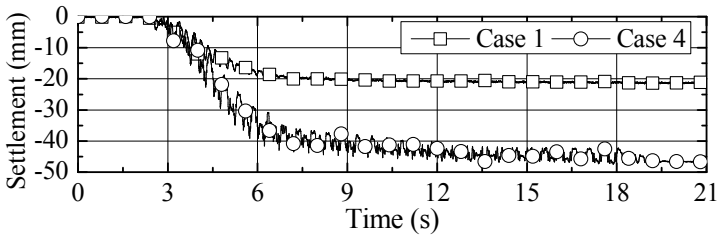

Figure 3.7 Time history of settlement of ground

ground. The density of the ground increased due to the dilatancy and the shear stiffness of the ground increased. After the shaking, the settlement of the ground in Case 1 and Case 4 were 21.3 and 46.6 mm, respectably. In comparison with the settlement of the ground in Case 4, that in Case 1 was small since the ground deformation was restricted due to the side wall of the rigid box.

3.4 Influence of Pipe Thickness on Bending Strain

Figure 3.8 shows the shear strain in laminar box for Case 4-6 and Case 7-9. The shear deformation as shown in **Figure 3.9** is the positive shear deformation. From **Figure 3.8(a)**, after the amplitude of the shear strain of the laminar box increased from 3 sec., the

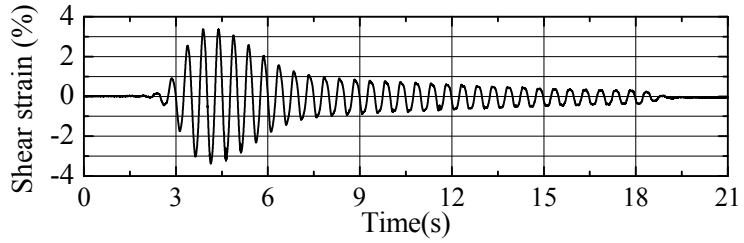

(a) Case 4-6

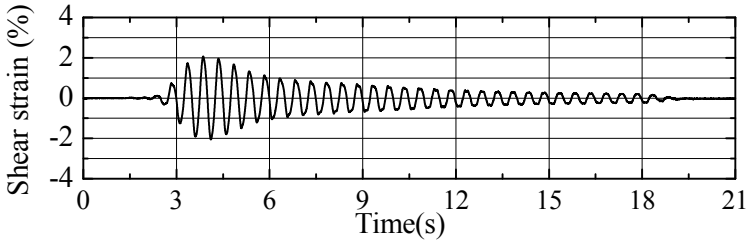

(b) Case 7-9

Figure 3.8 Time history of shear strain of box

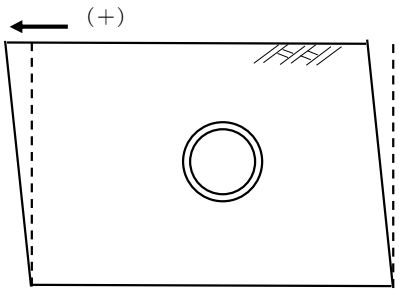

Figure 3.9 Positive shear deformation

amplitude reached at approximately 3%. This was caused by the phase difference between the ground over and under the pipe as shown in **Figure 3.6**. After the amplitude of the shear strain reached at the peak, the amplitude decreased due to the increment of the shear stiffness of the ground. As shown in **Figure 3.9(b)**, the maximum amplitude was approximately 2%. In comparison with the maximum amplitude in Case 4-6, the maximum amplitude was small. This indicated that the shear deformation of the ground was controlled by the concrete block.

Figure 3.10 shows the bending strain distribution in Case 1-3, Case4-6 and Case 7-9. **Figure 3.10(a)** shows the bending strain in Case 1-3 at 3.714 seconds when the deflection of the pipe in 135-315 degrees direction. **Figure 3.10(b)** shows the bending strain in Case 4-6 at 3.860 seconds when the shear strain of the laminar box was 3% and

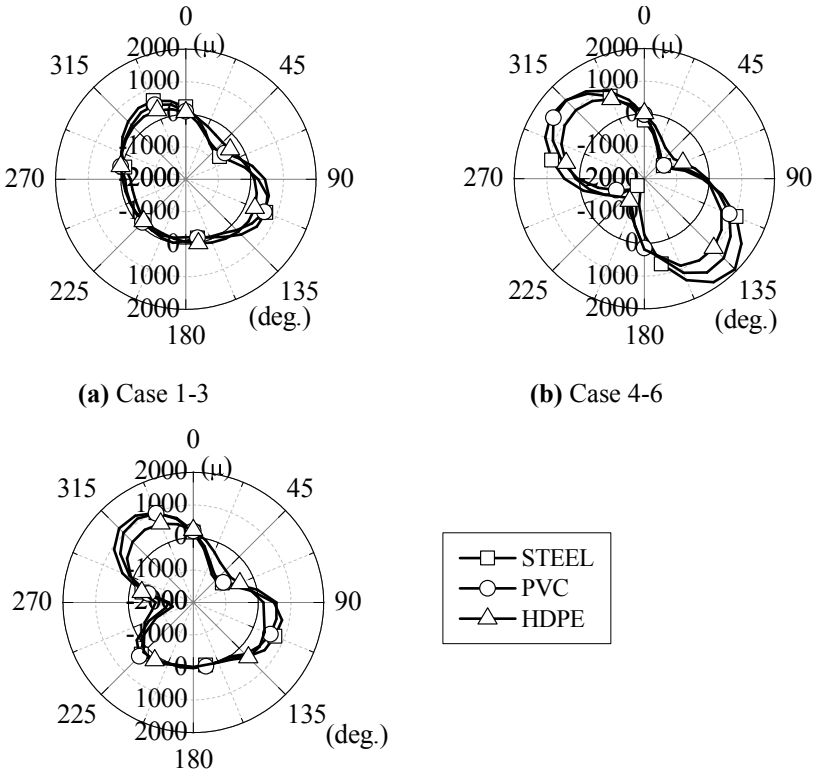

(a) Case 1-3

(b) Case 4-6

(c) Case 7-9

Figure 3.10 Bending strain distributions

Figure 3.10(c) shows the bending strain in Case 7-9 at 3.846 seconds when the shear strain was 2.0 %. The bending strain was defined in Chapter 2. A tensile strain outer circumferential strain is positive. Since the measured strain increased relative to the direction from neutral axis, the bending strain of the steel pipe and the PVC pipe were multiplied by the ratio the thickness of the steel pipe and the PVC pipe to the HDPE pipe, respectively.

The influence of the thickness of the pipe on the bending strain distribution was small in spite of the boundary condition and the base material. As shown in **Figure 3.10(a)**, the peak position and the value of the tensile and compressive strain in all pipes were corresponding. From **Figure 3.10(b)**, the tensile and compressive bending strain of all pipes were large at 135 and 315 deg. and 45 and 225 deg., respectively. The bending strain distribution of all pipes for using the concrete block as the base material was also corresponding.

When the underground structure was laid near the buried pipe, the deformation of the pipe was controlled. For the rigid box, the bending strain was generated hardly at 225 deg. as shown in **Figure 3.10(a)** although the compressive bending strain for the laminar box was large. The results were caused by the difference between the condition of the rigid box and the laminar box. The ground deformation is restricted due to the side wall of the rigid box.

When the stiffness of the base material was difference largely from the stiffness of the backfill material, the pipe was deformed at the boundary between the base material and the backfill material. In comparison with the bending strain distribution in Case 4-6, the bending strain from 135 to 225 degrees in Case 7-9 was approximately zero since the deformation of the pipe was controlled through the rigid concrete block. In comparison with the bending strain in Case 7-9, the compressive bending strain was large at 270 degrees. This result indicated that the stress concentration was generated due to the stiffness difference between the base and the back material.

3.5 Influence of Pipe Thickness on Axial Stress

Figure 3.11 shows the axial stress distribution in Case 1-3, Case4-6 and Case 7-9. The axial stress distribution shows at the same time as the bending strain distribution. The axial stress was defined in Chapter 2. A tensile stress is positive. The axial stress distribution in Case 1-3 was large and non-uniform according to the thickness of the pipe as shown in **Figure 3.11(a)**. The axial stress distribution in Case 4-6 and Case 7-9 exhibited the similar tendency as shown in **Figure 3.11(b)** and **Figure 3.11(c)**. These results indicated that the influence of the thickness of the pipe on the axial stress distribution was large in spite of the boundary condition and the base material condition. In addition, the axial stress was generated from 90 deg. to 270 deg. which the concrete block was set as shown in **Figure 3.11(c)** although the bending strain was hardly generated at the range as shown in **Figure 3.10(c)**.

Figure 3.12 shows the time history of the absolute maximum axial stress in Case

4-6 in order to evaluate the magnitude of the axial stress in each case. The absolute maximum axial stress increased as the amplitude of the shear strain of the laminar box increased. The peak of the absolute maximum axial stress in Case 4, Case 5 and Case 6 were 1.15, 0.24 and 0.14 N/mm^2, respectively. The peak of the absolute maximum axial

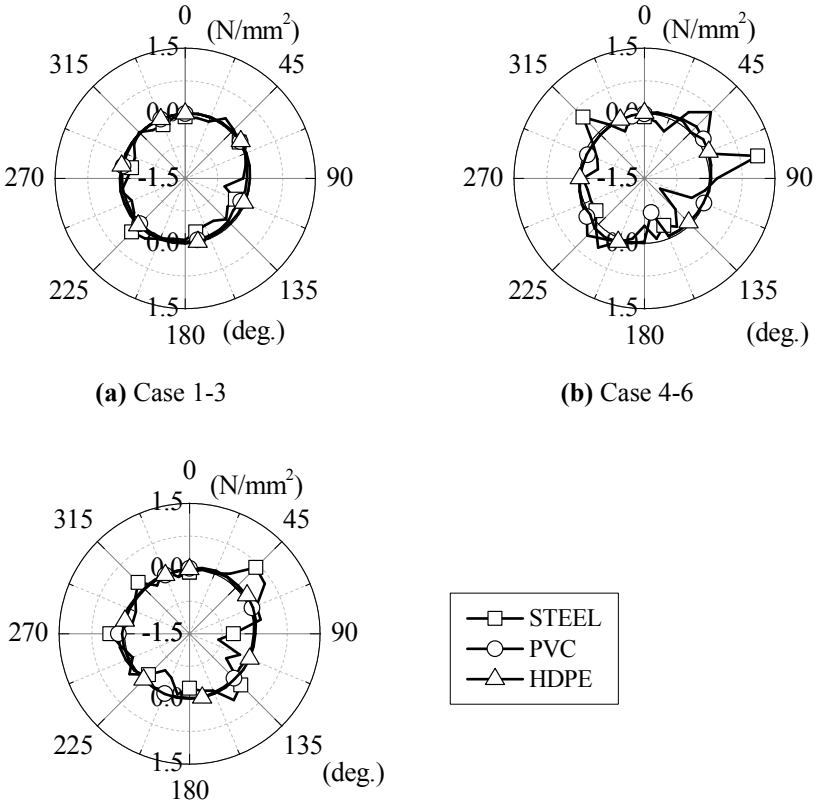

(a) Case 1-3

(b) Case 4-6

(c) Case 7-9

Figure 3.11 Axial stress distributions

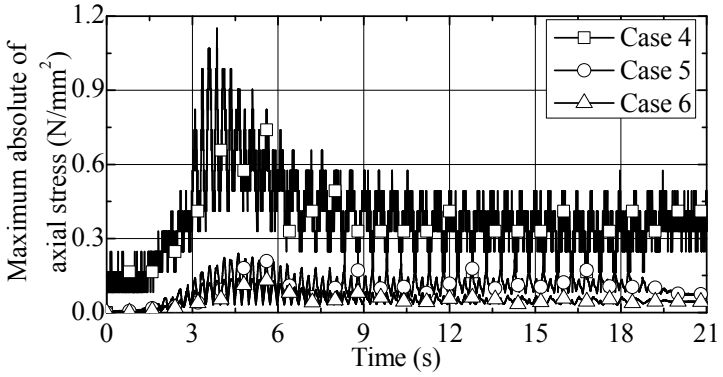

Figure 3.12 Time history of maximum absolute of axial stress

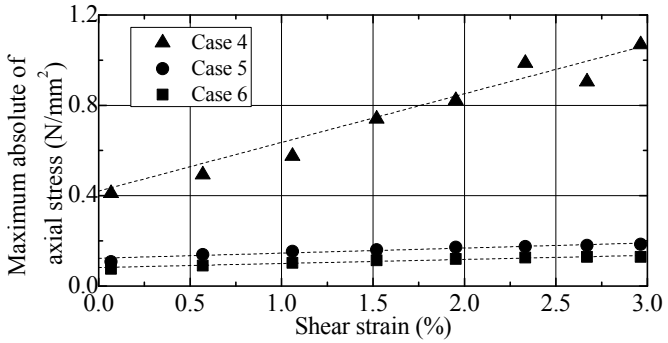

Figure 3.13 Relationships between shear strain and maximum absolute of axial stress

stress in Case 4 was about 8 times the peak in Case 6.

Figure 3.13 shows the relationships between the shear strain of the laminar box and the absolute maximum axial stress. Broken lines indicate linear approximation line of relationships. The absolute maximum axial stress to the shear strain had the linearity since the coefficient determination in Case 4, Case 5 and Case 6 were 0.94, 0.89 and 0.94, respectively. The slope of the absolute maximum axial stress to the shear strain in Case 4, Case 5 and Case 6 were 0.215, 0.023 and 0.018, respectively. The increment rate of the absolute maximum axial stress to the shear strain in Case 4 was approximately 10 times that in Case 5 and 12 times that in Case 6. As these results, it is founded that the absolute maximum axial stress increased according to the increment of the shear strain of the laminar box.

3.6 Conclusions

In this chapter, shaking table tests using these pipes were conducted in order to verify the influence of the thickness of pipe, a condition of test pit and bedding material on the dynamic behavior of pipes due to a shear deformation of a ground. The following findings were obtained through the test.

1. The pipe was deformed obliquely by the difference between the displacement of the ground over and under the buried pipe during the cyclic shear deformation in the

ground. When the underground structure was laid near the buried pipe, the deformation of the pipe was controlled.

2. The influence of the thickness of the pipe on the bending strain distribution was small in spite of the boundary condition and the base material.
3. When the stiffness of the base material was difference largely from the stiffness of the backfill material, the pipe was deformed at the boundary between the base material and the backfill material.
4. The influence of the thickness of the pipe on the axial stress distribution was large in spite of the boundary condition and the base material condition. In addition, the absolute maximum axial stress increased according to the increment of the shear strain of the laminar box.

References

Harada, K. (1998): (2014): Shallow Bury of Pipe in the Open Channel, *Water, Land and Environmental Engineering*, JSIDRE, pp.493-496.

Kokusho, T. and Iwatate, T. (1979): Scaled Model Tests and Numerical Analyses on Nonlinear Dynamic Response of Soft Grounds, JSCE, pp.57-67.

Tanaka, Y., Arimura, T. and Jibu M. (2005): Behavior of Buried Pipe with Flexible Joint in Liquefied Ground, *Report of Research Center for Urban Safety and Security*, Research Center for Urban Safety and Security Kobe University, No.8, pp.63-71.

CHAPTER 4

The contents of this chapter are based on:

Izumi, A., Sawada, Y., Miki, T., and Kawabata, T. : Influence of Ground Shear Deformation on Behavior of Buried Flexible Pipe, *Journal of Applied Mechanics*, JSCE (submitted)

Izumi, A., Miki, T., Sawada, Y. and Kawabata, T. : Influence of Shear Deformation on Buried Behavior of Rehabilitated Pipe, *Trans. of JSIDRE*, JSIDRE (submitted)

Chapter 4

Cross Section Behavior for Pipe Rehabilitation during Earthquake

4.1 Introduction

For a pipe rehabilitation which an aging outer pipe is repair inside the pipe, the aging outer pipe is permanently remained. In design standard (MAFF, 2009) for pipeline in Japan, the design of the pipe rehabilitation is not described. In the previous study, the influence of the damage of the outer pipe on the static behavior of the inner pipe was cleared. Sawada et al. (2014) and Ono et al. (2015) indicated that the strain concentration occurs at the top and the bottom of the outer pipe due to the point contact of the edge of the outer pipe.

The cross section behavior for pipe rehabilitation during earthquake was not cleared although the dynamic behavior of the buried pipe was investigated. Kawabata et al. (2005) verified the floating mechanism of the buried rigid pipe due to cyclic shear deformation of the ground using DEM analysis. Suehiro et al. (2003) conducted a shaking table test and DEM analysis in order to verify the floating mechanism of the buried rigid pipe in liquefied ground. A cross section force acting on a shield tunnel was calculated from a result of FEM analysis during earthquake (JSCE, Kansai branch, 2001).

In this chapter, in order to clarify the influence of a damage of the outer pipe on the dynamic behavior of the inner pipe, cyclic shear test using a lamina box was conducted under a different damage of outer pipes and a different density of backfill material.

4.2 Outline of Cyclic Shear Test

4.2.1 Test Equipment

The laminar box was made of aluminum and has a length of 700 mm, a width of 300 mm and a depth of 550 mm as shown in **Figure 4.1**. The laminar box consisted of ten flames. After each flame was horizontally displaced, a rubber sheet was set at both side wall in order to smoothen a gap between each flame. The top of the laminar box was fixed as a horizontal displacement distribution of the frame increased commensurately to a depth of the laminar box. The bottom of the laminar box was displaced horizontally by a motor.

4.2.2 Model Pipe

A hard polyvinyl chloride pipe (abbr. as VP) pipe, a thin polyvinyl (abbr. as VU) pipe, an aluminum (abbr. as AL) pipe were used as an inner pipe. Inner pipes has a length of 150 mm. Dummy pipes were set on both end of model pipes. **Table 4.1** shows property of pipes.

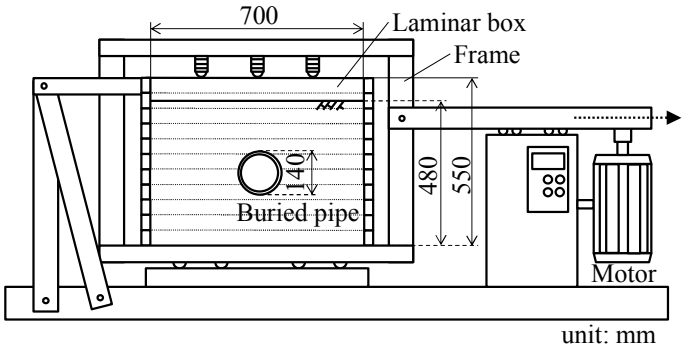

Figure 4.1 Schematic layouts of experiment

Aluminum segments were used as an outer pipe as shown in **Figure 4.2**. The outer pipes were divided into 2, 4, 8 and 16 segments in order to simulate an aging damage. It was assumed that the number of segment increased according to the development of the damage of outer pipes. The segments had a thickness of 10 mm and an outer diameter of 160 mm. The gap between the segments was 1 mm and was covered with a rubber sheet.

4.2.3 Model Ground

Silica sand was used as a soil material for the model ground. **Table 4.2** shows the properties of silica sand. **Figure 4.3** shows a grain size accumulation curve for silica sand. The laminar box was backfilled with silica sand in for different relative densities of 20, 45, 65 or 85% from the bottom of the pipe to the ground surface.

4.2.4 Procedure of Model Test and Test Condition

A cyclic horizontal sinusoidal wave was applied to the bottom of the laminar box after backfilling. The center of the pipe was a height of 240 mm from the bottom of the

Table 4.1 Properties of model pipe

Type of pipe	Thickness t_p (mm)	Outer diameter D_o (mm)	Ring Bending stiffness E_pI/D_c^3 (kN/m^2)
VU	4.1	140.0	8.8
VP	7.0	140.0	42.1
AL	2.0	150.0	14.2

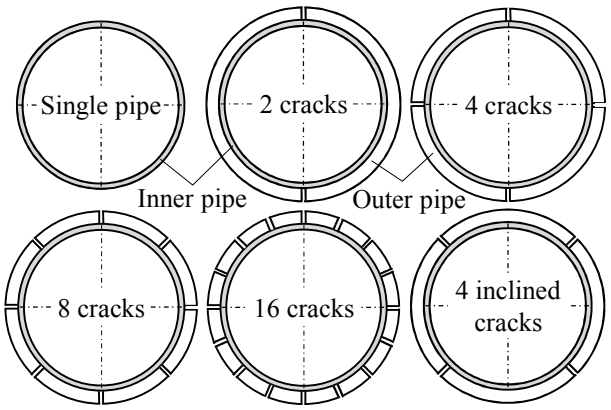

Figure 4.2 Schematic dialog of segments

laminar box. A maximum shear strain of the laminar box was 5 % and the sinusoidal wave had a frequency of 2 Hz as shown in **Figure 4.4**. The shear deformation of the laminar box was repeated thirty times. **Table 4.3** shows test conditions. In Series 1, the influence of the ring bending stiffness and the relative density of the backfill material condition on the behavior of the buried flexible pipes due to the cyclic shear deformation was evaluated. In Series 2, the influence of the shear deformation on a normal and tangential earth pressure acting on the AL pipe was evaluated. In Series 3, the influence of the damage of the outer pipe on the deflection of the inner pipe was evaluated.

4.2.5 Measurements

Strain of pipes, deflections of pipes and the normal and tangential earth pressure and the lateral displacement of the bottom of the laminar box were measured. In VU

Table 4.2 Properties of silica sand

Density of soil particles	ρ_s	2.63 g/cm^3
Minimum dry density	ρ_{dmin}	1.28 g/cm^3
Maximum dry density	ρ_{dmax}	1.63 g/cm^3

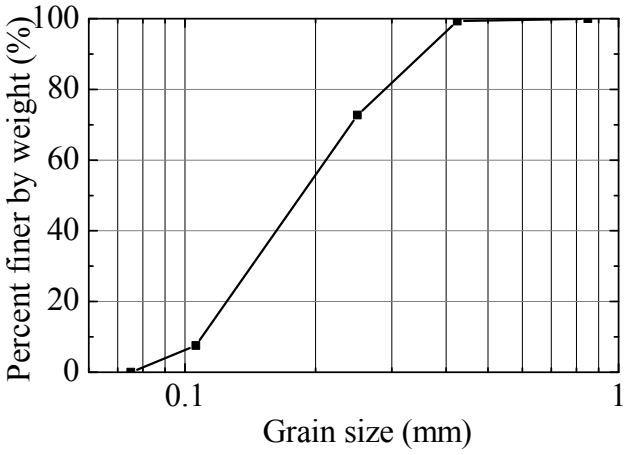

Figure 4.3 Grain size accumulation curve for silica sand

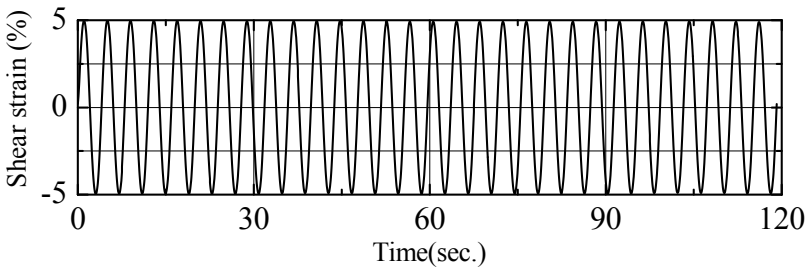

Figure 4.4 Time history of shear strain of laminar box

Table 4.3 Test conditions

Series	Case	Inner type	State of outer pipe	Relative density
Series 1	VUN-20	VU	None	20 %
	VUN-45			45 %
	VUN-65			65 %
	VUN-85			85 %
	VPN-20	VP	None	20 %
	VPN-45			45 %
	VPN-65			65 %
	VPN-85			85 %
Series 2	ALN-20	AL	None	20 %
	ALN-45			45 %
	ALN-65			65 %
	ALN-85			85 %
Series 3	VU2-20	VU	2 cracks	20 %
	VU2-45			45 %
	VU2-65			65 %
	VU2-85			85 %
	VU4C-20			20 %
	VU4C-45			45 %
	VU4C-65			65 %
	VU4C-85			85 %
	VU4I-20		4 cracks (inclined)	20 %
	VU4I-45			45 %
	VU4I-65			65 %
	VU4I-85			85 %
	VU8-20		8 cracks	20 %
	VU8-45			45 %
	VU8-65			65 %
	VU8-85			85 %
	VU16-20		16 cracks	20 %
	VU16-45			45 %
	VU16-65			65 %
	VU16-85			85 %
	VP2-45		2 cracks	45 %
	VP4C-45		4 cracks (cross)	45 %
	VP4I-45		4 cracks (inclined)	45 %
	VP8-45		8 cracks	45 %
	VP16-45		16 cracks	45 %

pipe and VP pipe, 24 strain gauges were attached circumferentially to the inner surfaces of each pipe at intervals of 15 degrees as show in **Figure 4.5(a)**. In all pipes, the deflection of pipes were measured using a phosphor bronze that strain gauges were attached in both side. As a top of pipe was defined as zero degrees, the phosphor bronzes were set inside pipe at the direction of 0-180 (vertical), 45-225, 90-270 (horizontal) and 135-315 degrees. The AL pipe included by-axial load cells by which the normal and tangential pressure at intervals of 18 deg. from the top of the pipe as shown in **Figure 4.5(b)**. Kawabata et al. (2003) investigated the normal and tangential earth pressure acted on the buried pipe in the reinforced embankment with settlement. The lateral displacement of the bottom of the laminar box were measured a displacement transducer. The shear strain of the laminar box was calculated by dividing the lateral displacement into the height of the laminar box. Shear deformations as shown in **Figure 4.6** were defined as positive.

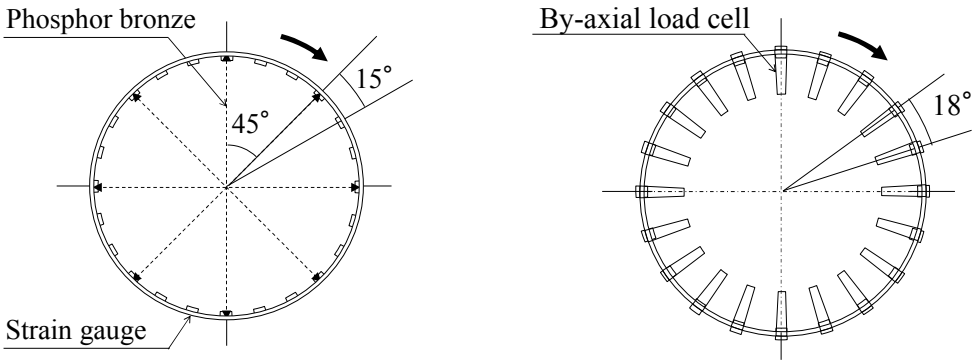

(a) Strain gauge and phosphor bronze **(b)** By-axial load cell

Figure 4.5 Installation position of measurements

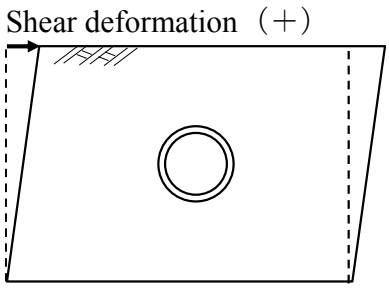

Figure 4.6 Shear deformation of laminar box

4.3 Buried Behavior for Flexible pipe

Figure 4.7 shows the relationship between the shear strain of the laminar box and the deflection of the pipe in VUN-45. The compressive deflection of the pipe in each direction is positive. The first cycle of the deflection of the pipe to the shear strain indicated a bolder line. As shown in **Figure 4.7(a)**, the tensile deflection of 0-180 degrees direction and the compressive of 90-270 degrees increased as the shear strain increased from zero to 5%. When the shear strain decreased from 5% to zero, each deflection was approximately zero at the shear strain of 3%. This is caused by the plastic deformation of the backfill material. In each deflection, the relationship between the shear strain and the deflection had a hysteresis characteristic. As shown in **Figure 4.7(b)**, the relationship had also the hysteresis characteristic in 45-225 and 135-315 degrees direction. The deflection of 0-180, 90-270, 45-225 and 135-315 degrees direction to the shear strain of 5% was 0.50, -0.37, 1.01 and -1.07 mm. As described in Chapter 3, the oblique deflections of the pipe to the shear strain were larger than the horizontal and vertical deflection. Thus, the oblique deflection of the pipe was only discussed from here onward.

Figure 4.8 shows the relationship between the cyclic number and 45-225 degrees direction deflection of the pipe to the shear strain which reached 5%. The deflection of the pipe in VUN20, VUN45, VUN65 and VUN85 at the first cycle were 0.62, 1.01, 1.34 and 1.87 mm, respectively. In general, a horizontal and vertical deflection of a buried flexible pipe for a dense ground is smaller than that for a loose ground since a ground stiffness increases according to a density of a ground. On the other hand, the oblique deflection of the pipe was large as the relative density of the backfill material increased. As the results, it was caused that the shear stress acting on the pipe for the dense ground was larger than that for the loose ground since the shear stiffness of the backfill material increased according to the relative density of the backfill material.

The deflection of the pipe in VUN20 increased according to the increment of the cycle. The deflection in VUN45 and VUN65 increased to 2 cycles and the change of the deflection was small. These results were caused by a negative dilatancy. The deflection of the pipe increased since the relative density increased due to the cyclic shear

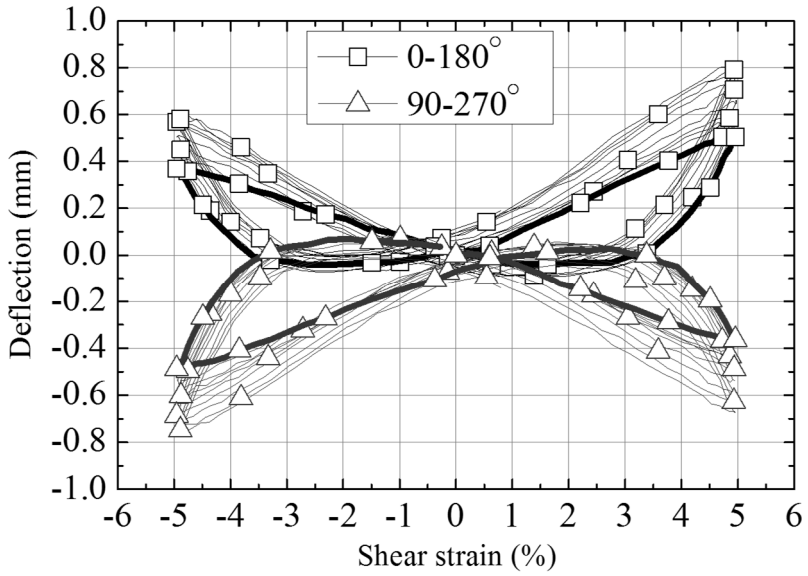

(a) 0-180 and 90-270 deg. direction

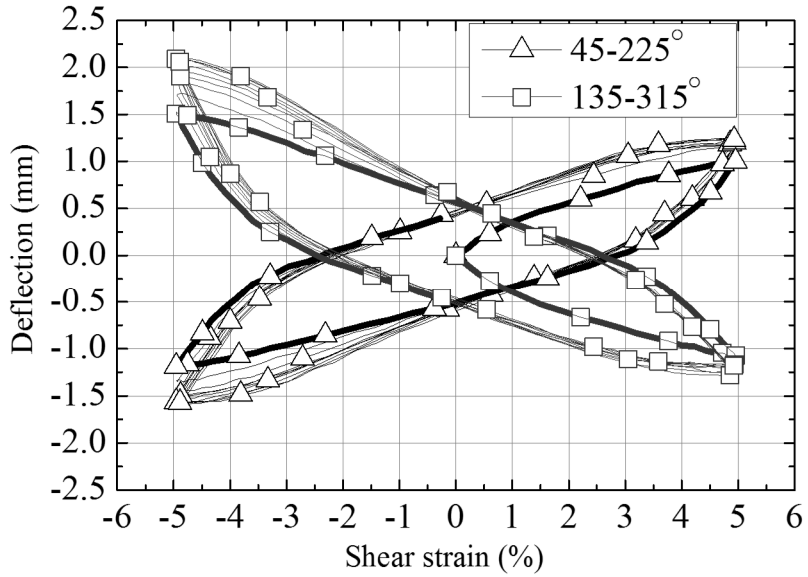

(b) 45-225 and 135-315 deg. direction

Figure 4.7 Relationships between shear strain and deflection of pipe in VUN45

deformation of the laminar box. On the other hand, the deflection of the pipe in VUN85 at the second cycles was smaller than that at the first cycle due to the positive dilatancy. In comparison with the deflection of the VU pipe in each relative density of the backfill material, that of the VP pipe was small due to the difference of the ring bending stiffness as described in Chapter 2.

Figure 4.9(a) shows the inner circumferential strain distribution in VUN-20, VUN-45, VUN-65 and VUN-85 to the shear strain which reached 5 % at the first cycle. **Figure 4.9(b)** shows the inner circumferential strain distribution in VPN-20, VPN-45,

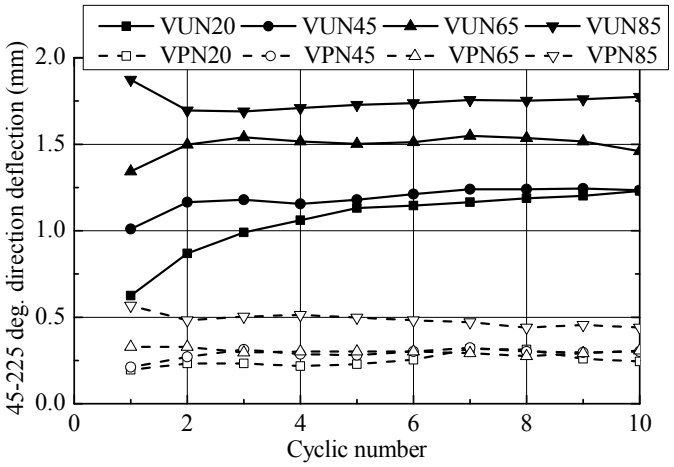

Figure 4.8 Relationships between cycle number and deflection of 45-225 degrees direction

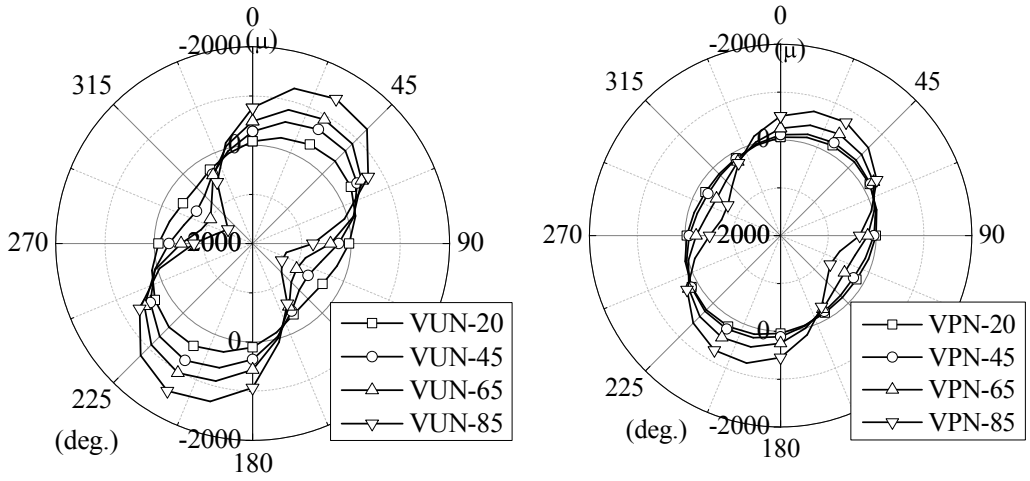

(a) VU pipe **(b)** VP pipe

Figure 4.9 Inner circumferential strain distribution

VPN-65 and VPN-85. A tensile strain is positive. In each case, the compressive strain increased from 90 to 180 degrees and from 270 to 360 degrees due to the shear deformation of the laminar box. In addition, the tensile strain increased from 0 to 90 degrees and from 180 to 270 degrees. These results were corresponding to the oblique deflection of the pipe as shown in **Figure 4.7(b)**. The compressive and tensile strain increased as the relative density of the backfill material. As shown in **Figure 4.9(b)**, the compressive and tensile strain in the VP pipe was smaller than that in the VU pipe in spite of the relative density of the backfill material since the ring bending stiffness of the VP pipe was large in comparison with that in the VU pipe.

Figure 4.10 shows the normal and tangential earth pressure distribution in ALN-20, ALN-45, ALN-65 and ALN-85 to the shear strain which reached 5 % at the first cycle. For the normal earth pressure, the compressive pressure is positive. For the tangential earth pressure, the clockwise pressure is positive. In each case, the normal earth pressure was generated from 60 to 210 degrees and from 240 to 360 degrees. The normal earth pressure increased according to the relative density of the backfill material. On the other hand, the normal earth pressure was hardly generated at the range of other. In each case, the negative tangential earth pressure was generated from 45 to 120 degrees and from 240 to 300 degrees. The positive tangential earth pressure was generated from 120 to 210

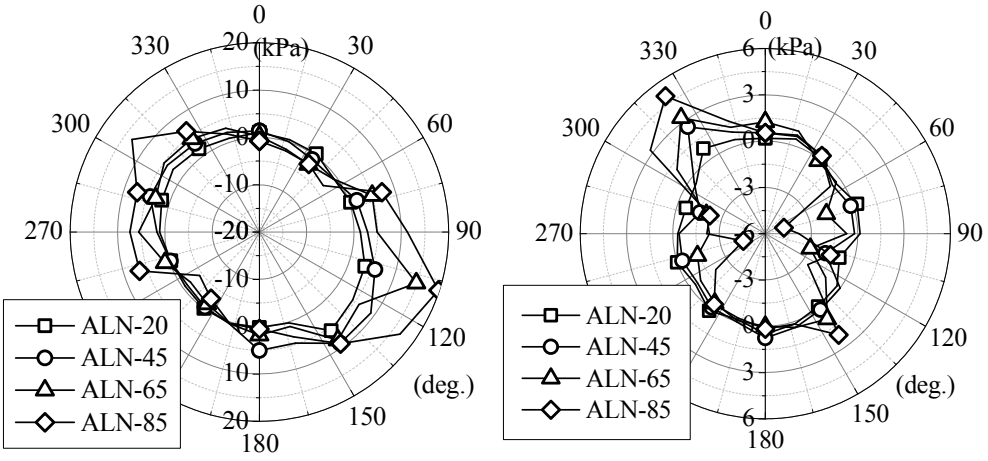

(a) Normal earth pressure **(b)** Tangential earth pressure

Figure 4.10 Normal and tangential earth pressure distribution

degrees and from 300 to 30 degrees. In comparison with the tangential earth pressure distribution, the normal earth pressure distribution was large. As the results, it was found that the normal earth pressure had a dominant influence on the deformation of the pipe during earthquake.

4.4 Influence of Damage Level of Outer Pipe

Figure 4.11 shows the relationship between the shear strain of the laminar box at the first cycle and the 45-225 deg. direction deflection of the pipe in VUN-45, VU2-45, VU4C-45, VU4I-45, VU8-45 and VU16-45. The slope of the deflection to the shear strain in VU2-45, VU4C-45, VU4I-45, VU8-45 and VU16-45 were smaller than that in VUN-45. The deflection of the pipe in VUN45 to the shear strain which reached 5 %was the smallest in all case. These results indicated that the deflection of the inner pipe was controlled with the outer pipe in spite of the damage level of the outer pipe.

The influence of the damage level of the outer pipe on the deflection of the inner pipe was categorized into two broad types. **Table 4.5** shows the 45-225 deg. direction deflection of the pipe to the shear strain which reached 5 % and **Table 4.6** shows the

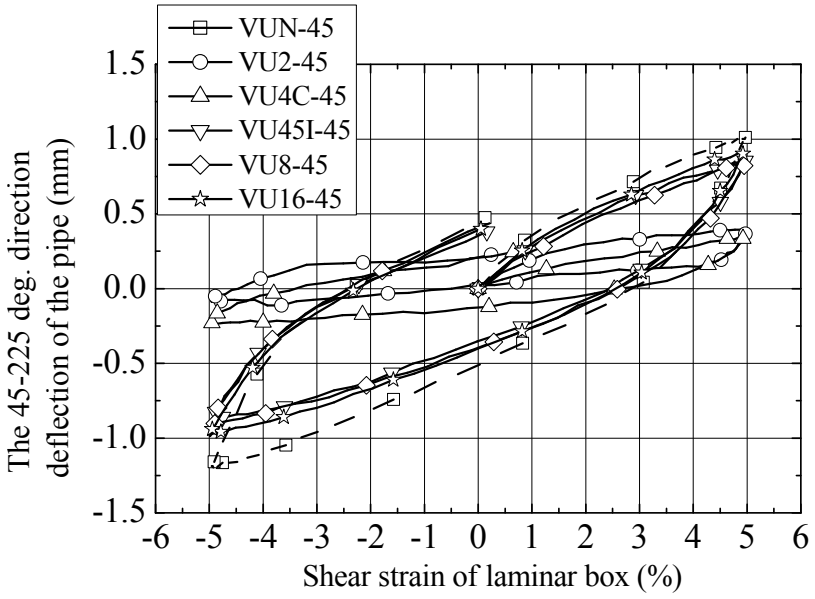

Figure 4.11 Relationships between shear strain and 45-225 deg. direction deflection of pipe

deflection rate of the pipe with the outer pipe to the pipe without the outer pipe in each relative density of the backfill material. As shown in **Table 4.6**, the deflection ratio for the outer pipe without inclined cracks (2 cracks and 4 cross cracks) was approximately 0.3 ~ 0.4 % for using the VU pipe as the inner pipe. On the other hand, the deflection ratio for the outer pipe with incline (4 inclined cracks, 8 cracks, 16 cracks) was approximately 0.8 ~ 1.0. From the results, it is found that the outer pipe without inclined cracks restrain that the earth pressure as show in **Figure 4.10** from acting on the inner pipe. When the outer pipe had the inclined cracks, the restraint efficacy to the deflection of the inner pipe was small. In the case of using the VP pipe as the inner pipe, the deflection rate was obtain a similar results to that in the VU pipe as the inner pipe. However, the deflection ratio of VP2-45 to VPN-45 was 0. It was caused that the deflection of the VPN-45 was extremely small as show in **Table 4.4**.

Figure 4.12 shows the inner circumferential strain distribution of the pipe in VUN-45, VU2-45, VU4C-45, VU4I-45, VU8-45 and VU16-45 pipe to the shear strain which reached 5 % at the first cycle. A tensile strain is positive. The strain distribution in VU2-45 and in VU4C-45 were smaller than that in VUN-45. On the other hand, the strain distribution in VU4I-45 was similar to that in VUN-45 except 135 deg. at which the outer pipe had the crack. The tensile strain was concentrated at the crack. Sawada et al (2014) and Ono et al. (2015) indicated that the concentrated force acted on the points of cracks due to the contact with the edge of the damaged pipe from the results of vertical and eccentric loading tests. The distribution in VU8-45 and VU16-45 was almost similar to that in VUN-45. From these results, when the damage level of the outer pipe was incipient, the strain of the inner pipe due to earthquake was restricted. In addition, for the outer pipe with 4 inclined, the concentrated strain was generated at the crack. As the damage level of the outer pipe was developed, the influence of the outer pipe in the strain of the inner pipe was almost negligible.

Table 4.5 45-225 deg. direction deflection of inner pipe to shear strain which reached 5 %

VU pipe	Relative density of backfill material			
State of outer pipe	20 %	45 %	65 %	85 %
None	0.62 mm	1.01 mm	1.34 mm	1.87 mm
2 cracks	0.23 mm	0.34 mm	0.39 mm	0.40 mm
4 cracks	0.22 mm	0.34 mm	0.49 mm	0.64 mm
4 inclined cracks	0.56 mm	0.85 mm	1.12 mm	1.20 mm
8 cracks	0.57 mm	0.84 mm	1.06 mm	1.19 mm
16 cracks	0.62 mm	0.90 mm	1.25 mm	1.39 mm
VU pipe	Relative density of backfill material			
State of outer pipe	20 %	45 %	65 %	85 %
None		0.21 mm		
2 cracks		0.00 mm		
4 cracks		0.10 mm		
4 inclined cracks		0.22 mm		
8 cracks		0.23 mm		
16 cracks		0.17 mm		

Table 4.6 Deflection ratio of pipe with the outer pipe to the pipe without the outer pipe

VP pipe	Relative density of backfill material			
State of outer pipe	20 %	45 %	65 %	85 %
None	1.00	1.00	1.00	1.00
2 cracks	0.38	0.34	0.29	0.21
4 cracks	0.36	0.33	0.36	0.34
4 inclined cracks	0.92	0.83	0.79	0.63
8 cracks	1.01	0.89	0.93	0.74
16 cracks	0.91	0.85	0.83	0.64
VP pipe	Relative density of backfill material			
State of outer pipe	20 %	45 %	65 %	85 %
None		1.00		
2 cracks		0.00		
4 cracks		0.48		
4 inclined cracks		1.03		
8 cracks		1.08		
16 cracks		0.83		

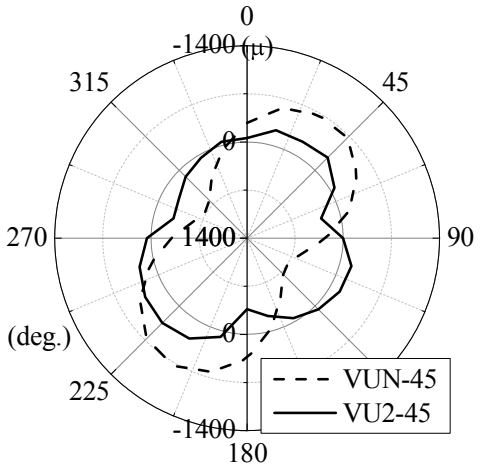

(a) VU2-45

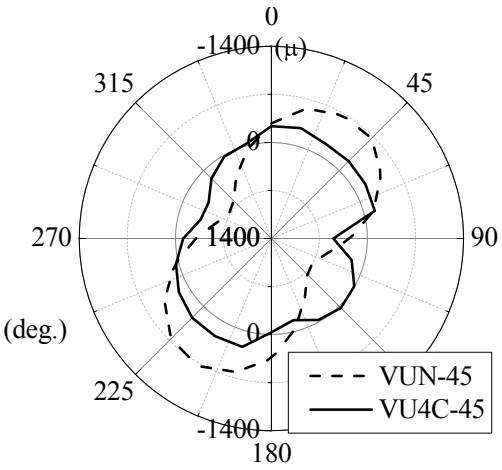

(b) VU4C-45

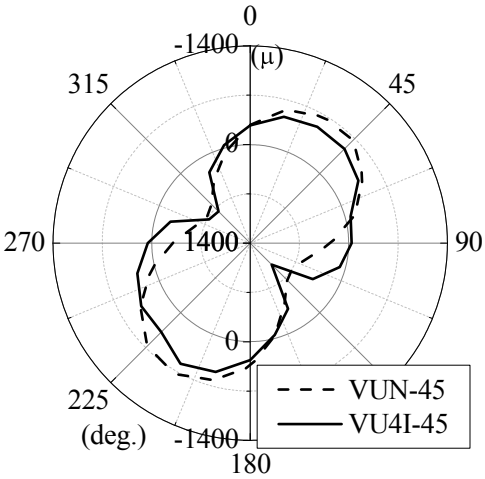

(c) VU4I-45

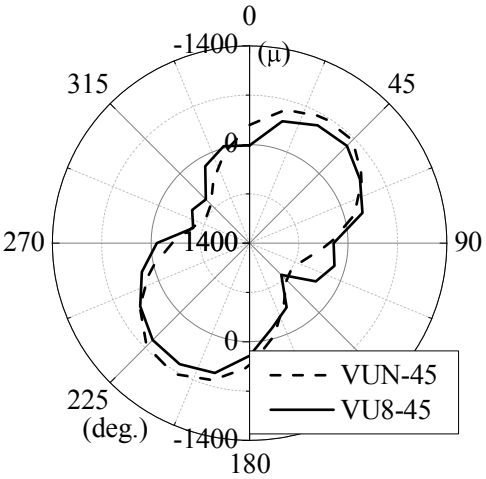

(d) VU8-45

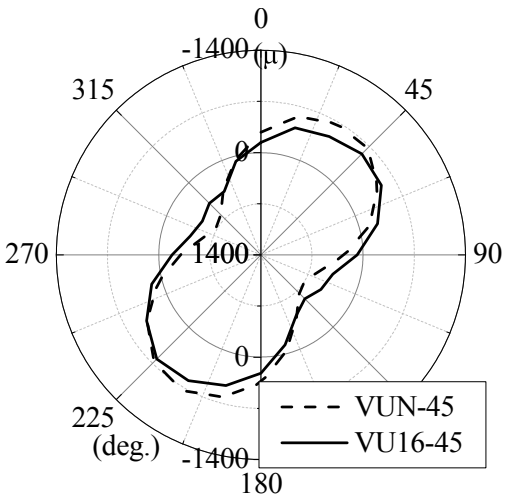

(d) VU16-45

Figure 4.12 Inner circumferential strain distribution

4.5 Conclusions

In this chapter, in order to clarify the influence of a damage of the outer pipe on the dynamic behavior of the inner pipe, cyclic shear test using a lamina box was a conducted under a different damage of outer pipes and a different density of backfill material. The following findings were obtained through the test.

1. The relationship between the shear strain of the laminar box and the deflection of the flexible pipe had a hysteresis characteristic. The oblique deflections of the pipe to the shear strain were larger than the horizontal and vertical deflection.
2. The deflection of the flexible pipe for the loose ground increased according to the increment of the cycle due to the negative dilatancy. On the other hand, the deflection for the dense ground at the second cycles was smaller than that at the first cycle due to the positive dilatancy.
3. The compressive strain increased from 90 to 180 deg. and from 270 to 360 deg. due to the shear deformation of the laminar box. In addition, the tensile strain increased from 0 to 90 deg. and from 180 to 270 deg.
4. The normal earth pressure on the flexible pipe was generated from 60 to 210 deg. and from 240 to 360 deg. The normal earth pressure increased according to the relative density of the backfill material. The negative tangential earth pressure was generated from 45 to 120 deg. and from 240 to 300 deg. and the positive tangential earth pressure was generated from 120 to 210 deg. and from 300 to 30 deg.
5. The deflection of the inner pipe was controlled with the outer pipe in spite of the damage level of the outer pipe. The outer pipe without inclined cracks restrain that the earth pressure from acting on the inner pipe. When the outer pipe had the inclined cracks, the restraint efficacy to the deflection of the inner pipe was small.
6. The strain of the inner pipe due to earthquake was restricted. In addition, for the outer pipe with 4 inclined, the concentrated strain was generated at the crack. As the damage level of the outer pipe was developed, the influence of the outer pipe in the strain of the inner pipe was almost negligible.

References

JSCE, Kansai branch (2001): Economic Seismic design guideline draft for shield tunnel (in Japanese), available from https://www.jsce.or.jp/library/eq10/book/bklist/49198/eqbk01.htm.

Kawabata, T., Uchida, K., Hirai, T., Mohri, Y., Lin, H.I. and Koyama, N. (2003): Experiments on Buried Pipe Using Backfill of Cover with Geosynthetics, Proc. of the Int. Conf. of pipeline 2008, ASCE, pp.1271-1278.

Kawabata, T., Oishi, J., Nakase, H., Mohri, Y. and Uchida, K. (2005), Mechanism of Uplifting for Buried Pipe Subjected to Cyclic Simple Shear, *Trans. of JSIDRE*, JSIDRE,. pp.59-66 (in Japanese with English Summary).

Ministry of Agriculture, Forestry and Fisheries of Japan (2009): Design standard for pipeline (in Japanese).

Ono, K., Sonoda, Y., Sawada, Y., Ling, H.I., Kawabata, T. (2015): Centrifuge Modeling for Mechanical Behavior of Liners in Damaged Host Pipes, *Transp. Infrastruct. Geotech.*, Springer, Vol.2, pp.139-154.

Sawada, Y., Sonoda, Y., Ono, K., Inoue, K., Mohri, Y., Ariyoshi, M. and Kawabata, T. (2014): Influence of Damage Levels of Outer Aging Pipes on Mechanical Behavior of Rehabilitated Pipes, *Trans. of JSIDRE*, JSIDRE, No.291, pp.157-163 (in Japanese with English Summary).

Suehiro, T., Nakase, H., Mohri, U., and Yasuda, S. (2003): Shaking Table Test to Underground Structures and Simulation Study on Mechanism of Uplifting Using Distinct Element Method, *Journal of JSCE, Earthquake Engineering*, JSCE, No.27, 0323, pp.1-8 (in Japanese with English Summary).

CHAPTER 5

The contents of this chapter are based on:

Izumi, A., Sawada, Y., Miki, T., and Kawabata, T. : Influence of Ground Shear Deformation on Behavior of Buried Flexible Pipe, *Journal of Applied Mechanics*, JSCE (submitted)

Izumi, A., Miki, T., Sawada, Y. and Kawabata, T. : Influence of Shear Deformation on Buried Behavior of Rehabilitated Pipe, *Trans. of JSIDRE*, JSIDRE (submitted)

Izumi, A. and Kawabata, T. : Analysis Method on Underground Structure with DEM, *Trans. of JSIDRE*, JSIDRE (submitted)

Chapter 5

DEM Analyses on Cross-Section Behavior of Pipe Rehabilitation

5.1 Introduction

In chapter 4, the deflection of the inner pipe was controlled with the outer pipe in spite of the damage level of the outer pipe. The outer pipe without inclined cracks restrain that the earth pressure from acting on the inner pipe. When the outer pipe had the inclined cracks, the restraint efficacy to the deflection of the inner pipe was small. In addition, for the outer pipe with 4 inclined, the concentrated strain was generated at the crack. As the damage level of the outer pipe was developed, the influence of the outer pipe in the strain of the inner pipe was almost negligible.

In this chapter, two dimensional discrete element method (DEM) analyses were conducted in order to verify the deformation mechanism of the inner pipe with and without the outer pipe during earthquake and formulate the oblique deflection of the inner pipe to shear strain of the ground. In DEM analyses, soil and a structure are regarded as assembly of elements and the mechanical behavior is simulated by solving the equations of motions for each element (Cundall, 1971).

5.2 Algorithm of DEM

5.2.1 Equation of Motion

In an equation of motion of elements, elements are regarded as a rigid body, an elastic and an inelastic characteristic of elements are expressed as a spring coefficient and a damping coefficient, respectively. Where an equation of motion of an element *i* is defined from the following equation.

$$m_i \cdot \ddot{u} + C_i \cdot \dot{u} + F_i = 0 \tag{5.1}$$

$$I_i \cdot \ddot{\varphi} + D_i \cdot \dot{\varphi} + M_i = 0 \tag{5.2}$$

where m_i is the element mass, u is the displacement vector of an element, φ is the rotational displacement of an element, C_i, D_i are the damping constants, I_i is the inertia moment of an element, F_i is the resultant force acted on an element and M_i is the resultant moment acted on an element. In addition, $\dot{x} = dx / dt$ and $\ddot{x} = d^2x / dt^2$.

5.2.2 Contact Detection

When the following inequality holds, two elements, *i* and *j* are contacted.

$$r_i + r_j \geq R_{ij} \tag{5.3}$$

where r_i is the radius of an element *i*, r_j is the radius of an element *j* and R_{ij} is the center distance between two elements, *i* and *j*. When two elements were contacted as shown in **Figure 5.1**, a relative displacement increment from t-Δt to t is given as

$$\Delta u_n = (\Delta u_i - \Delta u_j)\cos\alpha_{ij} + (\Delta v_i - \Delta v_j)\sin\alpha_{ij} \tag{5.4}$$

$$\Delta u_s = -(\Delta u_i - \Delta u_j)\sin\alpha_{ij} + (\Delta v_i - \Delta v_j)\cos\alpha_{ij} + (r_i\Delta\varphi_i - r_j\Delta\varphi_j) \tag{5.5}$$

where, Δu_n is the normal relative displacement between two elements *i* and *j*, Δu_s is the tangential relative displacement between two elements *i* and *j*, Δu_i is the *x* direction displacement increment of an element *i*, Δu_j is the *x* direction displacement increment of an element *j*, Δv_i is the *y* direction displacement increment of an element *i*, Δv_j is the *y* direction displacement increment of an element *j*, $\Delta\varphi_i$ is the rotational increment of an element *i*, $\Delta\varphi_j$ is the *x* direction displacement increment of an element *i*, α_{ij} is the angle making a straight line connecting a center of element *i* with a center of element *j* and *x* axial.

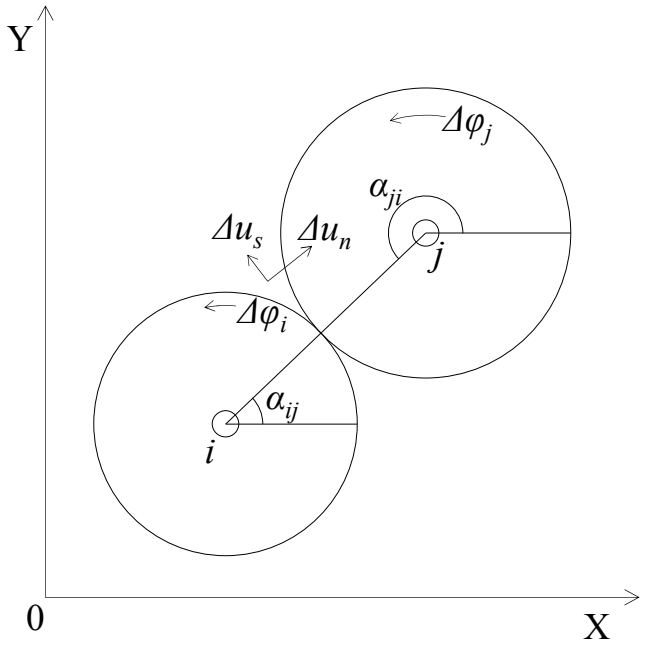

Figure 5.1 Contact detection

5.2.3 Force between Two Elements

A force between two elements is divided into the normal compressive force f_n and the tangential shear force f_s. **Figure 5.2** shows a relationship between two elements. K_n is the normal spring coefficient, K_s is the tangential spring coefficient, η_n is the normal damping coefficient, η_s is the tangential damping coefficient and μ is the frictional coefficient.

1) Normal direction

Since in the time increment Δt, the normal elastic force Δe_n is proportionate to the relative displacement Δu and the normal damping force Δd_n is proportionate to a relative displacement velocity Δu / t, the following equation is given.

$$\Delta e_n = K_n \Delta u_n \tag{5.6}$$

$$\Delta d_n = \eta_n \Delta u_n / \Delta t \tag{5.7}$$

Thus, the normal elastic force $[e_n]_t$ and the normal damping force $[d_n]_t$ at a time t are expressed as

$$[e_n]_t = [e_n]_{t-\Delta t} + \Delta e_n \tag{5.8}$$

$$[e_n]_t = \Delta d_n \tag{5.9}$$

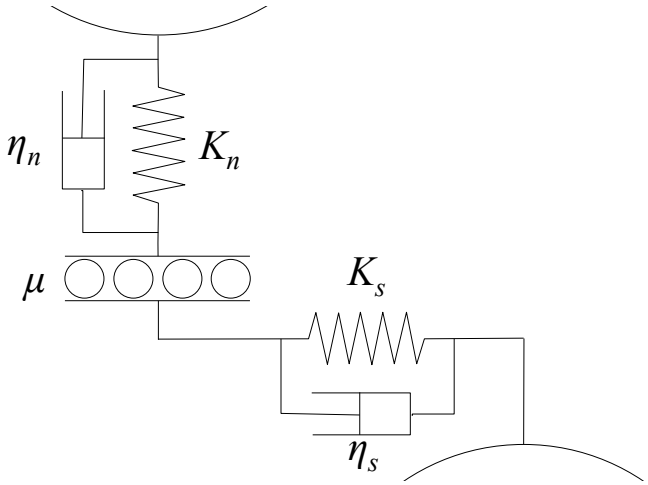

Figure 5.2 Relationship between two elements

where, since a normal tensile force is 0,

$$[e_n]_t < 0 \rightarrow [e_n]_t = [d_n]_t = 0 \tag{5.10}$$

From the above, the normal compressive force $[f_n]_t$ was given as

$$[f_n]_t = [e_n]_t + [d_n]_t \tag{5.11}$$

2) Tangential direction

Since a tangential shear force is given as the following equation as well as a normal compressive force.

$$\Delta e_s = K_s \Delta u_s \tag{5.12}$$

$$\Delta d_s = \eta_s \Delta u_s / \Delta t \tag{5.13}$$

Thus, the tangential elastic force $[e_s]_t$ and the tangential damping force $[d_s]_t$ at a time t are expressed as

$$[e_s]_t = [e_s]_{t-\Delta t} + \Delta e_s \tag{5.14}$$

$$[e_s]_t = \Delta d_s \tag{5.15}$$

where since a slip is generated between two elements as upper value multiplied by a normal compressive force to friction coefficient,

$$[e_n]_t < 0 \rightarrow [e_s]_t = [d_s]_t = 0 \tag{5.16}$$

$$\left|[e_s]_t\right| > \mu [e_n]_t \rightarrow [e_s]_t = \mu [e_n]_t \times SIGN\left([e_s]_t\right) \text{ and } [d_s]_t = 0 \tag{5.17}$$

From the above, a normal compressive force $[f_n]_t$ was given as

$$[f_s]_t = [e_s]_t + [d_s]_t \tag{5.18}$$

5.3 Outline of DEM Analyses

5.3.1 Model pipe

A model inner pipe consisted of a truss structure of a polygonal element of a tricontadigon as shown in **Figure 5.3**. Nakase et al. (2002) proposed that any structures are modeled using a circle element and an edge element. The VU pipe, the VP pipe and the AL pipe used in the test were modeled. In the truss structure, 64 elements were set on the double circle and each element was connected by the spring.

The normal spring coefficient of the model inner pipe was determined by a relationship between the normal spring coefficient and the elastic modulus. In DEM analyses, two point loading tests were conducted under various conditions including a center diameter of a model inner pipe d_c, a normal spring coefficient K_n, a distance between two elements of an outer circumferential of a polygonal element l, a normal distance t_m between an inner and an outer circumferential of a polygonal element as shown in **Figure 5.4**. The vertical deflection and the linear load obtained from these results was substituted in the equation (2.1) in Chapter 2. Thus, the relationship between $\frac{E_p t_p^{\,3}}{l t_m^{\,2}}\left(\frac{d_c}{D_c}\right)^3$ and K_n as shown in **Figure 5.5** was obtained. A broken line indicates a linear approximation line of relationships and the following equation is obtained by the linear

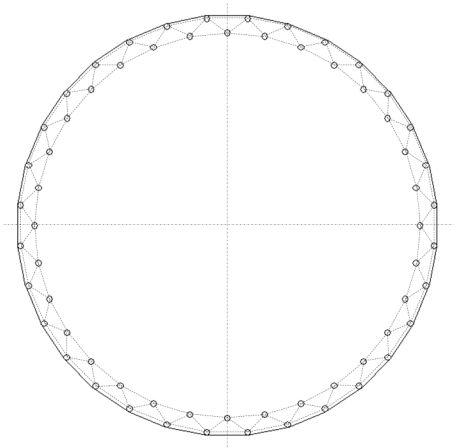

Figure 5.3 Model inner pipe

approximation.

$$K_n = 0.362 \frac{E_{p'} t_p^{\,3}}{l t_m^{\,2}} \left(\frac{d_c}{D_c} \right)^3 \tag{5.19}$$

where $E_{p'}$ is an elastic modulus per unit depth (N/mm^2/mm). In addition, when a center diameter of a test pipe was equivalent to that of a model pipe, equation (5.19) is expressed as

$$K_n = 0.362 \frac{t_p^{\,3}}{l t_m^{\,2}} E_{p'} \tag{5.20}$$

From the equation (5.20), the normal spring coefficient was calculated. **Table 5.1** shows the DEM parameters for model pipes. The outer diameter of the model pipe was equivalent to that of the test pipe and the element density of the model pipe was also equivalent to that of the test pipe. The thickness of the VU model pipe and the VP model pipe were equivalent to that of the VU test pipe and the VP test pipe. Since the calculation about the model pipe having the thickness of 2.0 mm diverged, the thickness of the AL

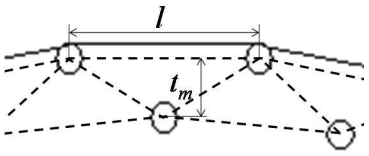

Figure 5.4 Definition of l and t_m

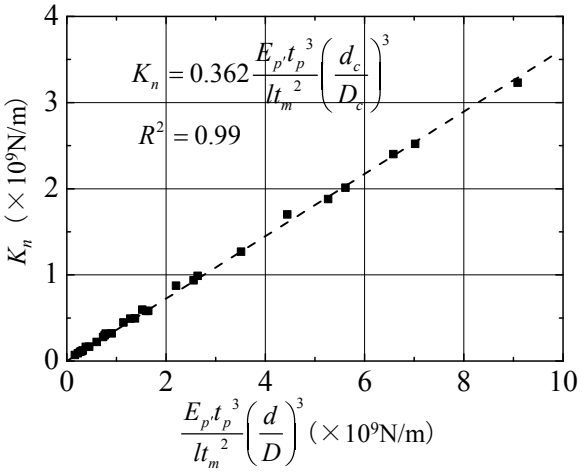

Figure 5.5 Relationship between $\frac{E_{p'} t_p^{\,3}}{l t_m^{\,2}} \left(\frac{d_c}{D_c} \right)^3$ and K_n

Table 5.1 Parameters for model inner pipe

Type of pipe	VU	VP	AL
Element radius (mm)	4.0	4.0	4.0
Outer diameter (mm)	140	140	150
Thickness of pipe (mm)	4.1	7.0	7.0
Element density (kg/m^3)	12,520	20,920	12,206
Normal spring coefficient (×10^{9}N/m)	1.70	1.27	0.49
Normal damping constant	0.5	0.5	0.5
Tangential spring coefficient (×10^{9}N/m)	4.25	3.18	1.24
Tangential damping constant	0.1	0.1	0.1
Surface friction coefficient	0.54	0.54	0.54

model pipe was 7.0 mm and the normal spring coefficient was determined as the ring bending stiffness of the AL model pipe was equivalent to that of the AL test pipe. The tangential spring coefficient was one-forty of the normal spring coefficient. The surface friction coefficient was determined by the result for the direct shear tests for silica sand and the vinyl chloride plate.

Figure 5.6 shows the model outer pipe. The model outer pipe consisted of a truss structure of a polygonal element as well as the model inner pipe. Each segment was connected by the spring. An edge element which was set on the outer circumferential prevent from a backfill material to penetrating the gap between segments. The normal spring coefficient was a value sufficient to not deform. The tangential spring coefficient and the normal and tangential damping constant was determined in the same manner as the model inner pipe. The surface friction coefficient between each segment was zero.

5.3.2 Model Backfill Material

The scale in DEM was equivalent to the scale in cyclic shear test as show in **Figure 5.7**. The model backfill material consisted a particle which had the average diameter of 2.0 mm and the uniformity coefficient of 1.52 since the calculation for the average diameter of silica sand used the cyclic shear test diverged. A rolling friction proposed by Sakaguchi et al. (1993) was used in order to express a shear strength had an actual soil material. The rolling friction M_r is expressed as

$$M_r = R \times F_n \times \tan\theta_r \tag{5.21}$$

where R is the radius of an element, F_n is the normal force at each contact and θ_r is the rolling friction angle.

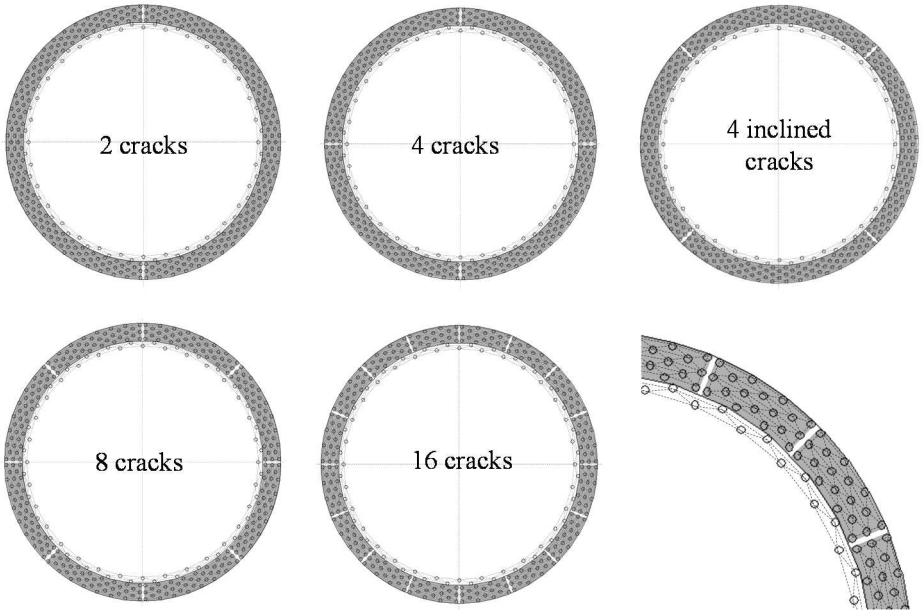

Figure 5.6 Schematic dialog of model outer pipe

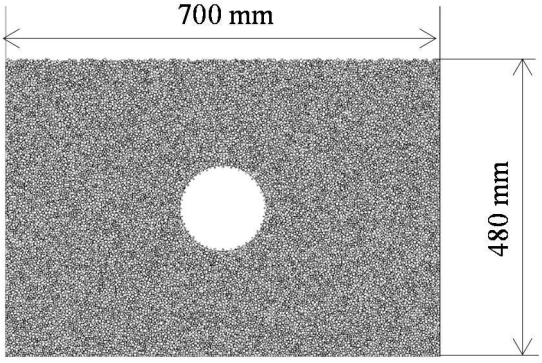

Figure 5.7 Schematic view of analysis

The parameters for model backfill material for relative density of 20, 45 and 65 % was determined through a trial and error process as the relationship between the shear strain of the laminar box and the 45-225 deg. deflection of the flexible pipe obtained from the results for cyclic shear simulation by DEM were fitted to that from the result for cyclic shear test at first cycle from 0 % to 5 %. The variables were the element density, the friction angel at each element and the rolling friction angle. The element density was determined as the density of the model backfill material was equivalent to that of silica

Table 5.2 Parameters for model backfill material

Relative density	20 %	40 %	65 %	85 %
Average diameter (mm)	2.0	2.0	2.0	2.0
Coefficient of uniformity	1.52	1.52	1.52	1.52
Element density (kg/m^3)	1,643	1,742	1,830	1928
Normal spring coefficient (×10^{9}N/m)	1.00	1.00	1.00	1.00
Normal damping constant	0.2	0.2	0.2	0.2
Tangential spring coefficient (×10^{9}N/m)	8.00	8.00	8.00	8.00
Tangential damping constant	0.2	0.2	0.2	0.2
Friction angel at each element (deg.)	20.0	26.1	29.9	36.8
Rolling friction angel (deg.)	20.0	26.1	29.9	36.8

sand for the test. **Table 5.2** shows the parameters for model backfill material. The procedure of the cyclic shear simulation was the same manner for the test.

5.3 Reproducibility of Test Resulting

Figure 5.8(a) shows the relationship between the shear strain of the laminar box and the 45-225 deg. deflection of the inner pipe in VUN-20, VUN-45 and VUN-65. **Figure 5.8(b)** shows the relationship in VUN-45, ALN-45 and VPN-45. For each relative density, the deflection of the pipe to the shear strain in analysis result was corresponding to that in the test result as shown in **Figure 5.8(a)**. For each ring bending stiffness, the analysis result was corresponding to the test result as show in **Figure 5.8(b)**. These results indicated that the deflection of the pipe to the shear strain in the laminar box was simulated for any relative density of the backfill material and any ring bending stiffness.

Figure 5.9 shows the relationship between the shear strain of the laminar box and the 45-225 degrees deflection of the inner pipe in VU2-45, VU4C-45, VU4I-45, VU8-45 and VU16-45. In VU2-45, VU4C-45 and VU4I-45, the deflection of the inner pipe to the shear strain in the analysis result was corresponding to that in the test result. In VU8-45 and VU16-45, although the deflection to the shear strain from zero to -5% in the analysis result was larger than that in the test result, the deflection to the other shear strain in the analysis result was corresponding to that in the test result. From these results, it was confirmed that the influence of the damage level of the outer pipe on the oblique

deflection of the inner pipe was simulated by DEM analyses.

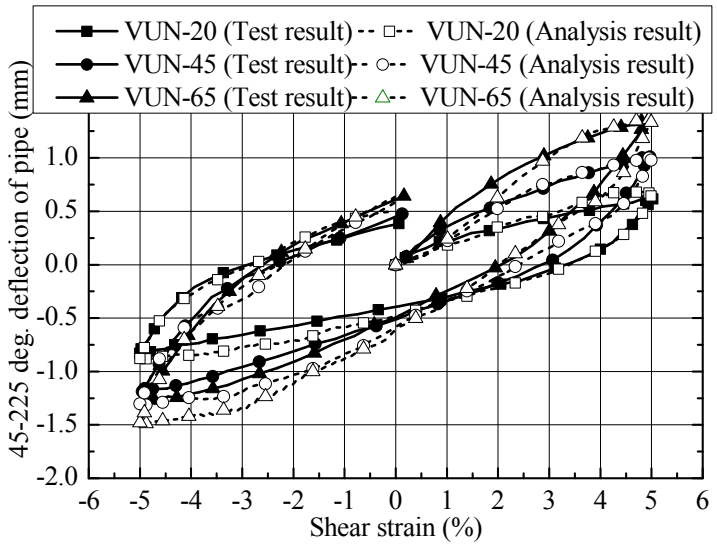

(a) VUN-20, VUN-45 and VUN-65

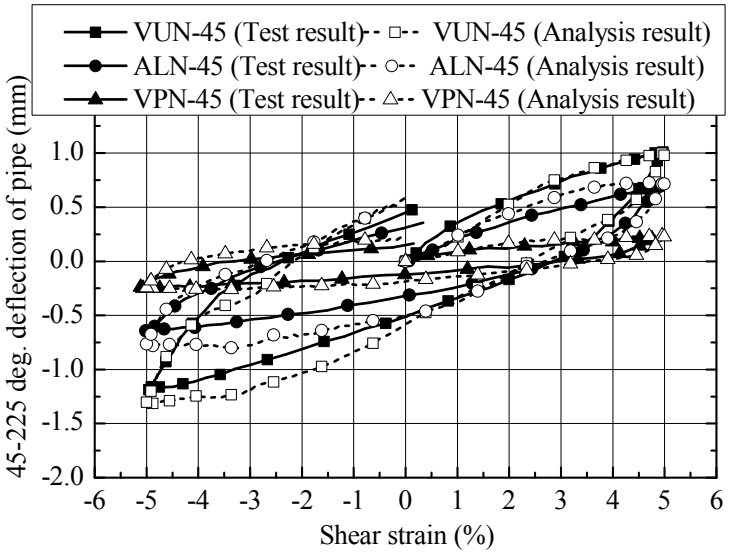

(b) VUN-45, ALN-45 and VPN-45

Figure 5.8 Relationships between shear strain and 45-225 deg. deflection of flexible pipe

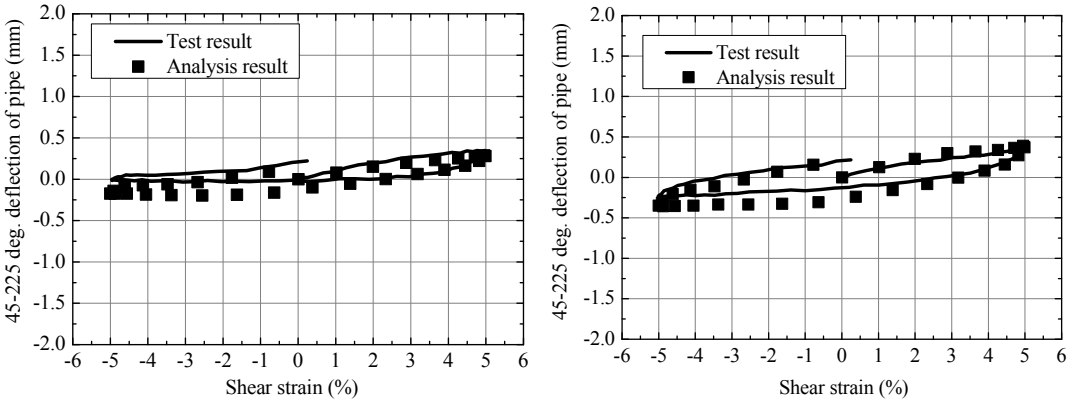

(a) VU2-45 **(b)** VU4C-45

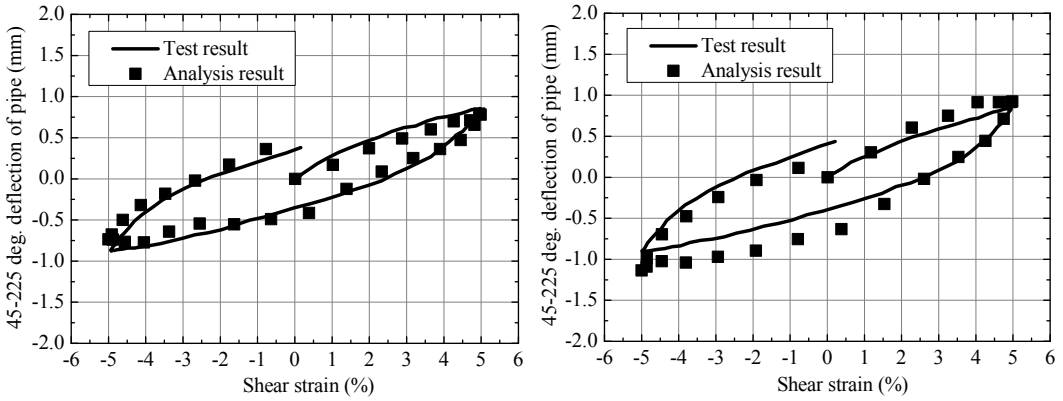

(c) VU4I-45 **(d)** VU8-45

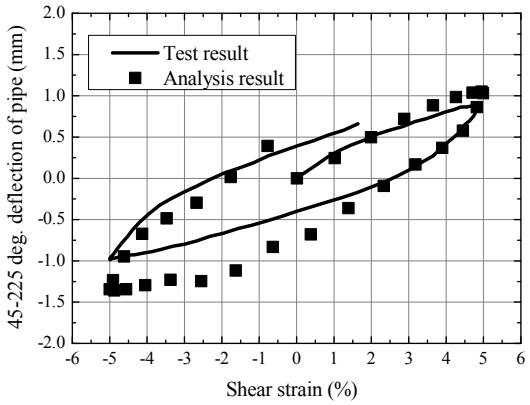

(e) VU16-45

Figure 5.9 Relationship between shear strain and 45-225 deg. deflection of inner pipe

Figure 5.10 shows the earth pressure distribution on the pipe when the shear strain of the side boundary reached at 5% in ALN-45. In DEM, the normal and tangential earth pressure was calculated by dividing the normal and tangential force into which the force acted on the edge element between each element was resolved by the length of the edge element of the model pipe, respectively. The normal and tangential earth pressure distribution in the analysis result was similar to that in the test result although the distribution in the analysis had more variable than that in the test result. It was assumed that the bias in the force transmitting in the backfill material was generated since the average diameter of the model backfill material in DEM was larger than that of silica sand used in the test.

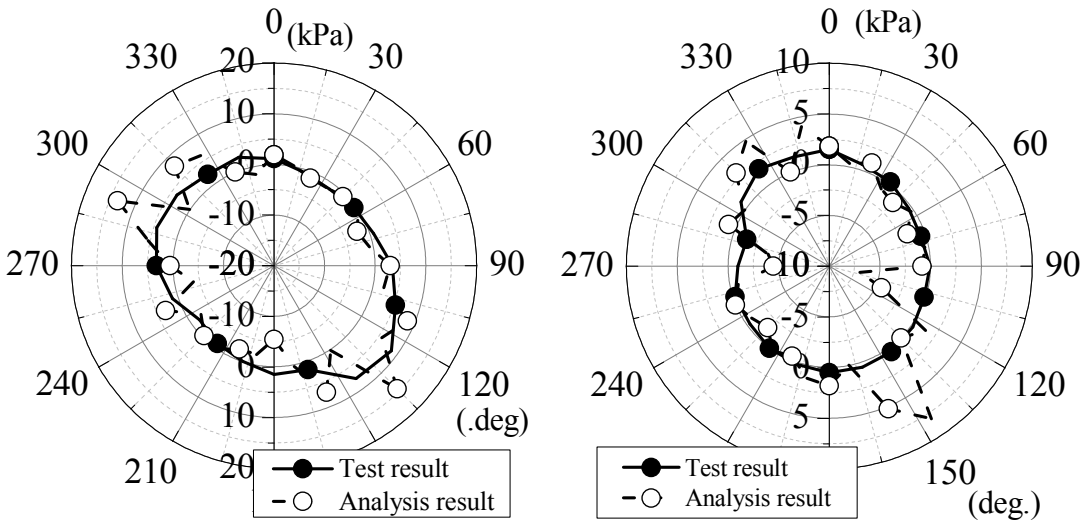

(a) Normal earth pressure **(b)** Tangential earth pressure

Figure 5.10 Earth pressure distribution in ALN-45

5.4 Deformation Mechanism of Inner pipe

Figure 5.11 shows the contact force distribution when the shear strain of the side boundary reached at 5% in VUN-45. A broken line indicates the installation position of the phosphor bronze in the cyclic shear test. The contact force was developed from the upper left boundary to the lower right boundary. Thus, when the model ground deformed into a parallelogram due to the shear deformation of the side boundary, the compressive force was acted on the shorter diagonal. The contact force which was more than 80 N was acted on the pipe from 90 to 135 degrees and from 270 to 315 degrees. These range was corresponding to the range to which the tensile inner circumferential strain was concentrated as shown in **Figure 4.9(a)** in chapter 4.

Figure 5.12 shows the deflection of the pipe to each direction when the shear strain reached at 5% in VUN-45. A tensile deflection is positive. 33.75-213.75 degrees deflection was large than 45-225 degrees deflection of the pipe which was measured in the test. 123.75-303.75 degrees deflection was smaller than 135-315 degrees measured in the test.

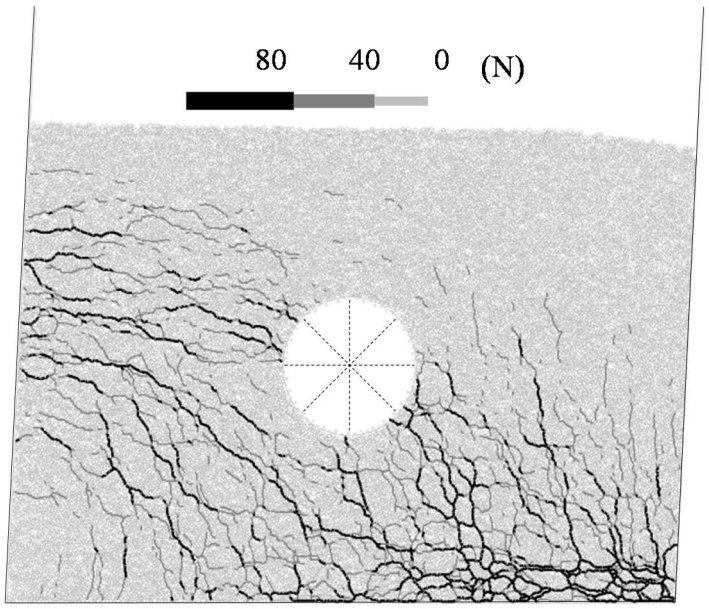

Figure 5.11 Contact force distribution in VUN-45

The deformation mechanism of the inner pipe judging from above results are shown in **Figure 5.13**. When the shear deformation was generated under the ground due to earthquake, the compressive normal earth pressure was acted on the pipe from 90 to 135 degrees and from 270 to 315 degrees, and the tangential earth pressure was acted along the pipe from the range of the normal earth pressure. As the results, the oblique deflection of the pipe was developed.

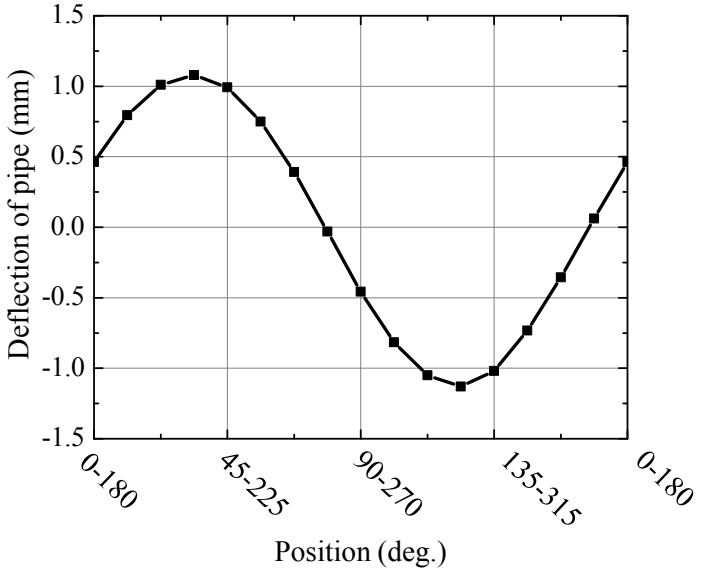

Figure 5.12 Deflection distribution in VUN-45

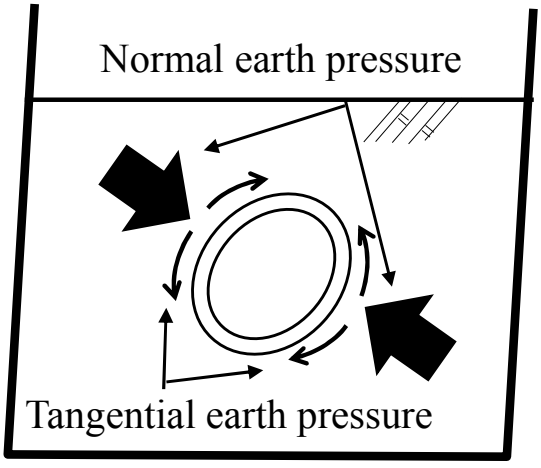

Figure 5.13 Deformation mechanism of inner pipe due to shear deformation

5.5 Formulation for Oblique Deflection of Inner Pipe

In order to formulate the oblique deflection of the inner pipe due to the shear deformation, a deformation modulus of the backfill material was determined by the consolidated triaxial compression test under the change of confining pressure in each relative density of the silica sand. As shown in **Figure 5.14**, the deformation modulus E_{50} is given as

$$E_{50} = \frac{q_n / 2}{\varepsilon_{50}} \tag{5.22}$$

where q_n is the maximum deviator stress, ε_{50} is the axial strain to half maximum deviator stress. **Figure 5.15** shows the relationship between the mean stress and the deformation modulus. A solid line shows a linear approximation line. The deformation modulus in each relative density was defined as the value of the intercept $E_{50\text{-}0}$, since the overburden pressures acted on the top of the pipe in Dr = 20, 45, 65 and 85 % were 2.1, 2.3, 2.4 and 2.5 kPa, respectively. Also, $E_{50\text{-}0}$ in Dr = 20, 45, 65 and 85 % were 5.46, 9.28, 14.7 and 20.7 MPa, respectively.

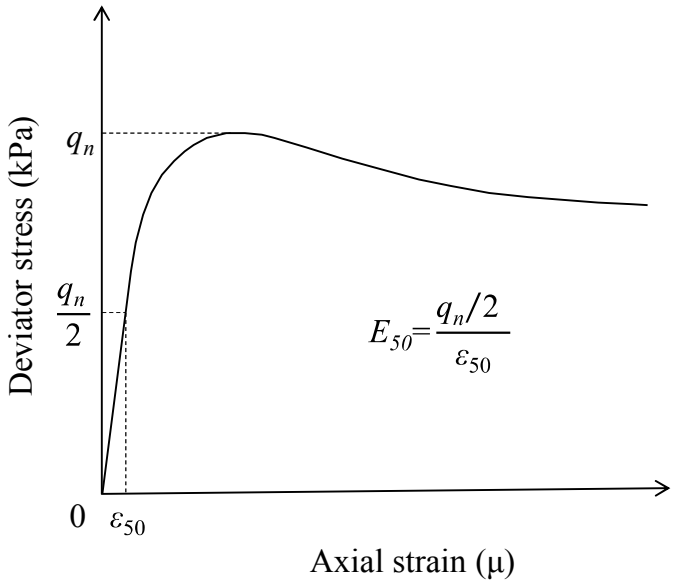

Figure 5.14 Relationship axial strain and deviator stress

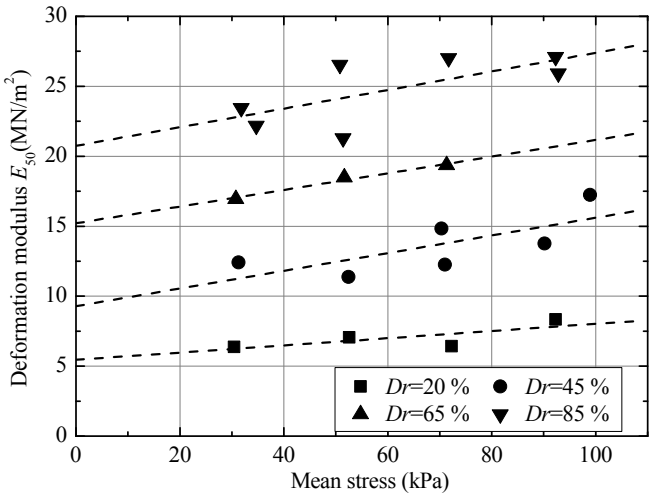

Figure 5.15 Relationships between mean stress and deformation modulus

Figure 5.16 shows the relationship between $E_{50} / (E_p I / D_c^3)$ and δ / D_c, where δ is the 45-225 deg. deflection of the pipe. The oblique deflection rate of the inner pipe increased in DEM analyses. Total twenty cases under various conditions including four types of the relative density of the model backfill material (*Dr*=20, 45, 65 and 85%) and five types of the different ring bending ($E_p I / D_c^3$ =2.89, 8.8, 14.2, 42.1, 130 kN/m^2). When the pipe was rigid, the deflection was zero to any shear strain. As the value of $E_{50} / (E_p I / D_c^3)$ increased, the deflection increased. It was assumed that the deflection rate converged at an asymptotic value.

The asymptotic value was determined by a geometric calculation. It was hypothesized that a shear deformation of a backfill material and a flexible pipe is shown is **Figure 5.17**. In this deformation, γ is a shear strain (=tanα'), the oblique deflection of the pipe is Δ (= 2Δ'), the center of the ellipse is the origin and the following equation is given.

$$\frac{x^2}{a^2} + \frac{y^2}{b^2} = 1 \tag{5.23}$$

In addition, since the absolute of the compressive deflection in the direction of the 45-225 degrees were approximately equal to the absolute of the tensile deflection in the direction of the 135-315 degrees at the first cycle as shown in **Figure 4.7(b)**, the following equation is assumed.

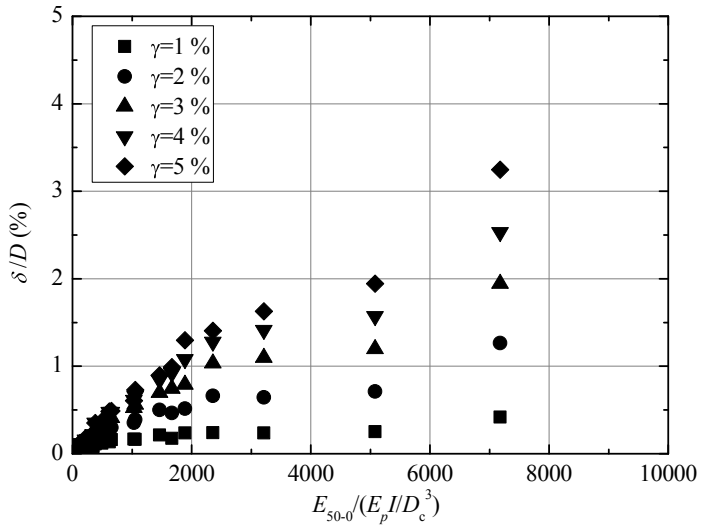

Figure 5.16 Relationships between $E_{50} / (E_p I / D_c^3)$ and δ / D_c for analyses results

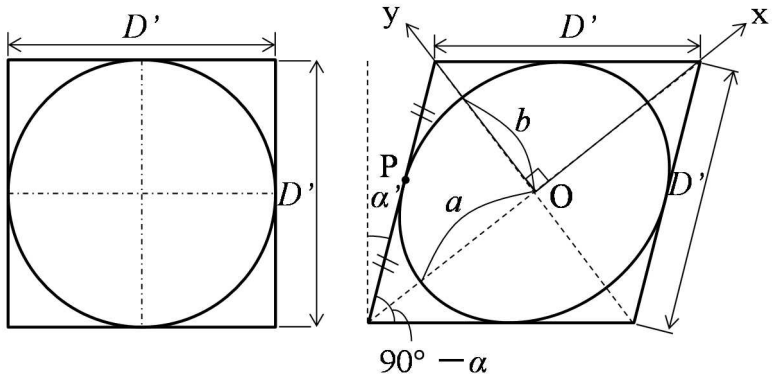

Figure 5.17 Geometric deformation of a flexible pipe due to a shear deformation

$$a + b = D' \tag{5.24}$$

The ellipse equations at a point P is expressed as

$$\frac{\left(\frac{1}{2}D'\cos\frac{90-\alpha'}{2}\right)^2}{a^2} + \frac{\left(\frac{1}{2}D'\sin\frac{90-\alpha'}{2}\right)^2}{b^2} = 1 \tag{5.25}$$

The equation (5.24) is rearrangement as

$$a = \frac{D'}{2} + \Delta', b = \frac{D'}{2} + \Delta' \tag{5.26}$$

The equation (5.26) is substituted in the equation (5.25) and the following equation is obtained.

$$A^2\left(\frac{D'^2}{4} - D'\Delta' + \Delta'^2\right) + B^2\left(\frac{D'^2}{4} + D'\Delta' + \Delta'^2\right) = \left(\frac{D'^2}{4} - D'\Delta' + \Delta'^2\right)\left(\frac{D'^2}{4} + D'\Delta' + \Delta'^2\right) \tag{5.27}$$

where $A = \frac{1}{2}D'\cos\frac{90-\alpha'}{2}, B = \frac{1}{2}D'\sin\frac{90-\alpha'}{2}, A^2 + B^2 = \frac{D'^2}{4}$

The equation (5.27) is rearrangement as

$$\Delta'^3 - \frac{3}{4}D'^2\Delta' + (A^2 - B^2)D' = 0 \tag{5.28}$$

Δ' is obtained as the general solution of a cubic equation. From the calculation result for *Δ'* to various *D'*, *Δ* is expressed as

$$\Delta = \frac{2}{3}D'\gamma \tag{5.29}$$

The relationship between $E_{50}/(E_pI/D_c^3)$ and the 45-225 degrees deflection of the pipe was approximated by Box-Lucas model. Box-Lucas model expressed a curved line which passes from an origin to an asymptotic value and is basic and simple model. Box-Lucas model is expressed as

$$f(x) = p\left(1 - e^{-qx}\right) \tag{5.30}$$

$$\frac{dE(x)}{dx} = q\left(p - f(x)\right) \tag{5.31}$$

where the coefficient *p* is the asymptotic value. When the deflection to the shear strain from 1% to 5% was approximated by Box-Lucas model as *p* =*Δ*, coefficient *q* in *γ* =1, 2, 3, 4 and 5% were 1.7×10^4, 2.6×10^4, 2.8×10^4, 2.6×10^4 and 2.3×10^4, respectively. When the value of coefficient *q* was fixed at 2.5×10^4, the equation (5.30) was expressed as

$$\frac{\delta}{D}=\frac{2}{3}\gamma\left(1-\exp\left(-\frac{2.5\times10^{-4}E_{50-0}}{EI/D^3}\right)\right) \tag{5.32}$$

where δ is the 45-225 degrees deflection of the pipe.

Figure 5.18 shows the relationship between $E_{50}/(E_pI/D_c^3)$ and δ/D. Solid lines shows this approximate curve and plots shows the analysis results. Coefficients of determination in γ =1, 2, 3, 4 and 5% were 0.57, 0.93, 0.97, 0.98 and 0.97, respectively. The approximate curved lines gave good agreement with the analysis result in spite of case in γ =1 % because i the pipe was hardly deformed since the shear stress in γ =1%

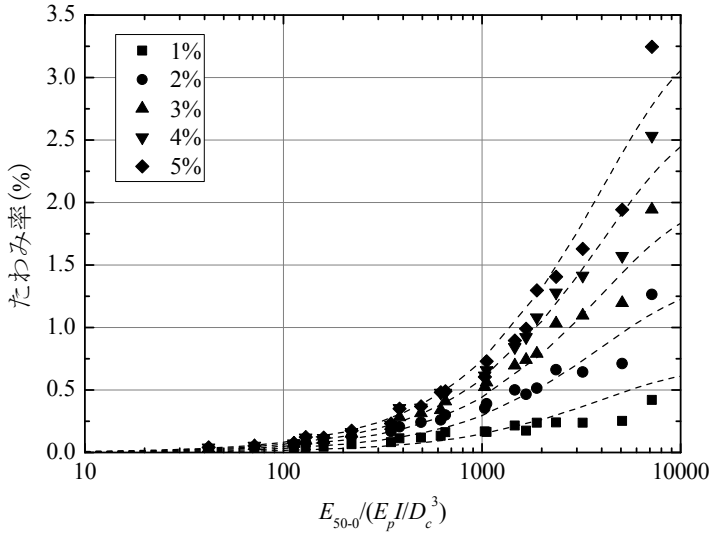

Figure 5.18 Relationships between $E_{50}/(E_pI/D_c^3)$ and δ/D_c for approximate curve line

acted on the pipe was extremely small.

The deflection of the inner pipe decreased according to the damage level or the outer pipe in comparison with that of the inner pipe without the outer pipe as described in Chapter 4. The effect of decreasing was expressed by introducing the decreasing coefficient C_h to the equation (5.32). C_h was multiplied by the right side of the equation and the following equation was obtained.

$$\frac{\delta}{D}=\frac{2}{3}C_h\gamma\left(1-\exp\left(-\frac{2.5\times10^{-4}E_{50-0}}{EI/D^3}\right)\right) \tag{5.33}$$

C_h was categorized as shown in **Table 5.3** on the basis of **Table 4.5** obtained from the test results. In Compaction 1, the relative density of the backfill material was 85% and over,

and in compaction 2, that was under 65%.

Figure 5.19 shows the relationship between $E_{50}/(E_pI/D_c^3)$ and δ/D for rehabilitated pipe. A broken line shows the approximate curved line obtained from the

Table 5.3 Categorization of decreasing coefficient

	Compaction	Damage level of outer pipe	C_h
Group 1	Compaction 1 and 2	cracks without inclined direction	0.35
Group 2	Compaction1	cracks with inclined direction	0.70
Group 3	Compaction 2		0.90

equation (5.33). The scatter plots show the values obtained from the test results. In all group, the test result was partially predicted by the approximated equation. From the result, it was found that the deflection of the rehabilitated pipe was calculated on the basis of the damage level of the outer pipe and the relative density of the backfill material by introducing the decreasing coefficient $C_{h.}$.

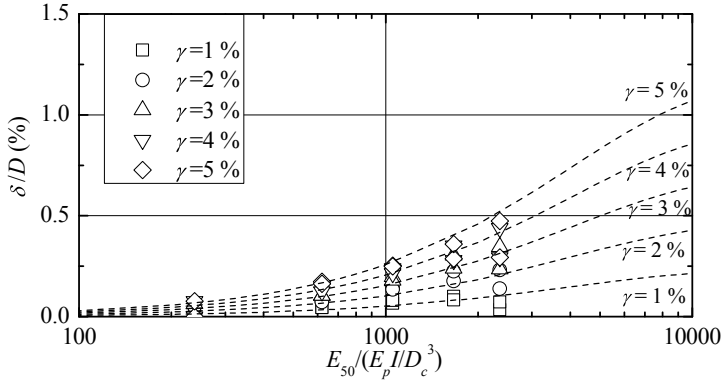

(a) Group 1

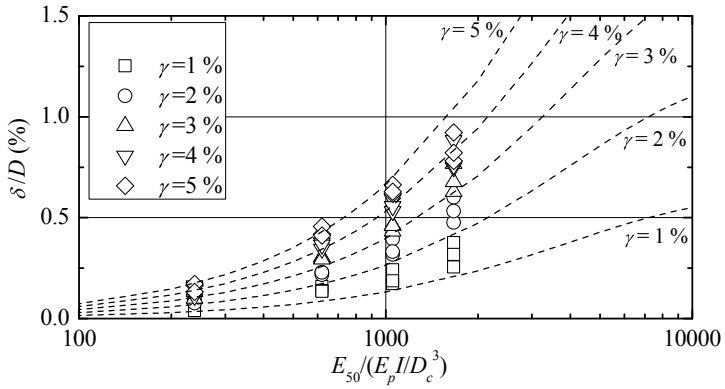

(b) Group 2

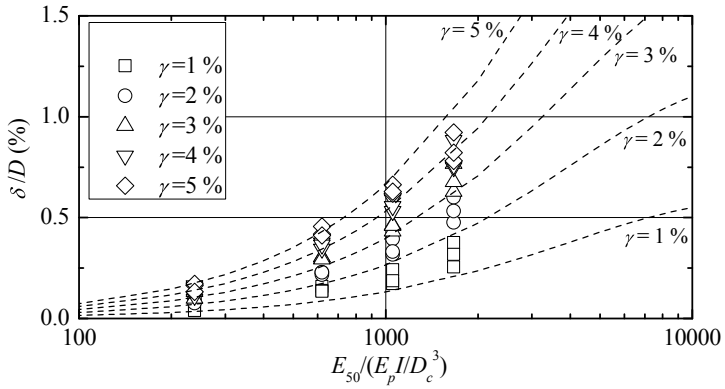

(c) Group 3

Figure 5.18 Relationship between $E_{50} / (E_p I / D_c^3)$ and δ / D_c introduced C_h

5.6 Conclusions

In this chapter, two dimensional discrete element method (DEM) analyses were conducted in order to verify the deformation mechanism of the inner pipe with and without the outer pipe during earthquake and formulate the oblique deflection of the inner pipe to shear strain of the ground. From the analysis results, the following findings were obtained.

1. The relationship between the normal spring coefficient and the elastic modulus had a linear. The pipe which had any bending ring stiffness could be modeled.
2. The deflection of the pipe to the shear strain in the laminar box was simulated for any relative density of the backfill material and any ring bending stiffness.
3. The influence of the damage level of the outer pipe on the oblique deflection of the inner pipe was simulated.
4. When the shear deformation was generated under the ground due to earthquake, the compressive normal earth pressure was acted on the pipe from 90 deg. to 135 deg. and from 270 deg. to 315 deg. (45 deg. to 90 deg. and 225 deg. to 270 deg.), and the tangential earth pressure was acted along the pipe from the range of the normal earth pressure. As the results, the oblique deflection of the pipe was developed.
5. The oblique deflection rate of the flexible pipe to $E_{50}/(E_pI/D_c^3)$ had the asymptotic value. The asymptotic value was determined by a geometric calculation. The relationship between $E_{50}/(E_pI/D_c^3)$ and the 45-225 deg. deflection of the pipe was approximated by Box-Lucas model. In addition, the deflection of the rehabilitated pipe was calculated on the basis of the damage level of the outer pipe and the relative density of the backfill material by introducing the decreasing coefficient C_h..

References

Cundall, P.A. and Strack, O.D.L. (1979): A Discrete Numerical Model for Granular

Assemblies, Géotechnique, 29, No.1. pp. 47-65.

Nakase, H., Miyata, M., Nagao, T., Honda, A., Kyouno, T., Yasuda, K. and Sugano, T. (2002) : Application of DEM to Deformation Analysis for Caisson Type Breakwater, Journal of Applied Mechanics, vol.5, pp. 461-472.

Sakaguchi H., Ozaki, E. and Igarashi, T. (1993) : Plugging of flow of granular materials during the discharge from a silo, Int. Journal of Modern Physics B, Vol. B7, pp. 1949-1963.

CHAPTER 6

The contents of this chapter are based on:

Izumi., A, Ono, K., Takahara, S., Sawada, Y., Ariyoshi, M. and Kawabata, T. : Shaking Table Test for Axial Behavior of Buried Inner Rehabilitated Pipes Affected by Aging Pipes in Liquefied Ground, *Proc. of Pipeline 2015*, ASCE, pp.316-324, 2015

Izumi., A, Ono, K., Takahara, S., Sawada, Y., Ariyoshi, M. and Kawabata, T. : Axial Behavior of Buried Rehabilitated Pipes in Liquefied Ground, *Transportation Infrastructure Geotechnology*, Springer (submitted)

.

Chapter 6

Axial Behavior for Pipe Rehabilitation in Liquefied Ground

6.1 Introduction

It is important to clear axial behavior of pipes during earthquake as with to cross section behavior. In chapters 4 and 5, cross-section behavior for pipe rehabilitation during earthquake was discussed from the results of cyclic shear tests and DEM analyses. An outer pipe such as a reinforced concrete pipe has joints. As the previous study, shaking table test, model test using sinking-soil-box and centrifuge test were conducted to verify the influence of ground deformation on axial behavior of pipes or joints of pipes. From test results of shaking table test, Fujita et al. (2007) evaluated an allowable range of joint for expansion and bending on pipeline that formed with flexible joints and Tanaka et al. (2005) cleared that the use of ball type flexible joint has reduced significantly the vertical thrust on the joint that usually observed during the ground settlement after the liquefaction. In addition, Kitaura and Miyajima (1983) conducted shaking table test for a model pipe fixed at one end in liquefied ground to verify a destruction of pipes due to floating of its. Takada and Yamabe (1982) proposed a model test using a sinking-soil-box and measured stress acting on pipes and deformation of joints of pipes when ground sank. Hachiya et al. (2005) proposed a rational design method for buried pipelines subjected to differential

ground settlement on the basis of a data set from 3D centrifuge model tests. Alireza et al. (2014) monitoring the performance of pipe rehabilitation using acoustic emission technique, subjected to static and dynamic loading. Particularly, two damage mechanisms are investigated-delamination between outer pipe and inner pipe, and incipient failure of the inner pipe. Da et al. (2008) were conducted two pairs of centrifuge tests designed to investigate the differences in behavior of buried high-density polyethylene pipelines subjected to normal and strike -strip faulting.

The influence of damaged outer pipes on inner pipes in the axial direction during an earthquake is unclear. In this chapter, shaking table tests were conducted at the National Institute for Rural Engineering in Japan to verify the dynamic behavior of the axial direction of the inner pipe used for the method. To model inner pipes, polyvinyl-chloride (PVC) and polyethylene (PE) pipe, which were 3,040 mm in length and 140 mm in diameter, were used. To model outer pipes, different types of concrete pipes in length were used.

6.2 Outline of Shaking Table Test

6.2.1 Test Equipment

The shaking table used for the test had plane dimensions of 6 m × 4 m, with the maximum loading capacity of 50 tf. Its excitation system was an electro-hydraulic servo. The test pit (5.6 m length, 3.6 m width, and 1.3 m height) as shown in **Figure 6.1**, was installed on the shaking table. At the bottom of the test pit, a bed of crushed stone was included to enhance the capabilities of pouring water into the ground.

For the model pipe, the bending strain in the axial direction and the horizontal acceleration, the horizontal displacement of the pipe end, and the pore water pressure in the model ground were measured. **Figure 6.1** shows the layout of measurements.

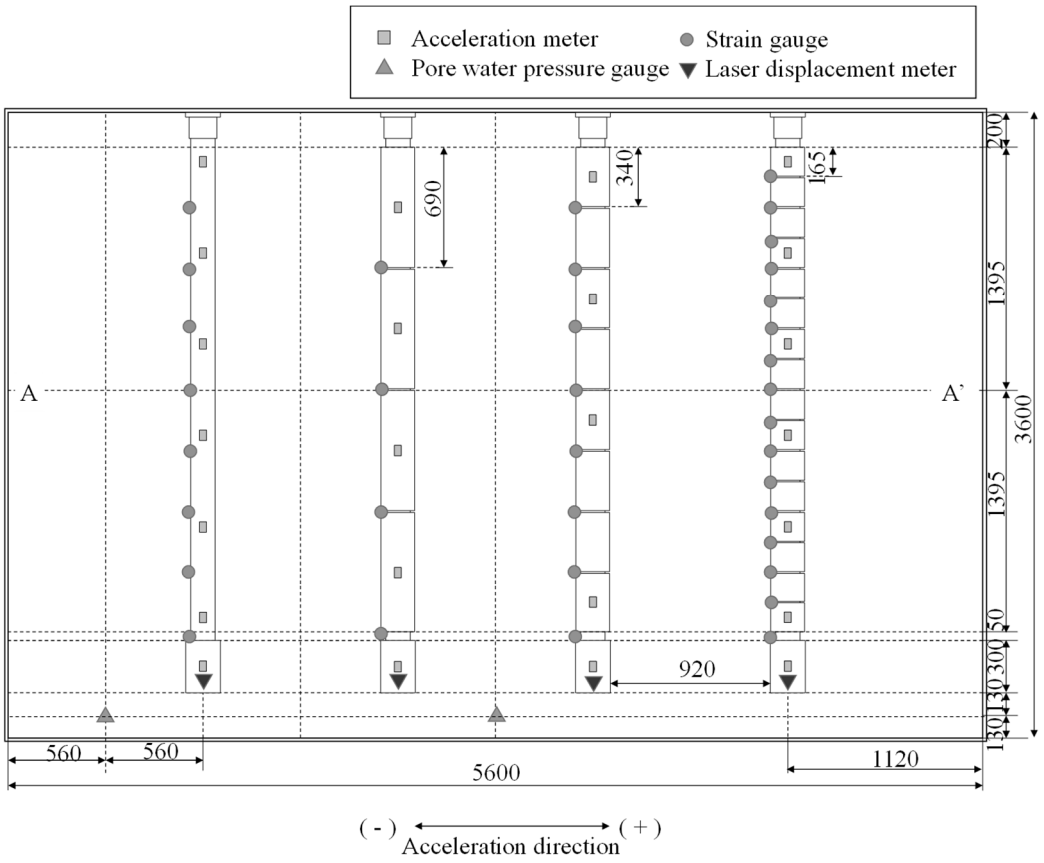

(a) Top view

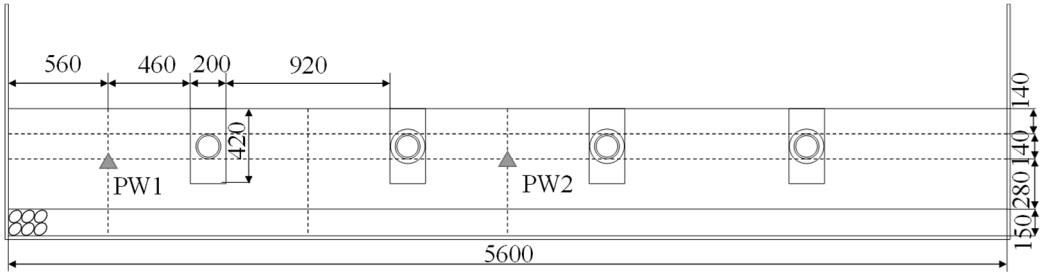

(b) Cross-section view

Figure 6.1 Schematic layouts of model pipes and sensors

6.2.2 Model Ground

Kasumigaura-sand was used as a soil material for the model ground. **Table 6.1** shows the properties of Kasumigaura-sand. The unsaturated ground was adequately compacted to achieve the target relative density of 50%.

Table 6.1 Properties of Kasumigaura-sand

Density of soil particle ρ_s	2.72 g/cm^3
Maximum dry density ρ_{dmax}	1.58 g/cm^3
Minimum dry density ρ_{dmin}	1.36 g/cm^3
Maximum void ratio e_{max}	0.99
Minimum void ratio e_{min}	0.72
Relative density D_r	50%

6.2.3 Model Pipe

PVC and PE pipes were used as inner pipes. Their properties are shown in **Table 6.2**. One end of the inner pipe was rigidly-connected to the test-pit wall, as shown in **Figure 6.1**. Lead shot and silica sand were inserted into the inner pipes to prevent the model pipe from floating during liquefaction. Both ends of the inner pipe were waterproofed. A concrete block weighting 50 kg was installed at the other end. When inertia forces were applied to the concrete block during shaking, it was expected that deflections of the pipe efficiently amplified. The block was hoisted by chains to avoid sinking in the liquefied ground.

Table 6.2 Properties of Inner pipe

	Length L (mm)	Thickness t (mm)	Outer Diameter D (mm)	Bending stiffness EI (kN · m)
PVC	3,000	4.1	140	15,354
PE	3,000	7.0	140	7,250

Concrete pipes were made to simulate RC pipes as outer pipes. These pipes had an inner diameter of 140 mm and a thickness of 27 mm. They were made in three-different lengths: with four segments (three joints), eight segments (seven joints), and 16 segments (15 joints) as shown in **Figure 6.2**. They were divided in the axial. After curing for seven days, the unconfined compression strength of the concrete was 22.72 N/mm^2.

Figure 6.2 Concrete pipe

The outer diameter of the inner pipe corresponded to the inner diameter of the outer pipe. Outer pipes were tightly fit to inner pipes. To prevent outer pipes from sliding, the pipe was restricted by a band. The gap between outer pipes was 10 mm and was covered by membranes to simulate a joint structure in the axial direction.

6.2.4 Procedure of Test

Experiments were conducted using different types of inner pipe and outer pipe as shown in **Table 6.3**. Horizontal shakings were applied after backfilling. The model pipes were buried at a depth of 140 mm (1D). The ground was saturated from the bottom of the pit. Input acceleration generated a sinusoidal wave at the frequency of 2 Hz with the maximum acceleration of 500 Gal as shown in **Figure 6.3**. **Figure 6.4** shows the response of the horizontal displacement of the shaking table.

Table 6.3 Test cases

Series	Case	Type of inner pipe	Type of outer pipe
A	PVC00	PVC	N/A
	PVC03		Three joints
	PVC07		Seven joints
	PVC15		15 joints
B	PE00	PE	N/A
	PE07		Seven joints
	PE15		15 joints

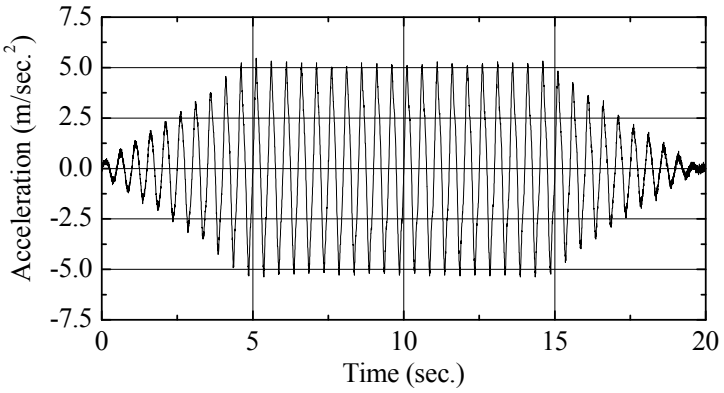

Figure 6.3 Response of acceleration of shaking table

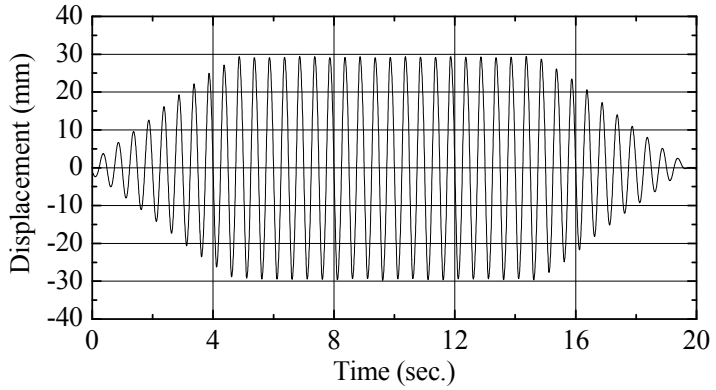

Figure 6.4 Response of horizontal displacement of shaking table

6.3 Response of Horizontal Displacement of Pipe

Figure 6.5 shows response of excess pore water pressure ratio. Liquefaction occurred during the shaking, judging from the excess pore water pressure ratio as shown in **Figure 6.5** in both series. An excess pore water pressure ratio was calculated as the ratio of the initial effective stress to the change of the excess pore water pressure. The excess pore water pressure ratio increased at approximately 2.5 seconds from the start of the shaking. However, the excess pore water pressure ratios did not reach 1.0, indicating that the ground did not liquefy completely.

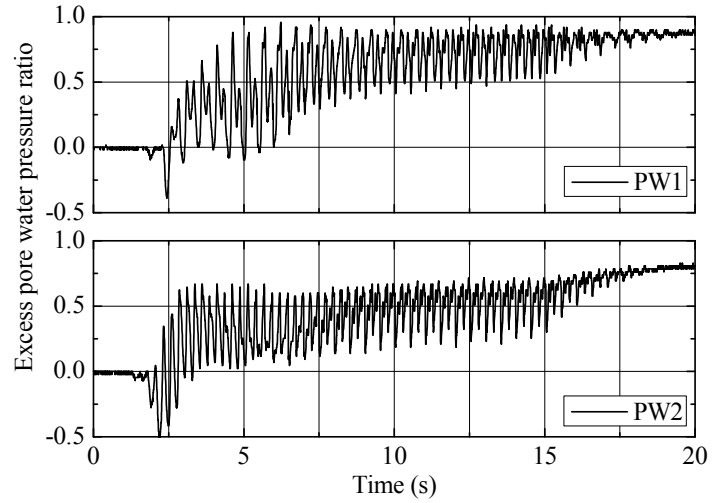

(a) Series A

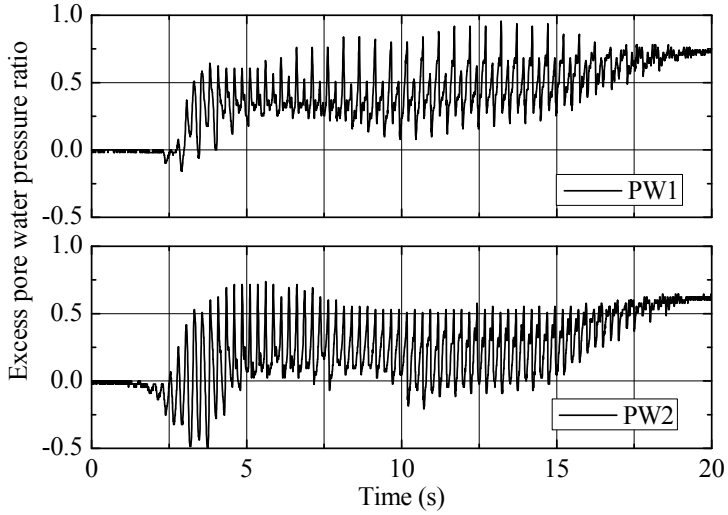

(b) Series B.

Figure 6.5 Response of excess pore water pressure ratio

The influence of the number of joint structures on the horizontal displacement of the pipe was extremely small. **Figure 6.6(a)** shows the response of the horizontal displacement of the pipe end in Series A. In every case, the end of the pipe moved horizontally due to the liquefaction as shown in **Figure 6.5**. The horizontal displacement of the pipe end increased with the increment of acceleration of the shaking table. The difference between the maximum displacement and the minimum for PVC00, PVC03, PVC07, and PVC15 is 107 mm, 114 mm, 112 mm and 105 mm, respectively. As shown in **Figure 6.6 (b)**, the horizontal displacement in Series B was also similar to that in Series A.

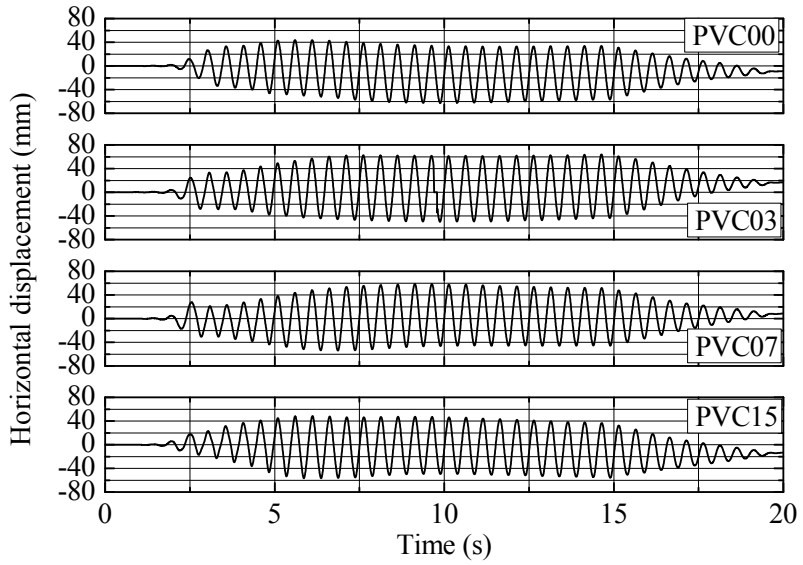

(a) Series A

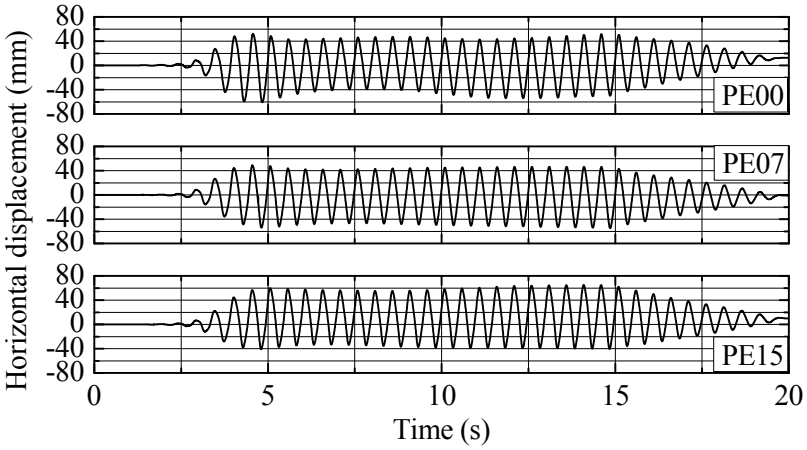

(b) Series B

Figure 6.6 Response of horizontal displacement of end of pipe

6.4 Influence of Damage Levels of Outer Aging Pipe

The amplitude of the bending strain that PVC pipe had on the outer pipe was large when the liquefaction occurred. **Figure 6.7(a)** shows the response of the bending strain at the center (A-A' section as shown in **Figure 6.2**) in Series A. In PVC00, the amplitude

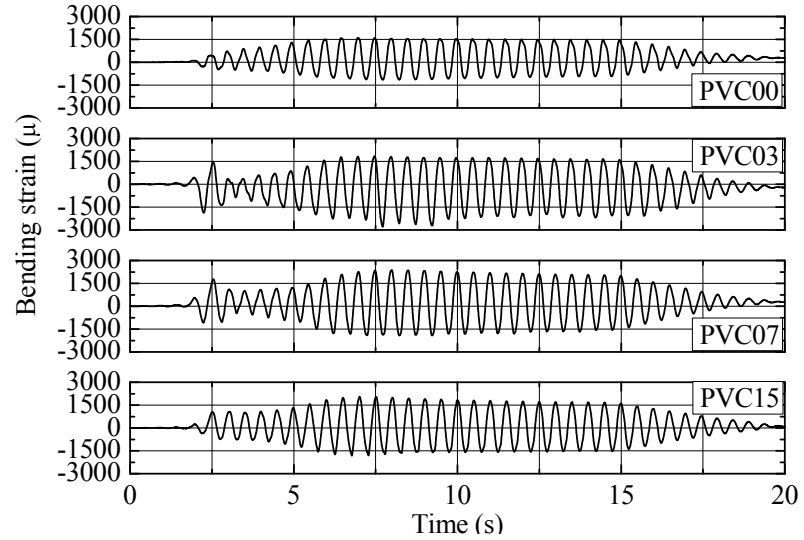

(a) Series A

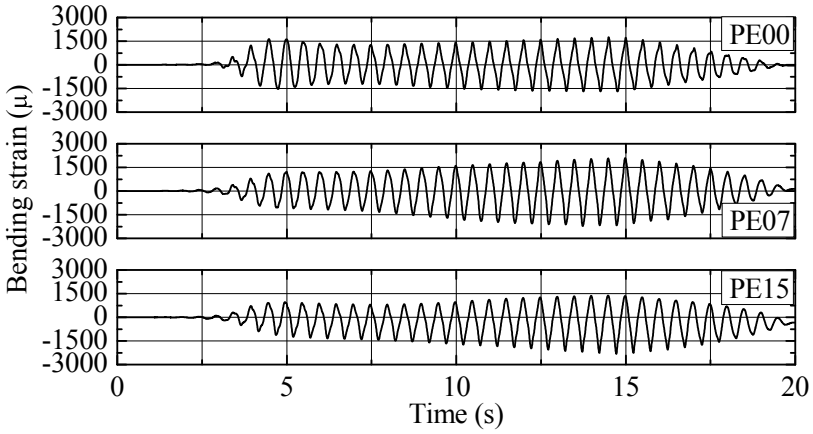

(b) Series B

Figure 6.7 Response of bending strain of inner pipe at center

of the bending strain increased, depending on the increasing amplitude of acceleration of the shaking table. For PVC00, PVC03, PVC07 and PVC15, the amplitude reached 284 μ, 1,793 μ, 1,075 μ and 358 μ, respectively, at approximately 2.3 sec. when the ground liquefied. Tease results indicate that the outer pipe restricted the deformation of inner pipe when it was moved. Therefore, the stress was concentrated at the gaps between the outer pipes.

Figure 6.8 shows relationships between the horizontal displacement of the pipe end and the bending strain at the center in every case. A broken line indicates linear approximate line of relationships. The gradient of approximate line in PVC00, PVC03, PVC07 and PVC15 were 57.9, 166.1, 76.9 and 40.3, respectively. **Figure 6.9** shows the

relationship between the length of outer pipe and the gradient. A solid line indicates linear approximate line of the relationship. The slope increased in proportion to the length of the outer pipe. From the result, it was revealed that the value of strain of inner pipe at the gaps between the outer pipes depended on the length of the outer pipes

On the other hand, the concentration at the gaps between the outer pipes did not occur in the PE pipe. **Figure 6.7(b)** shows the response of the bending strain at the center in Series B. The wave form for PE00 showed no difference from the wave form for PE07

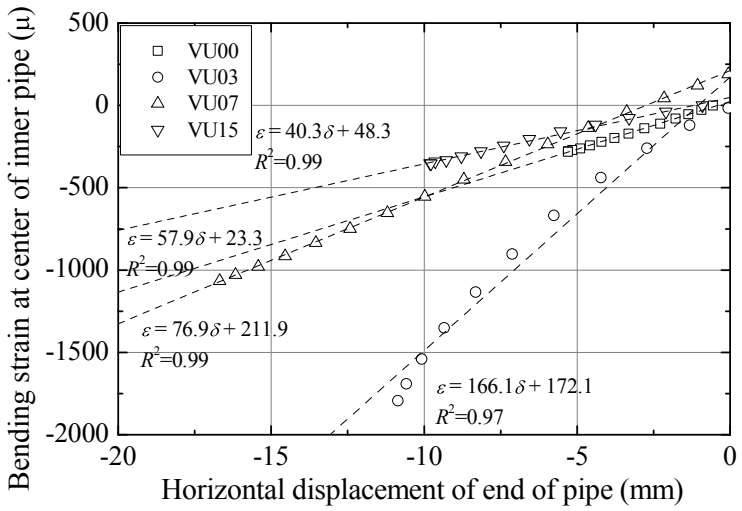

Figure 6.8 Relationships between horizontal displacement of the pipe end and bending strain at the center

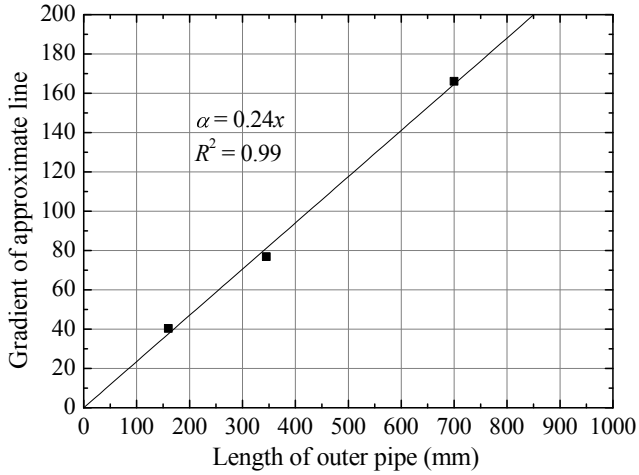

(b) Series B

Figure 6.9 Relationship between length of outer pipe and gradient of approximate line

and PE15 at the time when the ground liquefied. In addition, the amplitude of the bending strain increased from 7.5 to 15 seconds in every case, although the amplitude of the acceleration of the shaking table was constant at 5.0 m/ seconds squared. The creep of the PE pipe is considered to cause this result.

6.5 Deflection Mode of Inner Pipe

The deflection mode of the model pipes was categorized, in every case, into two main types: bow-shaped and pendulum-shaped deformation. **Figure 6.10** shows the acceleration distribution, and **Figure 6.11** shows the bending strain distribution in Series A. The displacement of the shaking table is 0 mm (t = 8.0) in **Figure 6.10(a)** and **Figure 6.11 (a)**, and the displacement is the maximum at approximately 30 mm (t = 8.125) in **Figure 6.10(b)** and **Figure 6.11(b)**. The acceleration distribution looks bow-shaped as shown in **Figure 6.10(a)**, and the bending strains at the rigid ends and around the centers developed as shown in **Figure 6.11(a)**. However, the model pipes were deformed like a pendulum-shaped, judging from **Figure 6.10(b)** and **Figure 6.11(b)**. The bending strain of a bow-shaped deformation is clearly larger than that the bending strain of a pendulum-shaped deformation. Deflection mode of PE pipe is similar to that of PVC. **Figure 6.12** shows the acceleration distribution, and **Figure 6.13** shows the bending strain distribution of in Series B. When the displacement of the shaking table was 0 mm, the PE pipe was deformed similarly to the PVC pipe as shown in **Figure 6.12(a)** and **Figure 6.13(a)**. In addition, the PE pipe was also deformed like pendulum-shaped when the displacement of the shaking table was approximately 30 mm as shown in **Figure 12(b)** and **Figure 13(b)**.

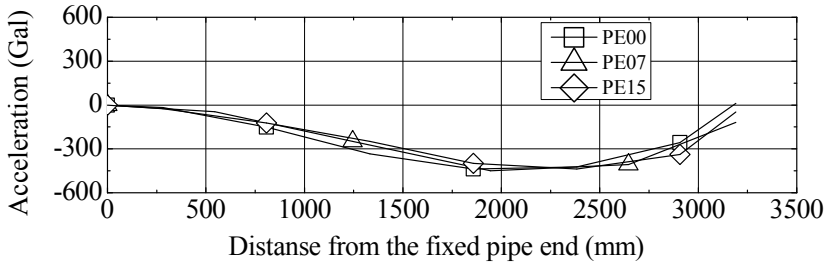

(a) t = 8.0

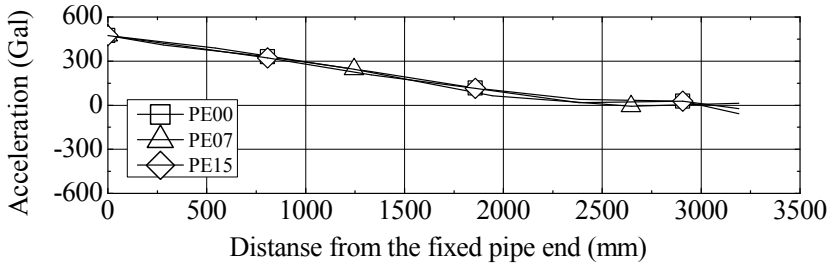

(b) t = 8.125

Figure 6.12 Acceleration distribution of model pipe in Series B

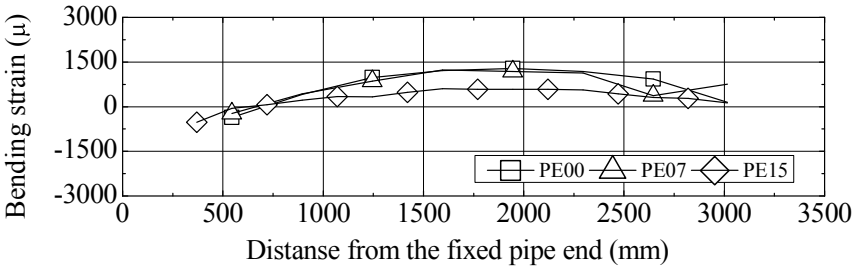

(a) t = 8.0

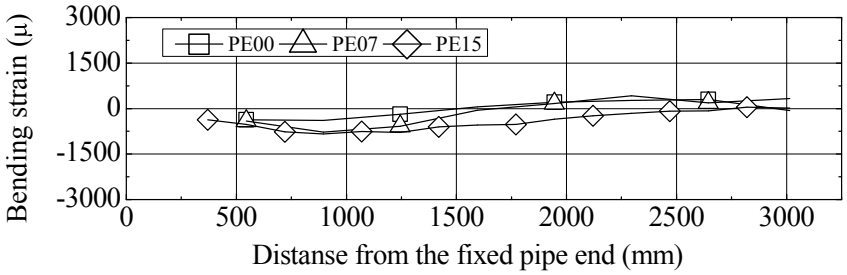

(b) t = 8.125

Figure 6.13 Bending strain distribution of model pipe in Series B

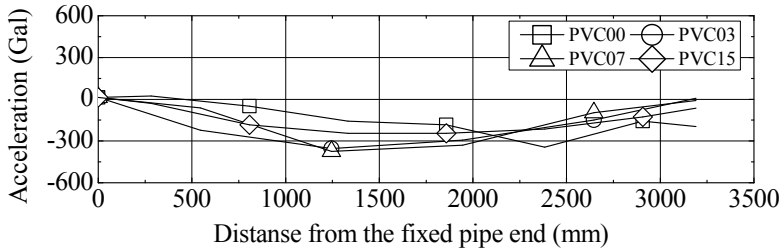

(a) t = 8.0

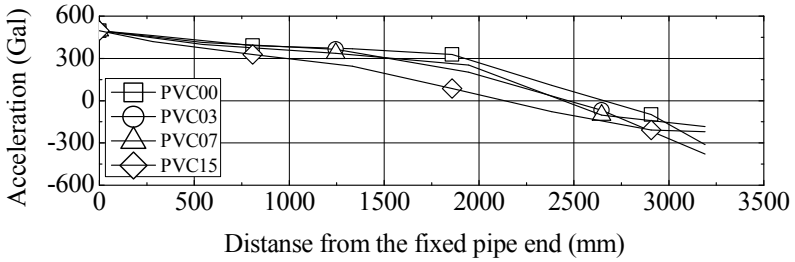

(b) t = 8.125

Figure 6.10 Acceleration distribution of model pipe in Series A

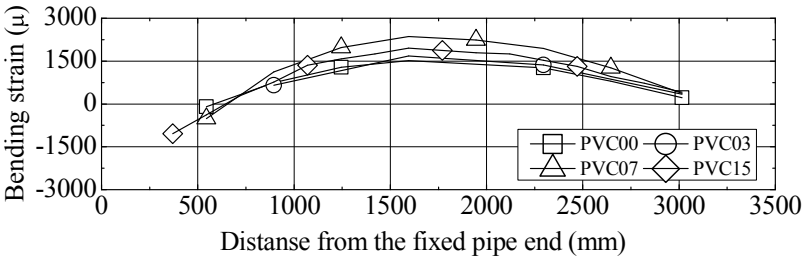

(a) t = 8.0

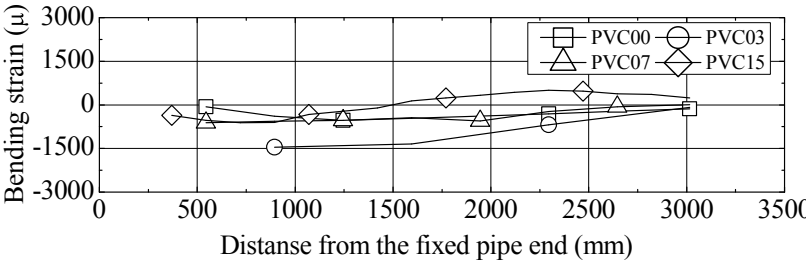

(b) t = 8.125

Figure 6.11 Bending strain distribution of model pipe in Series A

6.8 Conclusions

In this chapter, the shaking table tests were conducted to verify the dynamic behavior in the axial direction for the pipe rehabilitation method during liquefaction. The following points were clarified from the test results:

1. The influence of the number of joint structures on the horizontal displacement of the pipe was extremely small.
2. The amplitude of the bending strain of PVC pipe having the outer pipe was large when liquefaction occurred due to the stress concentrated at the gaps between the outer pipes.
3. The deflection mode of the pipe was categorized into two main types: bow-shaped and pendulum-shaped deformation during earthquake in liquefied ground. Compared with the bending strain of a pendulum-shaped deformation, the bending strain of a bow-shaped deformation was large.

References

Alireza, F., Ehsan D., Zilan, Z., Salvatore S., Amjad A. and Andre, F. (2014): Post-earthquake Evaluation of Pipelines Rehabilitated with Cured in Place Lining Technology Using Acousitic Emission, *Construction and Building Materials*, Vol.54, pp.326-338.

Da Ha, Tarek H. Abdoun, Michael J. O'Rourke, Michael D. Symans, Thomas D. O'Rourke, Michael C. Palmer and Harry E. Stewart (2008): Buried High-density Polyethylene Pipelines Subjected to Normal and Strike-slip Faulting- A Centrifuge Investigation, *Canadian Geotechnical Journal*, Vol. 45, pp.1733-1742.

Fujita, N., Mohri, Y. and Suzuki, H. (2007): Performance of Flexible Joints Formed Underground Pipeline for Seismic Motion, *Trans. of JSIDRE*, No. 249, pp.63-73

(in Japanese with English Summary).

Hachiya, M., Tohda, J., Tokumasu, K., Takatsuka, Y. and Sano Y. (2005): A New Design Method for Buried Pipelines Subjected to Differential Ground Settlement, *Journal of JSCE*, No. 799, pp.109-122.

Kitara, M. and Miyajima, M. (1983): Dynamic Behavior of a Model Pipe Fixed at One End during Liquefaction, *Journal of JSCE*, No. 336, pp.31-38.

Kobayashi, M., Ando, H. and Oguchi, N. (1998): Effects of Velocity and Cyclic Displacement of Subsoil on Its Axial Restraint Force Acting on Polyethylene Coated Steel Pipes during Earthquakes, *Journal of JSCE*, No. 591, pp.299-312.

Takada, S. and Yamabe, Y. (1982): An Experiment on A Seismic Behavior of Buried Pipelines Subjected to Large Ground Deformations Using The Sinking-Soil-Box, *Journal of JSCE*, No. 323, pp.55-65.

Tanaka, Y., Arimura, T. and Jibu M. (2005): Behavior of Buried Pipe with Flexible Joint in Liquefied Ground, *Report of Research Center for Urban Safety and Security*, No. 8, pp.63-71.

CHAPTER 7

Chapter 7

Conclusions and Perspectives

In this thesis, the dynamic behavior of rehabilitated pipe was discussed. The following shows the conclusions of the previous chapters.

In chapter 2, the model tests for several flexible pipes, which each pipe has a different thickness and equivalent bending ring stiffness were conducted in a steel pit to discuss the influence of the thickness of pipe and ground stiffness behavior of pipes. For flexible pipes having different thickness and equivalent ring bending stiffness, the influence of the thickness of the pipe on the deflection and the bending strain distribution of the pipe was extremely small. On the other hand, the axial stress of the pipe which was generated due to the vertical pressure and the dispersion of the axial strain distribution increased according to the decrease of the pipe thickness. The maximum change rate of axial stress to the distance between a strain gauge and an adjacent strain gauge in the thin steel pipe was 9 times as large as that in the HDPE pipe for loose ground.

In chapter 3, shaking table tests using these pipes were conducted in order to verify the influence of the thickness of pipe, a condition of test pit and bedding material on the dynamic behavior of pipes due to a shear deformation of a ground on the basis of the study in Chapter 3. As the results, the influence of the thickness of the pipe on the bending strain distribution was small in spite of the boundary condition and the base

material. The influence of the thickness of the pipe on the axial stress distribution was large in spite of the boundary condition and the base material condition. In addition, the absolute maximum axial stress increased according to the increment of the shear strain of the laminar box.

In chapter 4, in order to clarify the influence of a damage of the outer pipe on the dynamic behavior of the inner pipe, cyclic shear test using a lamina box was a conducted under a different damage of outer pipes and a different density of backfill material. The relationship between the shear strain of the laminar box and the deflection of the flexible pipe had a hysteresis characteristic. The oblique deflections of the pipe to the shear strain were larger than the horizontal and vertical deflection. The deflection of the flexible pipe for the loose ground increased according to the increment of the cycle due to the negative dilatancy. On the other hand, the deflection for the dense ground at the second cycles was smaller than that at the first cycle due to the positive dilatancy. The compressive strain increased from 90 to 180 deg. and from 270 to 360 deg. due to the shear deformation of the laminar box. In addition, the tensile strain increased from 0 to 90 deg. and from 180 to 270 deg. The normal earth pressure on the flexible pipe was generated from 60 to 210 deg. and from 240 to 360 deg. The normal earth pressure increased according to the relative density of the backfill material. The negative tangential earth pressure was generated from 45 to 120 deg. and from 240 to 300 deg. and the positive tangential earth pressure was generated from 120 to 210 deg. and from 300 to 30 deg. The deflection of the inner pipe was controlled with the outer pipe in spite of the damage level of the outer pipe. The outer pipe without inclined cracks restrain that the earth pressure from acting on the inner pipe. When the outer pipe had the inclined cracks, the restraint efficacy to the deflection of the inner pipe was small. The strain of the inner pipe due to earthquake was restricted. In addition, for the outer pipe with 4 inclined, the concentrated strain was generated at the crack. As the damage level of the outer pipe was developed, the influence of the outer pipe in the strain of the inner pipe was almost negligible.

In chapter 5, two dimensional discrete element method (DEM) analyses were conducted in order to verify the deformation mechanism of the inner pipe with and

without the outer pipe during earthquake and formulate the oblique deflection of the inner pipe to shear strain of the ground. The relationship between the normal spring line and elastic modulus of the flexible pipe had a linear and the model pipe had any ring bending stiffness was modeled. The deflection of the pipe to the shear strain in the laminar box was simulated for any relative density of the backfill material and any ring bending stiffness. The influence of the damage level of the outer pipe on the oblique deflection of the inner pipe was simulated. When the shear deformation was generated under the ground due to earthquake, the compressive normal earth pressure was acted on the pipe from 90 deg. to 135 deg. and from 270 deg. to 315 deg. (45 deg. to 90 deg. and 225 deg. to 270 deg.), and the tangential earth pressure was acted along the pipe from the range of the normal earth pressure. As the results, the oblique deflection of the pipe was developed. The oblique deflection rate of the flexible pipe to $E_{50}/(E_pI/D_c^3)$ had the asymptotic value. The asymptotic value was determined by a geometric calculation. The relationship between $E_{50}/(E_pI/D_c^3)$ and the 45-225 deg. deflection of the pipe was approximated by Box-Lucas model. In addition, the deflection of the rehabilitated pipe was calculated on the basis of the damage level of the outer pipe and the relative density of the backfill material by introducing the decreasing coefficient C_h.

In this chapter 6, the shaking table tests were conducted to verify the dynamic behavior in the axial direction for the pipe rehabilitation method during liquefaction. The influence of the number of joint structures on the horizontal displacement of the pipe was extremely small. The amplitude of the bending strain of PVC pipe having the outer pipe was large when liquefaction occurred due to t the stress concentrated at the gaps between the outer pipes. The deflection mode of the pipe was categorized into two main types: bow-shaped and pendulum-shaped deformation during earthquake in liquefied ground. Compared with the bending strain of a pendulum-shaped deformation, the bending strain of a bow-shaped deformation was large.

In chapter 2~6, experiments and analyses used for fine-grained and homogeneous backfill material were conducted. Experiments and analyses under many types of the backfill material, the depth of the cover, the pipe diameter are need in order to evaluate more quantitatively the buried behavior In addition, aluminum segments which was

divided into 2, 4, 8 and 16 segments were used as the damaged outer pipe in chapter 4 and 5. In order to clear the influence of the outer pipe on the buried behavior of the inner pipe, the deterioration state of pipes should be investigated in the field.

Appendix

Contact force distribution

The contact force distribution discussed in chapter 5 is shown in this appendix for details.

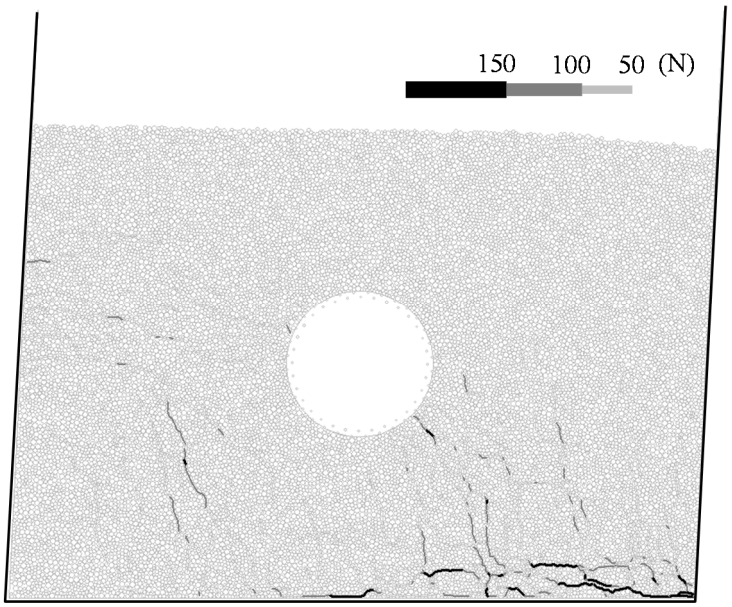

Figure A.1 Contact force distribution in ALN-20 at γ =5%

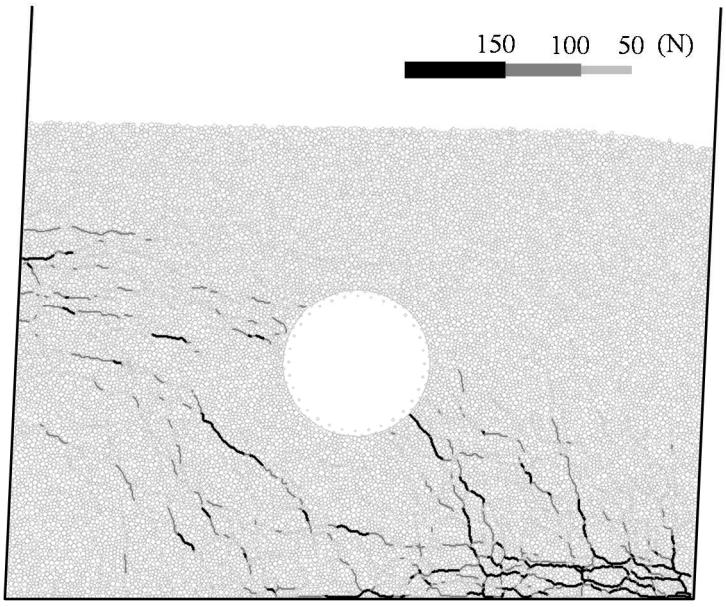

Figure A.2 Contact force distribution in ALN-45 at γ =5%

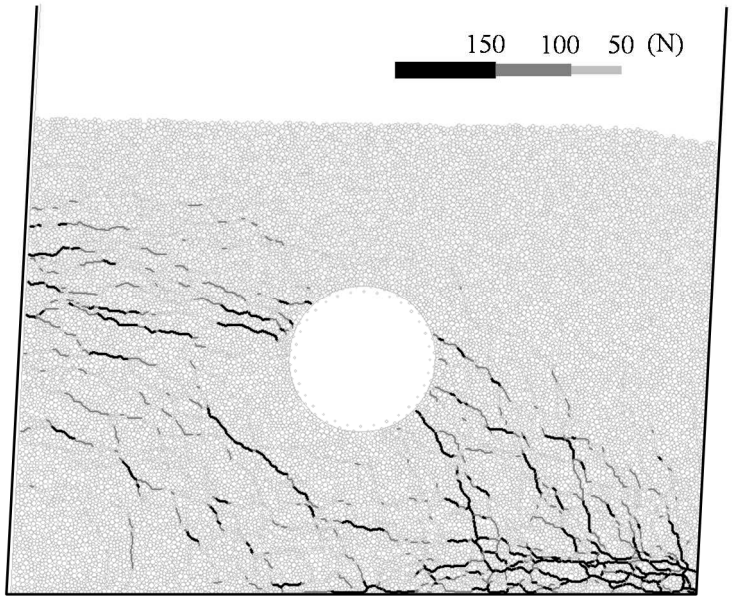

Figure A.3 Contact force distribution in ALN-65 at γ =5%

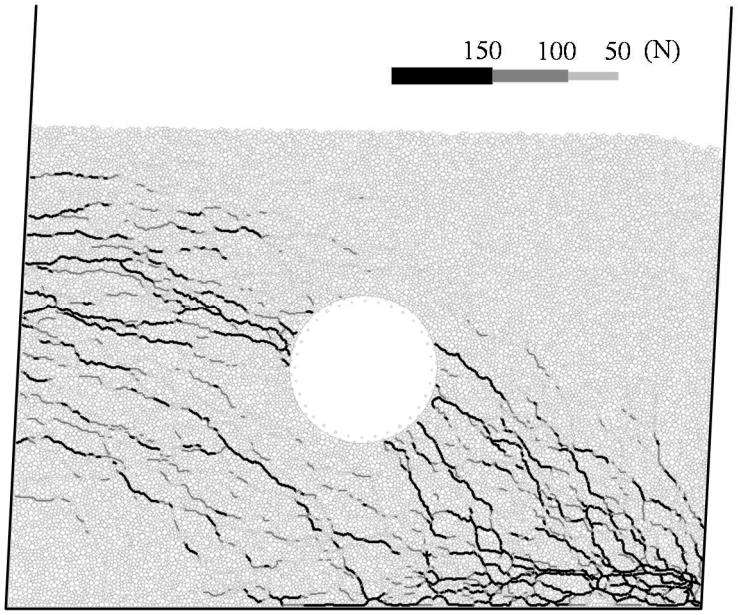

Figure A.4 Contact force distribution in ALN-85 at γ =5%

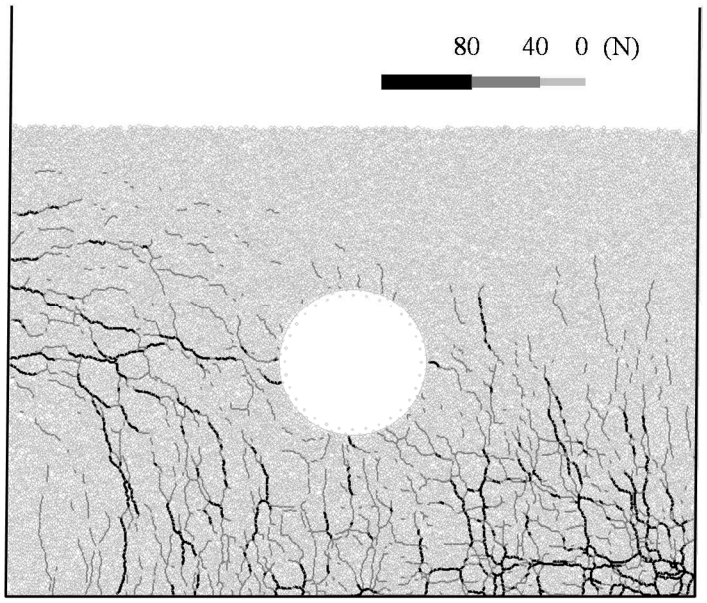

Figure A.5 Contact force distribution in ALN-45 at γ =1% (t = 0.129)

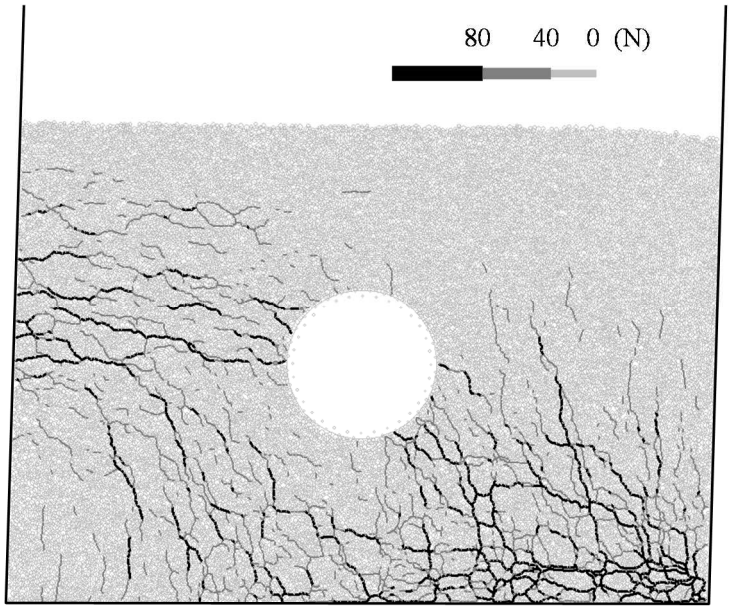

Figure A.6 Contact force distribution in ALN-45 at γ =3% (t = 0.410)

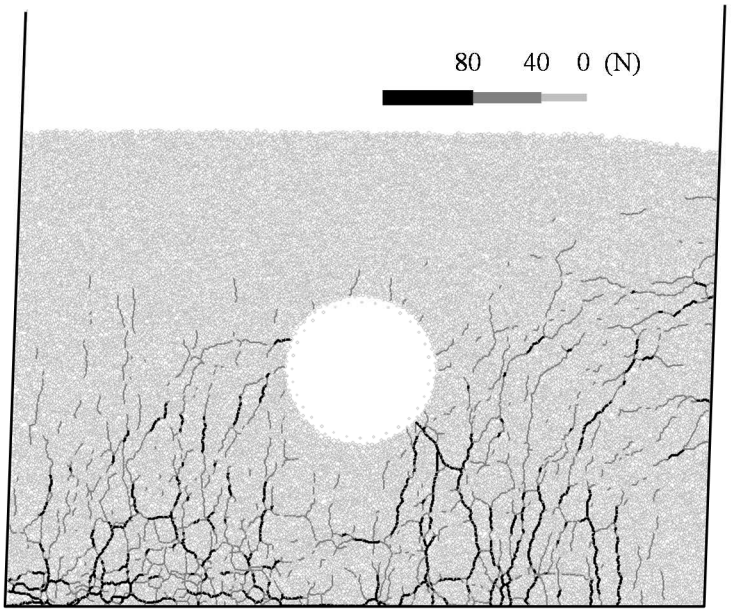

Figure A.7 Contact force distribution in ALN-45 at γ =3.5% (t = 1.506)

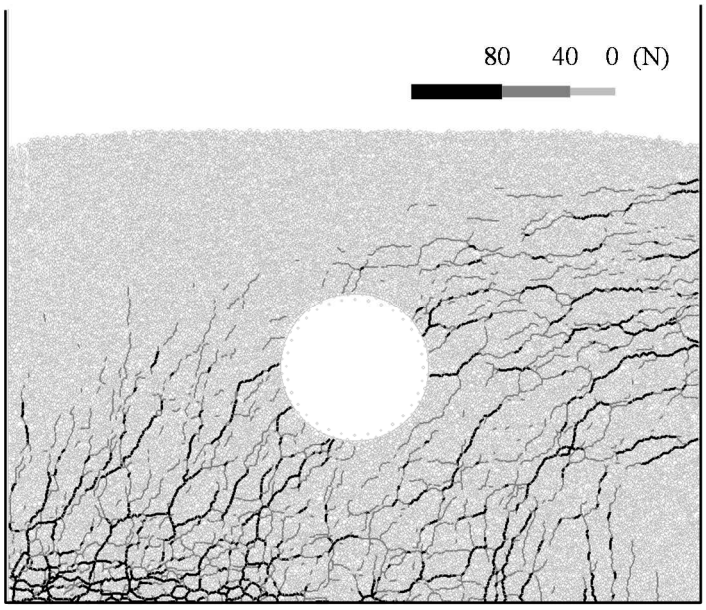

Figure A.8 Contact force distribution in ALN-45 at γ =0% (t = 2.000)